

GW241011 and GW241110: Exploring Binary Formation and Fundamental Physics with Asymmetric, High-Spin Black Hole Coalescences

A. G. ABAC ¹, I. ABOUELFETTOUH, ² F. ACERNESE, ^{3,4} K. ACKLEY ⁵, C. ADAMCEWICZ ⁶, S. ADHICARY ⁷,
D. ADHIKARI, ^{8,9} N. ADHIKARI ¹⁰, R. X. ADHIKARI ¹¹, V. K. ADKINS, ¹² S. AFROZ ¹³, A. AGAPITO, ¹⁴
D. AGARWAL ¹⁵, M. AGATHOS ¹⁶, N. AGGARWAL, ¹⁷ S. AGGARWAL, ¹⁸ O. D. AGUIAR ¹⁹, I.-L. AHREND, ²⁰
L. AIELLO ^{21,22}, A. AIN ²³, P. AJITH ²⁴, T. AKUTSU ^{25,26}, S. ALBANESI ^{27,28}, W. ALI, ^{29,30} S. AL-KERSHI, ^{8,9}
C. ALLÉNE, ³¹ A. ALLOCCA ^{32,4}, S. AL-SHAMMARI, ³³ P. A. ALTIN ³⁴, S. ALVAREZ-LOPEZ ³⁵, W. AMAR, ³¹
O. AMARASINGHE, ³³ A. AMATO ^{36,37}, F. AMICUCCI ^{38,39}, C. AMRA, ⁴⁰ A. ANANYEVA, ¹¹ S. B. ANDERSON ¹¹,
W. G. ANDERSON ¹¹, M. ANDIA ⁴¹, M. ANDO, ⁴² M. ANDRÉS-CARCASONA ⁴³, T. ANDRIĆ ^{44,45,8,9}, J. ANGLIN, ⁴⁶
S. ANSOLDI ^{47,48}, J. M. ANTELLIS ⁴⁹, S. ANTIER ³³, F. ANTONINI, ³³ M. AOUMI, ⁵⁰ E. Z. APPAVURAVTHER, ^{51,52}
S. APPERT, ¹¹ S. K. APPLE ⁵³, K. ARAI ¹¹, C. ARAÚJO-ÁLVAREZ, ⁵⁴ A. ARAYA ⁴², M. C. ARAYA ¹¹,
M. ARCA SEDDA ^{44,45}, J. S. AREEDA ⁵⁵, N. ARITOMI, ² F. ARMATO ^{29,30}, S. ARMSTRONG ⁵⁶, N. ARNAUD ⁵⁷,
M. AROGETI ⁵⁸, S. M. ARONSON ¹², K. G. ARUN ⁵⁹, G. ASHTON ⁶⁰, Y. ASO ^{25,61}, L. ASPREA, ²⁸ M. ASSIDUO, ^{62,63}
S. ASSIS DE SOUZA MELO, ⁶⁴ S. M. ASTON, ⁶⁵ P. ASTONE ³⁸, P. S. ASWATHI, ³⁴ F. ATTADIO ^{39,38}, F. AUBIN ⁶⁶,
K. AULTONEAL ⁶⁷, G. AVALLONE ⁶⁸, E. A. AVILA ⁴⁹, S. BABAK ²⁰, C. BADGER, ⁶⁹ S. BAE ⁷⁰, S. BAGNASCO ²⁸,
L. BAIOTTI ⁷¹, R. BAJPAI ⁷², T. BAKA, ^{73,37} A. M. BAKER, ⁶ K. A. BAKER, ⁷⁴ T. BAKER ⁷⁵, G. BALDI ^{76,77},
N. BALDICCHI ^{78,51}, M. BALL, ⁷⁹ G. BALLARDIN, ⁶⁴ S. W. BALLMER, ⁸⁰ S. BANAGIRI ⁶, B. BANERJEE ⁴⁴,
D. BANKAR ⁸¹, T. M. BAPTISTE, ¹² P. BARAL ¹⁰, M. BARATTI ^{82,83}, J. C. BARAYOGA, ¹¹ B. C. BARISH, ¹¹ D. BARKER, ²
N. BARMAN, ⁸¹ P. BARNEO ^{84,85,86}, F. BARONE ^{87,4}, B. BARR ⁸⁸, L. BARSOTTI ³⁵, M. BARSUGLIA ²⁰,
D. BARTA ⁸⁹, A. M. BARTOLETTI, ⁹⁰ M. A. BARTON ⁸⁸, I. BARTOS, ⁴⁶ A. BASALAEV ^{8,9}, R. BASSIRI ⁹¹,
A. BASTI ^{83,82}, M. BAWAJ ^{78,51}, P. BAXI, ⁹² J. C. BAYLEY ⁸⁸, A. C. BAYLOR ¹⁰, P. A. BAYNARD II, ⁵⁸
M. BAZZAN, ^{93,94} V. M. BEDAKIHALE, ⁹⁵ F. BEIRNAERT ⁹⁶, M. BEJGER ⁹⁷, D. BELARDINELLI ²², A. S. BELL ⁸⁸,
D. S. BELLIE, ⁹⁸ L. BELLIZZI ^{82,83}, W. BENOIT ¹⁸, I. BENTARA ⁵⁷, J. D. BENTLEY ⁹⁹, M. BEN YAALA, ⁵⁶
S. BERA ^{100,101}, F. BERGAMIN ³³, B. K. BERGER ⁹¹, S. BERNUZZI ²⁷, M. BEROIZ ¹¹, C. P. L. BERRY ⁸⁸,
D. BERSANETTI ²⁹, T. BERTHEAS, ¹⁰² A. BERTOLINI, ^{37,36} J. BETZWIESER ⁶⁵, D. BEVERIDGE ⁷⁴, G. BEVILACQUA ¹⁰³,
N. BEVINS ¹⁰⁴, R. BHANDARE, ¹⁰⁵ R. BHATT, ¹¹ D. BHATTACHARJEE ^{106,107}, S. BHATTACHARYYA, ¹⁰⁸ S. BHAUMIK ⁴⁶,
V. BIANCALANA ¹⁰³, A. BIANCHI, ^{37,109} I. A. BILENKO, ¹¹⁰ G. BILLINGSLEY ¹¹, A. BINETTI ¹¹¹, S. BINI ^{11,76,77},
C. BINU, ¹¹² S. BIOT, ¹¹³ O. BIRNHOLTZ ¹¹⁴, S. BISCOVEANU ⁹⁸, A. BISHT, ⁹ M. BITOSSI ^{64,82}, M.-A. BIZOUARD ¹¹⁵,
S. BLABER, ¹¹⁶ J. K. BLACKBURN ¹¹, L. A. BLAGG, ⁷⁹ C. D. BLAIR, ^{74,65} D. G. BLAIR, ⁷⁴ N. BODE ^{8,9}, N. BOETTNER, ⁹⁹
G. BOILEAU ¹¹⁵, M. BOLDRINI ³⁸, G. N. BOLINGBROKE ¹¹⁷, A. BOLLIAND, ^{118,40} L. D. BONAVENA ⁴⁶,
R. BONDARESCU ⁸⁴, F. BONDU ¹¹⁹, E. BONILLA ⁹¹, M. S. BONILLA ⁵⁵, A. BONINO, ¹²⁰ R. BONNAND ^{31,118},
A. BORCHERS, ^{8,9} S. BORHANIAN, ⁷ V. BOSCHI ⁸², S. BOSE, ¹²¹ V. BOSSILKOV, ⁶⁵ Y. BOTHRA ^{37,109}, A. BOUDON, ⁵⁷
L. BOURG, ⁵⁸ M. BOYLE, ¹²² A. BOZZI, ⁶⁴ C. BRADASCHIA, ⁸² P. R. BRADY ¹⁰, A. BRANCH, ⁶⁵ M. BRANCHESI ^{44,45},
I. BRAUN, ¹⁰⁶ T. BRIANT ¹²³, A. BRILLET, ¹¹⁵ M. BRINKMANN, ^{8,9} P. BROCKILL, ¹⁰ E. BROCKMUELLER ^{8,9},
A. F. BROOKS ¹¹, B. C. BROWN, ⁴⁶ D. D. BROWN, ¹¹⁷ M. L. BROZZETTI ^{78,51}, S. BRUNETT, ¹¹ G. BRUNO, ¹⁵
R. BRUNTZ ¹²⁴, J. BRYANT, ¹²⁰ Y. BU, ¹²⁵ F. BUCCI ⁶³, J. BUCHANAN, ¹²⁴ O. BULASHENKO ^{84,85}, T. BULIK, ¹²⁶
H. J. BULTEN, ³⁷ A. BUONANNO ^{127,1}, K. BURTONYK, ² R. BUSCICCHIO ^{128,129}, D. BUSKULIC, ³¹ C. BUY ¹⁰²,
R. L. BYER, ⁹¹ G. S. CABOURN DAVIES ⁷⁵, R. CABRITA ¹⁵, V. CÁCERES-BARBOSA ⁷, L. CADONATI ⁵⁸,
G. CAGNOLI ¹³⁰, C. CAHILLANE ⁸⁰, A. CALAFAT, ¹⁰⁰ J. CALDERÓN BUSTILLO, ⁵⁴ T. A. CALLISTER, ^{131,132} E. CALLONI, ^{32,4}
S. R. CALLOS ⁷⁹, G. CANEVA SANTORO ⁴³, K. C. CANNON ⁴², H. CAO, ³⁵ L. A. CAPISTRAN, ¹³³ E. CAPOCASA ²⁰,
E. CAPOTE ^{2,11}, G. CAPURRI ^{83,82}, G. CARAPPELLA, ^{68,134} F. CARBOGNANI, ⁶⁴ M. CARLASSARA, ^{8,9} J. B. CARLIN ¹²⁵,
T. K. CARLSON, ¹³⁵ M. F. CARNEY, ¹⁰⁶ M. CARPINELLI ^{128,64}, G. CARRILLO, ⁷⁹ J. J. CARTER ^{8,9}, G. CARULLO ^{120,136},
A. CASALLAS-LAGOS, ¹³⁷ J. CASANUEVA DIAZ ⁶⁴, C. CASENTINI ^{138,22}, S. Y. CASTRO-LUCAS, ¹³⁹ S. CAUDILL, ¹³⁵
M. CAVAGLIÀ ¹⁰⁷, R. CAVALIERI ⁶⁴, A. CEJA, ⁵⁵ G. CELLA ⁸², P. CERDÁ-DURÁN ^{140,141}, E. CESARINI ²²,
N. CHABBRA, ³⁴ W. CHAIBI, ¹¹⁵ A. CHAKRABORTY ¹³, P. CHAKRABORTY ^{8,9}, S. CHAKRABORTY, ¹⁰⁵
S. CHALATHADKA SUBRAHMANYA ⁹⁹, J. C. L. CHAN ¹⁴², M. CHAN, ¹¹⁶ K. CHANG, ¹⁴³ S. CHAO ^{144,143},
P. CHARLTON ¹⁴⁵, E. CHASSANDE-MOTTIN ²⁰, C. CHATTERJEE ¹⁴⁶, DEBARATI CHATTERJEE ⁸¹,
DEEP CHATTERJEE ³⁵, M. CHATURVEDI, ¹⁰⁵ S. CHATY ²⁰, K. CHATZHOANNOU ¹¹, A. CHEN ¹⁴⁷, A. H.-Y. CHEN, ¹⁴⁸
D. CHEN ¹⁴⁹, H. CHEN, ¹⁴⁴ H. Y. CHEN ¹⁵⁰, S. CHEN, ¹⁴⁶ YANBEI CHEN, ¹⁵¹ YITIAN CHEN ¹²², H. P. CHENG, ¹⁵²
P. CHESA ^{78,51}, H. T. CHEUNG ⁹², S. Y. CHEUNG, ⁶ F. CHIADINI ^{153,134}, D. CHIARAMELLO, ²⁸ G. CHIARINI, ^{8,9,94}
A. CHIBA, ¹⁵⁴ A. CHINCARINI ²⁹, M. L. CHIOFALO ^{83,82}, A. CHIUMMO ^{4,64}, C. CHOU, ¹⁴⁸ S. CHOUDHARY ⁷⁴

- N. CHRISTENSEN ^{115,155} S. S. Y. CHUA ³⁴ G. CIANI ^{76,77} P. CIECIELAG ⁹⁷ M. CIEŚLAR ¹²⁶ M. CIFALDI ²²
 B. CIROK ¹⁵⁶ F. CLARA ² J. A. CLARK ^{11,58} T. A. CLARKE ⁶ P. CLEARWATER ¹⁵⁷ S. CLESSE ¹¹³ F. CLEVA ^{115,118}
 E. COCCIA ^{44,45,43} E. CODAZZO ^{158,159} P.-F. COHADON ¹²³ S. COLACE ³⁰ E. COLANGELI ⁷⁵ M. COLLEONI ¹⁰⁰
 C. G. COLLETTE ¹⁶⁰ J. COLLINS ⁶⁵ S. COLLOMS ⁸⁸ A. COLOMBO ^{161,129} C. M. COMPTON ² G. CONNOLLY ⁷⁹
 L. CONTI ⁹⁴ T. R. CORBITT ¹² I. CORDERO-CARRIÓN ¹⁶² S. COREZZI ^{78,51} N. J. CORNISH ¹⁶³ I. CORONADO ¹⁶⁴
 A. CORSI ¹⁶⁵ R. COTTINGHAM ⁶⁵ M. W. COUGHLIN ¹⁸ A. COUINEAUX ³⁸ P. COUVARES ^{11,58} D. M. COWARD ⁷⁴
 R. COYNE ¹⁶⁶ A. COZZUMBO ⁴⁴ J. D. E. CREIGHTON ¹⁰ T. D. CREIGHTON ¹⁶⁷ P. CREMONESE ¹⁰⁰ S. CROOK ⁶⁵
 R. CROUCH ² J. CSIZMAZIA ² J. R. CUDELL ¹⁶⁸ T. J. CULLEN ¹¹ A. CUMMING ⁸⁸ E. CUOCO ^{169,170}
 M. CUSINATO ¹⁴⁰ L. V. DA CONCEIÇÃO ¹⁷¹ T. DAL CANTON ⁴¹ S. DAL PRA ¹⁷² G. DÁLYA ¹⁰²
 B. D'ANGELO ²⁹ S. DANILISHIN ^{36,37} S. D'ANTONIO ³⁸ K. DANZMANN ^{9,8,9} K. E. DARROCH ¹²⁴ L. P. DARTEZ ⁶⁵
 R. DAS ¹⁰⁸ A. DASGUPTA ⁹⁵ V. DATILO ⁶⁴ A. DAUMAS ²⁰ N. DAVARI ^{173,174} I. DAVE ¹⁰⁵ A. DAVENPORT ¹³⁹ M. DAVIER ⁴¹
 T. F. DAVIES ⁷⁴ D. DAVIS ¹¹ L. DAVIS ⁷⁴ M. C. DAVIS ¹⁸ P. DAVIS ^{175,176} E. J. DAW ¹⁷⁷ M. DAX ¹
 J. DE BOLLE ⁹⁶ M. DEENADAYALAN ⁸¹ J. DEGALLAIX ¹⁷⁸ M. DE LAURENTIS ^{32,4} F. DE LILLO ²³
 S. DELLA TORRE ¹²⁹ W. DEL POZZO ^{83,82} A. DEMAGNY ³¹ F. DE MARCO ^{39,38} G. DEMASI ^{179,63}
 F. DE MATTEIS ^{21,22} N. DEMOS ³⁵ T. DENT ⁵⁴ A. DEPASSE ¹⁵ N. DEPERGOLA ¹⁰⁴ R. DE PIETRI ^{180,181}
 R. DE ROSA ^{32,4} C. DE ROSSI ⁶⁴ M. DESAI ³⁵ R. DESALVO ¹⁸² A. DESIMONE ¹⁸³ R. DE SIMONE ^{153,134}
 A. DHANI ¹ R. DHURKUNDE ^{8,9,75} R. DIAB ⁴⁶ M. C. DÍAZ ¹⁶⁷ M. DI CESARE ^{32,4} G. DIDERON ¹⁸⁴ T. DIETRICH ¹
 L. DI FIORE ⁴ C. DI FRONZO ⁷⁴ M. DI GIOVANNI ^{39,38} T. DI GIROLAMO ^{32,4} D. DIKSHA ^{37,36} J. DING ^{20,185}
 S. DI PACE ^{39,38} I. DI PALMA ^{39,38} D. DI PIERO ^{186,48} F. DI RENZO ⁵⁷ DIVYAJYOTI ³³ A. DMITRIEV ¹²⁰
 J. P. DOCHERTY ⁸⁸ Z. DOCTOR ⁹⁸ N. DOERKSEN ¹⁷¹ E. DOHMEN ² A. DOKE ¹³⁵ A. DOMICIANO DE SOUZA ¹⁸⁷
 L. D'ONOFRIO ³⁸ F. DONOVAN ³⁵ K. L. DOOLEY ³³ T. DOONEY ⁷³ S. DORAVARI ⁸¹ O. DOROSH ¹⁸⁸
 W. J. D. DOYLE ¹²⁴ M. DRAGO ^{39,38} J. C. DRIGGERS ² L. DUNN ¹²⁵ U. DUPLETSA ⁴⁴ P.-A. DUVERNE ²⁰
 D. D'URSO ^{173,158} P. DUTTA ROY ⁴⁶ H. DUVAL ¹⁸⁹ S. E. DWYER ² C. EASSA ² W. E. EAST ¹⁸⁴
 M. EBERSOLD ^{190,31} T. ECKHARDT ⁹⁹ G. EDDOLLS ⁸⁰ A. EFFLER ⁶⁵ J. EICHHOLZ ³⁴ H. EINSLE ¹¹⁵
 M. EISENMANN ²⁵ M. EMMA ⁶⁰ K. ENDO ¹⁵⁴ R. ENFICIAUD ¹ L. ERRICO ^{32,4} R. ESPINOSA ¹⁶⁷ M. ESPOSITO ^{4,32}
 R. C. ESSICK ¹⁹¹ H. ESTELLÉS ¹ T. ETZEL ¹¹ M. EVANS ³⁵ T. EVSTAFYEVA ¹⁸⁴ B. E. EWING ⁷
 J. M. EZQUIAGA ¹⁴² F. FABRIZI ^{62,63} V. FAFONE ^{21,22} S. FAIRHURST ³³ A. M. FARAH ¹³¹ B. FARR ⁷⁹
 W. M. FARR ^{192,193} G. FAVARO ⁹³ M. FAVATA ¹⁹⁴ M. FAYS ¹⁶⁸ M. FAZIO ⁵⁶ J. FEICHT ¹¹ M. M. FEJER ⁹¹
 R. FELICETTI ^{186,48} E. FENYVESI ^{89,195} J. FERNANDES ¹⁹⁶ T. FERNANDES ^{197,140} D. FERNANDO ¹¹²
 S. FERRAIUOLO ^{198,39,38} T. A. FERREIRA ¹² F. FIDECARO ^{83,82} P. FIGURA ⁹⁷ A. FIORI ^{82,83} I. FIORI ⁶⁴
 M. FISHBACH ¹⁹¹ R. P. FISHER ¹²⁴ R. FITTIPALDI ^{199,134} V. FIUMARA ^{200,134} R. FLAMINIO ³¹ S. M. FLEISCHER ¹⁰¹
 L. S. FLEMING ²⁰² E. FLODEN ¹⁸ H. FONG ¹¹⁶ J. A. FONT ^{140,141} F. FONTINELE-NUNES ¹⁸ C. FOO ¹ B. FORNAL ²⁰³
 K. FRANCESCHETTI ¹⁸⁰ F. FRAPPEZ ³¹ S. FRASCA ^{39,38} F. FRASCONI ⁸² J. P. FREED ⁶⁷ Z. FREI ²⁰⁴ A. FREISE ^{37,109}
 O. FREITAS ^{197,140} R. FREY ⁷⁹ W. FRISCHHERTZ ⁶⁵ P. FRITSCHER ³⁵ V. V. FROLOV ⁶⁵ G. G. FRONZÉ ²⁸
 M. FUENTES-GARCIA ¹¹ S. FUJII ²⁰⁵ T. FUJIMORI ²⁰⁶ P. FULDA ⁴⁶ M. FYFFE ⁶⁵ B. GADRE ⁷³ J. R. GAIR ¹
 S. GALAUDAGE ¹⁸⁷ V. GALDI ²⁰⁷ R. GAMBA ⁷ A. GAMBOA ¹ S. GAMOJI ¹⁸² D. GANAPATHY ²⁰⁸ A. GANGULY ⁸¹
 B. GARAVENTA ²⁹ J. GARCÍA-BELLIDO ²⁰⁹ C. GARCÍA-QUIRÓS ¹⁹⁰ J. W. GARDNER ³⁴ K. A. GARDNER ¹¹⁶
 S. GARG ⁴² J. GARGIULO ⁶⁴ X. GARRIDO ⁴¹ A. GARRON ¹⁰⁰ F. GARUFI ^{32,4} P. A. GARVER ⁹¹
 C. GASBARRA ^{21,22} B. GATELEY ² F. GAUTIER ²¹⁰ V. GAYATHRI ¹⁰ T. GAYER ⁸⁰ G. GEMME ²⁹ A. GENNAI ⁸²
 V. GENNARI ¹⁰² J. GEORGE ¹⁰⁵ R. GEORGE ¹⁵⁰ O. GERBERDING ⁹⁹ L. GERGELY ¹⁵⁶ ARCHISMAN GHOSH ⁹⁶
 SAYANTAN GHOSH ¹⁹⁶ SHAON GHOSH ¹⁹⁴ SHROBANA GHOSH ^{8,9} SUPROVO GHOSH ²¹¹ TATHAGATA GHOSH ⁸¹
 J. A. GIAIME ^{12,65} K. D. GIARDINA ⁶⁵ D. R. GIBSON ²⁰² C. GIER ⁵⁶ S. GKAITATZIS ^{83,82} J. GLANZER ¹¹
 F. GLOTIN ⁴¹ J. GODFREY ⁷⁹ R. V. GODLEY ^{8,9} P. GODWIN ¹¹ A. S. GOETTEL ³³ E. GOETZ ¹¹⁶ J. GOLOMB ¹¹
 S. GOMEZ LOPEZ ^{39,38} B. GONCHAROV ⁴⁴ G. GONZÁLEZ ¹² P. GOODARZI ²¹² S. GOODE ⁶
 A. W. GOODWIN-JONES ¹⁵ M. GOSSELIN ⁶⁴ R. GOUATY ³¹ D. W. GOULD ³⁴ K. GOVORKOVA ³⁵ A. GRADO ^{78,51}
 V. GRAHAM ⁸⁸ A. E. GRANADOS ¹⁸ M. GRANATA ¹⁷⁸ V. GRANATA ^{213,134} S. GRAS ³⁵ P. GRASSIA ¹¹ J. GRAVES ⁵⁸
 C. GRAY ² R. GRAY ⁸⁸ G. GRECO ⁵¹ A. C. GREEN ^{37,109} L. GREEN ²¹⁴ S. M. GREEN ⁷⁵ S. R. GREEN ²¹⁵
 C. GREENBERG ¹³⁵ A. M. GRETARSSON ⁶⁷ H. K. GRIFFIN ¹⁸ D. GRIFFITH ¹¹ H. L. GRIGGS ⁵⁸ G. GRIGNANI ^{78,51}
 C. GRIMAUD ³¹ H. GROTE ³³ S. GRUNEWALD ¹ D. GUERRA ¹⁴⁰ D. GUETTA ²¹⁶ G. M. GUIDI ^{62,63}
 A. R. GUIMARAES ¹² H. K. GULATI ⁹⁵ F. GULMINELLI ^{175,176} H. GUO ¹⁴⁷ W. GUO ⁷⁴ Y. GUO ^{37,36}
 ANURADHA GUPTA ²¹⁷ I. GUPTA ⁷ N. C. GUPTA ⁹⁵ S. K. GUPTA ⁴⁶ V. GUPTA ¹⁸ N. GUPTE ¹ J. GURS ⁹⁹
 N. GUTIERREZ ¹⁷⁸ N. GUTTMAN ⁶ F. GUZMAN ¹³³ D. HABA ²¹⁸ M. HABERLAND ¹ S. HAINO ²¹⁹ E. D. HALL ³⁵
 E. Z. HAMILTON ¹⁰⁰ G. HAMMOND ⁸⁸ M. HANEY ³⁷ J. HANKS ² C. HANNA ⁷ M. D. HANNAM ³³
 O. A. HANNUKSELA ²²⁰ A. G. HANSELMAN ¹³¹ H. HANSEN ² J. HANSON ⁶⁵ S. HANUMASAGAR ⁵⁸ R. HARADA ⁴²
 A. R. HARDISON ¹⁸³ S. HARIKUMAR ¹⁸⁸ K. HARIS ^{37,73} I. HARLEY-TROCHIMCZYK ¹³³ T. HARMARK ¹³⁶ J. HARMS ^{44,45}

G. M. HARRY ²²¹ I. W. HARRY ⁷⁵ J. HART, ¹⁰⁶ B. HASKELL, ^{97, 222, 223} C. J. HASTER ²¹⁴ K. HAUGHIAN ⁸⁸
 H. HAYAKAWA, ⁵⁰ K. HAYAMA, ²²⁴ A. HEFFERNAN, ¹⁰⁰ M. C. HEINTZE, ⁶⁵ J. HEINZE ¹²⁰ J. HEINZEL, ³⁵ H. HEITMANN ¹¹⁵
 F. HELLMAN ²⁰⁸ A. F. HELMLING-CORNELL ⁷⁹ G. HEMMING ⁶⁴ O. HENDERSON-SAPIR ¹¹⁷ M. HENDRY ⁸⁸
 I. S. HENG, ⁸⁸ M. H. HENNIG ⁸⁸ C. HENSHAW ⁵⁸ M. HEURS ^{8, 9} A. L. HEWITT ^{225, 226} J. HEYENEN, ¹⁵ J. HEYNS, ³⁵
 S. HIGGINBOTHAM, ³³ S. HILD, ^{36, 37} S. HILL, ⁸⁸ Y. HIMEMOTO ²²⁷ N. HIRATA, ²⁵ C. HIROSE, ²²⁸ D. HOFMAN, ¹⁷⁸
 B. E. HOGAN, ⁶⁷ N. A. HOLLAND, ^{37, 109} I. J. HOLLOWES ¹⁷⁷ D. E. HOLZ ¹³¹ L. HONET, ¹¹³ D. J. HORTON-BAILEY, ²⁰⁸
 J. HOUGH ⁸⁸ S. HOURIHANE ¹¹ N. T. HOWARD, ¹⁴⁶ E. J. HOWELL ⁷⁴ C. G. HOY ⁷⁵ C. A. HRISHIKESH, ²¹ P. HSI, ³⁵
 H.-F. HSIEH ¹⁴⁴ H.-Y. HSIEH, ¹⁴⁴ C. HSIUNG, ²²⁹ S.-H. HSU, ¹⁴⁸ W.-F. HSU ¹¹¹ Q. HU ⁸⁸ H. Y. HUANG ¹⁴³
 Y. HUANG ⁷ Y. T. HUANG, ⁸⁰ A. D. HUDDART, ²³⁰ B. HUGHEY, ⁶⁷ V. HUI ³¹ S. HUSA ¹⁰⁰ R. HUXFORD, ⁷
 L. IAMPIERI ^{39, 38} G. A. IANDOLO ³⁶ M. IANNI, ^{22, 21} G. IANNONE ¹³⁴ J. IASCAU, ⁷⁹ K. IDE, ²³¹ R. IDEN, ²¹⁸
 A. IERARDI, ^{44, 45} S. IKEDA, ¹⁴⁹ H. IMAFUKU, ⁴² Y. INOUE, ¹⁴³ G. IORIO ⁹³ P. IOSIF ^{186, 48} M. H. IQBAL, ³⁴ J. IRWIN ⁸⁸
 R. ISHIKAWA, ²³¹ M. ISI ^{192, 193} K. S. ISLEIF ²³² Y. ITOH ^{206, 233} M. IWAYA, ²⁰⁵ B. R. IYER ²⁴ C. JACQUET, ¹⁰²
 P.-E. JACQUET ¹²³ T. JACQUOT, ⁴¹ S. J. JADHAV, ²³⁴ S. P. JADHAV ¹⁵⁷ M. JAIN, ¹³⁵ T. JAIN, ²²⁵ A. L. JAMES ¹¹
 K. JANI ¹⁴⁶ J. JANQUART ¹⁵ N. N. JANTHALUR, ²³⁴ S. JARABA ²³⁵ P. JARANOWSKI ²³⁶ R. JAUME ¹⁰⁰
 W. JAVED, ³³ A. JENNINGS, ² M. JENSEN, ² W. JIA, ³⁵ J. JIANG ¹⁵² H.-B. JIN ^{237, 238} G. R. JOHNS, ¹²⁴ N. A. JOHNSON, ⁴⁶
 M. C. JOHNSTON ²¹⁴ R. JOHNSTON, ⁸⁸ N. JOHNY, ^{8, 9} D. H. JONES ³⁴ D. I. JONES, ²¹¹ R. JONES, ⁸⁸ H. E. JOSE, ⁷⁹
 P. JOSHI ⁷ S. K. JOSHI, ⁸¹ G. JOUBERT, ⁵⁷ J. JU, ²³⁹ L. JU ⁷⁴ K. JUNG ²⁴⁰ J. JUNKER ³⁴ V. JUSTE, ¹¹³
 H. B. KABAGOZ ^{65, 35} T. KAJITA ²⁴¹ I. KAKU, ²⁰⁶ V. KALOGERA ⁹⁸ M. KALOMENOPOULOS ²¹⁴ M. KAMIIZUMI ⁵⁰
 N. KANDA ^{233, 206} S. KANDHASAMY ⁸¹ G. KANG ²⁴² N. C. KANNACHEL, ⁶ J. B. KANNER, ¹¹ S. A. KANTI MAHANTY, ¹⁸
 S. J. KAPADIA ⁸¹ D. P. KAPASI ⁵⁵ M. KARTHIKEYAN, ¹³⁵ M. KASPRZACK ¹¹ H. KATO, ¹⁵⁴ T. KATO, ²⁰⁵
 E. KATSAVOUNIDIS, ³⁵ W. KATZMAN, ⁶⁵ R. KAUSHIK ¹⁰⁵ K. KAWABE, ² R. KAWAMOTO, ²⁰⁶ D. KEITEL ¹⁰⁰
 L. J. KEMPERMAN ¹¹⁷ J. KENNINGTON ⁷ F. A. KERKOW, ¹⁸ R. KESHARWANI ⁸¹ J. S. KEY ²⁴³ R. KHADELA, ^{8, 9}
 S. KHADKA, ⁹¹ S. S. KHADKIKAR, ⁷ F. Y. KHALILI ¹¹⁰ F. KHAN ^{8, 9} T. KHANAM, ¹⁶⁵ M. KHURSHEED, ¹⁰⁵
 N. M. KHUSID, ^{192, 193} W. KIENDREBEOGO ^{115, 244} N. KIJBUNCHOO ¹¹⁷ C. KIM, ²⁴⁵ J. C. KIM, ²⁴⁶ K. KIM ²⁴⁷
 M. H. KIM ²³⁹ S. KIM ²⁴⁸ Y.-M. KIM ²⁴⁷ C. KIMBALL ⁹⁸ K. KIMES, ⁵⁵ M. KINNEAR, ³³ J. S. KISSEL ²
 S. KLIMENKO, ⁴⁶ A. M. KNEE ¹¹⁶ E. J. KNOX, ⁷⁹ N. KNUST ^{8, 9} K. KOBAYASHI, ²⁰⁵ S. M. KOEHLBECK ⁹¹
 G. KOEKOEK, ^{37, 36} K. KOHRI ^{249, 250} K. KOKEYAMA ^{33, 251} S. KOLEY ^{44, 168} P. KOLITSIDOU ¹²⁰
 A. E. KOLONIARI ²⁵² K. KOMORI ⁴² A. K. H. KONG ¹⁴⁴ A. KONTOS ²⁵³ L. M. KOPONEN, ¹²⁰ M. KOROBKO ⁹⁹
 X. KOU, ¹⁸ A. KOUSHIK ²³ N. KOVATSOS ⁶⁹ M. KOVALAM, ⁷⁴ T. KOYAMA, ¹⁵⁴ D. B. KOZAK, ¹¹ S. L. KRANZHOFF, ^{36, 37}
 V. KRINGEL, ^{8, 9} N. V. KRISHNENDU ¹²⁰ S. KROKER, ²⁵⁴ A. KRÓLAK ^{255, 188} K. KRUSKA, ^{8, 9} J. KUBISZ ²⁵⁶
 G. KUEHN, ^{8, 9} S. KULKARNI ²¹⁷ A. KULUR RAMAMOHAN ³⁴ ACHAL KUMAR, ⁴⁶ ANIL KUMAR, ²³⁴ PRAVEEN KUMAR ⁵⁴
 PRAYUSH KUMAR ²⁴ RAHUL KUMAR, ² RAKESH KUMAR, ⁹⁵ J. KUME ^{257, 258, 42} K. KUNS ³⁵ N. KUNTIMADDI, ³³
 S. KUROYANAGI ^{209, 259} S. KUWAHARA ⁴² K. KWAK ²⁴⁰ K. KWAN, ³⁴ S. KWON ⁴² G. LACAILLE, ⁸⁸
 D. LAGHI ^{190, 102} A. H. LAITY, ¹⁶⁶ E. LALANDE, ²⁶⁰ M. LALLEMAN ²³ P. C. LALREMRUATI, ²⁶¹ M. LANDRY, ²
 B. B. LANE, ³⁵ R. N. LANG ³⁵ J. LANGE, ¹⁵⁰ R. LANGGIN ²¹⁴ B. LANTZ ⁹¹ I. LA ROSA ¹⁰⁰ J. LARSEN, ²⁰¹
 A. LARTAUD-VOLLARD ⁴¹ P. D. LASKY ⁶ J. LAWRENCE ¹⁶⁷ M. LAXEN ⁶⁵ C. LAZARTE ¹⁴⁰ A. LAZZARINI ¹¹
 C. LAZZARO, ^{159, 158} P. LEACI ^{39, 38} L. LEALI, ¹⁸ Y. K. LECOEUQUE ¹¹⁶ H. M. LEE ²⁶² H. W. LEE ²⁶³ J. LEE, ⁸⁰
 K. LEE ²³⁹ R.-K. LEE ¹⁴⁴ R. LEE, ³⁵ SUNGHO LEE ²⁴⁷ SUNJAE LEE, ²³⁹ Y. LEE, ¹⁴³ I. N. LEGRED, ¹¹ J. LEHMANN, ^{8, 9}
 L. LEHNER, ¹⁸⁴ M. LE JEAN ^{178, 118} A. LEMAÎTRE ³¹ M. LENTI ^{63, 179} M. LEONARDI ^{76, 77, 265} M. LEQUIME, ⁴⁰
 N. LEROY ⁴¹ M. LESOVSKY, ¹¹ N. LETENDRE, ³¹ M. LETHUILLIER ⁵⁷ Y. LEVIN, ⁶ K. LEYDE, ⁷⁵ A. K. Y. LI, ¹¹
 K. L. LI ²⁶⁶ T. G. F. LI, ¹¹¹ X. LI ¹⁵¹ Y. LI, ⁹⁸ Z. LI, ⁸⁸ A. LIHOS, ¹²⁴ E. T. LIN ¹⁴⁴ F. LIN, ¹⁴³ L. C.-C. LIN ²⁶⁶
 Y.-C. LIN ¹⁴⁴ C. LINDSAY, ²⁰² S. D. LINKER, ¹⁸² A. LIU ²²⁰ G. C. LIU ²²⁹ JIAN LIU ⁷⁴ F. LLAMAS VILLARREAL, ¹⁶⁷
 J. LLOBERA-QUEROL ¹⁰⁰ R. K. L. LO ¹⁴² J.-P. LOCQUET, ¹¹¹ S. C. G. LOGGINS, ²⁶⁷ M. R. LOIZOU, ¹³⁵ L. T. LONDON, ⁶⁹
 A. LONGO ^{62, 63} D. LOPEZ ¹⁶⁸ M. LOPEZ PORTILLA, ⁷³ A. LORENZO-MEDINA ⁵⁴ V. LORIETTE, ⁴¹ M. LORMAND, ⁶⁵
 G. LOSURDO ^{268, 82} E. LOTTI, ¹³⁵ T. P. LOTT IV ⁵⁸ J. D. LOUGH ^{8, 9} H. A. LOUGHLIN, ³⁵ C. O. LOUSTO ¹¹²
 N. LOW, ¹²⁵ N. LU ³⁴ L. LUCCHESI ⁸² H. LÜCK, ^{9, 8, 9} D. LUMACA ²² A. P. LUNDGREN ^{269, 270} A. W. LUSSIER ²⁶⁰
 R. MACAS ⁷⁵ M. MACINNIS, ³⁵ D. M. MACLEOD ³³ I. A. O. MACMILLAN ¹¹ A. MACQUET ⁴¹ K. MAEDA, ¹⁵⁴
 S. MAENAUT ¹¹¹ S. S. MAGARE, ⁸¹ R. M. MAGEE ¹¹ E. MAGGIO ¹ R. MAGGIORE, ^{37, 109} M. MAGNOZZI ^{29, 30}
 P. MAHAPATRA, ^{33, 59} M. MAHESH, ⁹⁹ M. MAINI, ¹⁶⁶ S. MAJHI, ⁸¹ E. MAJORANA, ^{39, 38} C. N. MAKAREM, ¹¹ N. MALAGON, ¹¹²
 D. MALAKAR ¹⁰⁷ J. A. MALAQUIAS-REIS, ¹⁹ U. MALI ¹⁹¹ S. MALIAKAL, ¹¹ A. MALIK, ¹⁰⁵ L. MALICK ^{171, 191}
 A.-K. MALZ ⁶⁰ N. MAN, ¹¹⁵ M. MANCARELLA ¹⁰¹ V. MANDIC ¹⁸ V. MANGANO ^{173, 158} N. MANNING, ¹¹²
 B. MANNIX, ⁷⁹ G. L. MANSSELL ⁸⁰ M. MANSKE ¹⁰ M. MANTOVANI ⁶⁴ M. MAPELLI ^{93, 94, 271} C. MARINELLI ¹⁰³
 F. MARION ³¹ A. S. MARKOSYAN, ⁹¹ A. MARKOWITZ, ¹¹ E. MAROS, ¹¹ S. MARSAT ¹⁰² F. MARTELLI ^{62, 63}
 I. W. MARTIN ⁸⁸ R. M. MARTIN ¹⁹⁴ B. B. MARTINEZ, ¹³³ D. A. MARTINEZ, ⁵⁵ M. MARTINEZ, ^{43, 272} V. MARTINEZ ¹³⁰
 A. MARTINI, ^{76, 77} J. C. MARTINS ¹⁹ D. V. MARTYNOV, ¹²⁰ E. J. MARX, ³⁵ L. MASSARO, ^{36, 37} A. MASSEROT, ³¹

- M. MASSO-REID ⁸⁸, S. MASTROGIOVANNI ³⁸, T. MATCOVICH ⁵¹, M. MATIUSHECHKINA ^{8,9}, L. MAURIN, ²¹⁰
 N. MAVALVALA ³⁵, N. MAXWELL, ² G. MCCARROL, ⁶⁵ R. MCCARTHY, ² D. E. MCCLELLAND ³⁴, S. MCCORMICK, ⁶⁵
 L. MCCULLER ¹¹, S. MCEACHIN, ¹²⁴ C. MCELHENNY, ¹²⁴ G. I. MCGHEE ⁸⁸, J. MCGINN, ⁸⁸ K. B. M. MCGOWAN, ¹⁴⁶
 J. MCIVER ¹¹⁶, A. MCLEOD ⁷⁴, I. MCMAHON ¹⁹⁰, T. MCRAE, ³⁴ R. MCTEAGUE ⁸⁸, D. MEACHER ¹⁰,
 B. N. MEAGHER, ⁸⁰ R. MECHUM, ¹¹² Q. MEIJER, ⁷³ A. MELATOS, ¹²⁵ C. S. MENONI ¹³⁹, F. MERA, ² R. A. MERCER ¹⁰,
 L. MERENI, ¹⁷⁸ K. MERFELD, ¹⁶⁵ E. L. MERILH, ⁶⁵ J. R. MÉROU ¹⁰⁰, J. D. MERRITT, ⁷⁹ M. MERZOUGUI, ¹¹⁵ C. MESSICK ¹⁰,
 B. MESTICHELLI, ⁴⁴ M. MEYER-CONDE ²⁷³, F. MEYLAHN ^{8,9}, A. MHASKE, ⁸¹ A. MIANI ^{76,77}, H. MIAO, ²⁷⁴
 C. MICHEL ¹⁷⁸, Y. MICHIMURA ⁴², H. MIDDLETON ¹²⁰, D. P. MIHAYLOV ¹⁰⁶, S. J. MILLER ¹¹, M. MILLHOUSE ⁵⁸,
 E. MILOTTI ^{186,48}, V. MILOTTI ⁹³, Y. MINENKOV, ²² E. M. MINIHAN, ⁶⁷ LL. M. MIR ⁴³, L. MIRASOLA ^{158,159},
 M. MIRAVET-TENÉS ¹⁴⁰, C.-A. MIRITESCU ⁴³, A. MISHRA, ²⁴ C. MISHRA ¹⁰⁸, T. MISHRA ⁴⁶, A. L. MITCHELL, ^{37,109}
 J. G. MITCHELL, ⁶⁷ S. MITRA ⁸¹, V. P. MITROFANOV ¹¹⁰, K. MITSUHASHI, ²⁵ R. MITTLEMAN, ³⁵ O. MIYAKAWA ⁵⁰,
 S. MIYOKI ⁵⁰, A. MIYOKO, ⁶⁷ G. MO ³⁵, L. MOBILIA ^{62,63}, S. R. P. MOHAPATRA, ¹¹ S. R. MOHITE ⁷,
 M. MOLINA-RUIZ ²⁰⁸, M. MONDIN, ¹⁸² M. MONTANI, ^{62,63} C. J. MOORE, ²²⁵ D. MORARU, ² A. MORE ⁸¹, S. MORE ⁸¹,
 C. MORENO ¹³⁷, E. A. MORENO ³⁵, G. MORENO, ² A. MORESO SERRA, ⁸⁴ S. MORISAKI ^{42,205}, Y. MORIWAKI ¹⁵⁴,
 G. MORRAS ²⁰⁹, A. MOSCATELLO ⁹³, M. MOULD ³⁵, B. MOURS ⁶⁶, C. M. MOW-LOWRY ^{37,109},
 L. MUCCILLO ^{179,63}, F. MUCIACCIA ^{39,38}, D. MUKHERJEE ¹²⁰, SAMANWAYA MUKHERJEE, ²⁴ SOMA MUKHERJEE, ¹⁶⁷
 SUBROTO MUKHERJEE, ⁹⁵ SUVODIP MUKHERJEE ¹³, N. MUKUND ³⁵, A. MULLAVEY, ⁶⁵ H. MULLOCK, ¹¹⁶ J. MUNDI, ²²¹
 C. L. MUNGIOLI, ⁷⁴ M. MURAKOSHI, ²³¹ P. G. MURRAY ⁸⁸, D. NABARI ^{76,77}, S. L. NADJI, ^{8,9} A. NAGAR, ^{28,275}
 N. NAGARAJAN ⁸⁸, K. NAKAGAKI, ⁵⁰ K. NAKAMURA ²⁵, H. NAKANO ²⁷⁶, M. NAKANO, ¹¹
 D. NANADOUNGAR-LACROZE ⁴³, D. NANDI, ¹² V. NAPOLANO, ⁶⁴ P. NARAYAN ²¹⁷, I. NARDECCHIA ²², T. NARIKAWA, ²⁰⁵
 H. NAROLA, ⁷³ L. NATICCHIONI ³⁸, R. K. NAYAK ²⁶¹, L. NEGRI, ⁷³ A. NELA, ⁸⁸ C. NELLE, ⁷⁹ A. NELSON ¹³³,
 T. J. N. NELSON, ⁶⁵ M. NERY, ^{8,9} A. NEUNZERT ², S. NG, ⁵⁵ L. NGUYEN QUYNH ²⁷⁷, S. A. NICHOLS, ¹²
 A. B. NIELSEN ²⁷⁸, Y. NISHINO, ^{25,42} A. NISHIZAWA ²⁷⁹, S. NISSANKE, ^{280,37} W. NIU ⁷, F. NOCERA, ⁶⁴ J. NOLLER, ²⁸¹
 M. NORMAN, ³³ C. NORTH, ³³ J. NOVAK ^{118,235,282}, R. NOWICKI ¹⁴⁶, J. F. NUÑO SILES ²⁰⁹, L. K. NUTTALL ⁷⁵,
 K. OBAYASHI, ²³¹ J. OBERLING ², J. O'DELL, ²³⁰ E. OELKER ³⁵, M. OERTEL ^{235,118,283,282}, G. OGANESYAN, ^{44,45}
 T. O'HANLON, ⁶⁵ M. OHASHI ⁵⁰, F. OHME ^{8,9}, R. OLIVERI ^{118,283,282}, R. OMER, ¹⁸ B. O'NEAL, ¹²⁴ M. ONISHI, ¹⁵⁴
 K. OOHARA ²⁸⁴, B. O'REILLY ⁶⁵, M. ORSELLI ^{51,78}, R. O'SHAUGHNESSY ¹¹², S. O'SHEA, ⁸⁸ S. OSHINO ⁵⁰,
 C. OSTHELDER, ¹¹ I. OTA ¹², D. J. OTTAWAY ¹¹⁷, A. OUZRIAT, ⁵⁷ H. OVERMIER, ⁶⁵ B. J. OWEN ²⁸⁵, R. OZAKI, ²³¹
 A. E. PACE ⁷, R. PAGANO ¹², M. A. PAGE ²⁵, A. PAI ¹⁹⁶, L. PAIELLA, ⁴⁴ A. PAL, ²⁸⁶ S. PAL ²⁶¹,
 M. A. PALAIA ^{82,83}, M. PÁLFI, ²⁰⁴ P. P. PALMA, ^{39,21,22} C. PALOMBA ³⁸, P. PALUD ²⁰, H. PAN, ¹⁴⁴ J. PAN, ⁷⁴
 K. C. PAN ¹⁴⁴, P. K. PANDA, ²³⁴ SHIKSHA PANDEY, ⁷ SWADHA PANDEY, ³⁵ P. T. H. PANG, ^{37,73} F. PANNARALE ^{39,38},
 K. A. PANNONE, ⁵⁵ B. C. PANT, ¹⁰⁵ F. H. PANTHER, ⁷⁴ M. PANZERI, ^{62,63} F. PAOLETTI ⁸², A. PAOLONE ^{38,287},
 A. PAPADOPOULOS ⁸⁸, E. E. PAPALEXAKIS, ²¹² L. PAPALINI ^{82,83}, G. PAPIGKIOTIS ²⁵², A. PAQUIS, ⁴¹ A. PARISI ^{78,51},
 B.-J. PARK, ²⁴⁷ J. PARK ²⁸⁸, W. PARKER ⁶⁵, G. PASCALE, ^{8,9} D. PASCUCCI ⁹⁶, A. PASQUALETTI ⁶⁴,
 R. PASSAQUIETI ^{83,82}, L. PASSENGER, ⁶ D. PASSUELLO, ⁸² O. PATANE ², A. V. PATEL ¹⁴³, D. PATHAK, ⁸¹ A. PATRA, ³³
 B. PATRICELLI ^{83,82}, B. G. PATTERSON, ³³ K. PAUL ¹⁰⁸, S. PAUL ⁷⁹, E. PAYNE ¹¹, T. PEARCE, ³³ M. PEDRAZA, ¹¹
 A. PELE ¹¹, F. E. PEÑA ARELLANO ²⁸⁹, X. PENG, ¹²⁰ Y. PENG, ⁵⁸ S. PENN ²⁹⁰, M. D. PENULIAR, ⁵⁵ A. PEREGO ^{76,77},
 Z. PEREIRA, ¹³⁵ C. PÉRIGOIS ^{291,94,93}, G. PERNA ⁹³, A. PERRECA ^{76,77,44}, J. PERRET ²⁰, S. PERRIÈS ⁵⁷,
 J. W. PERRY, ^{37,109} D. PESIOS, ²⁵² S. PETERS, ¹⁶⁸ S. PETRACCA, ²⁰⁷ C. PETRILLO, ⁷⁸ H. P. PFEIFFER ¹, H. PHAM, ⁶⁵
 K. A. PHAM ¹⁸, K. S. PHUKON ¹²⁰, H. PHURAILATPAM, ²²⁰ M. PIARULLI, ¹⁰² L. PICCARI ^{39,38}, O. J. PICCINI ³⁴,
 M. PICHOT ¹¹⁵, M. PIENDIBENE ^{83,82}, F. PIERGIOVANNI ^{62,63}, L. PIERINI ³⁸, G. PIERRA ³⁸, V. PIERRO ^{292,134},
 M. PIETRZAK, ⁹⁷ M. PILLAS ¹⁶⁸, F. PILO ⁸², L. PINARD ¹⁷⁸, I. M. PINTO ^{292,134,293,32}, M. PINTO ⁶⁴,
 B. J. PIOTRZKOWSKI ¹⁰, M. PIRELLO, ² M. D. PITKIN ^{225,88}, A. PLACIDI ⁵¹, E. PLACIDI ^{39,38}, M. L. PLANAS ¹⁰⁰,
 W. PLASTINO ^{213,22} C. PLUNKETT ³⁵, R. POGGIANI ^{83,82}, E. POLINI, ³⁵ J. POMPER, ^{82,83} L. POMPILI ¹, J. POON, ²²⁰
 E. PORCELLI, ³⁷ E. K. PORTER, ²⁰ C. POSNANSKY ⁷, R. POULTON ⁶⁴, J. POWELL ¹⁵⁷, G. S. PRABHU, ⁸¹
 M. PRACCHIA ¹⁶⁸, B. K. PRADHAN ⁸¹, T. PRADIER ⁶⁶, A. K. PRAJAPATI, ⁹⁵ K. PRASAI ²⁹⁴, R. PRASANNA, ²³⁴
 P. PRASIA, ⁸¹ G. PRATTEN ¹²⁰, G. PRINCIPE ^{186,48}, G. A. PRODI ^{76,77}, P. PROSPERI, ⁸² P. PROSPERITO, ^{21,22}
 A. C. PROVIDENCE, ⁶⁷ A. PUECHER ¹, J. PULLIN ¹², P. PUPPO, ³⁸ M. PÜRRETT ¹⁶⁶, H. QI ¹⁶, J. QIN ³⁴,
 G. QUÉMÉNER ^{176,118}, V. QUETSCHKE, ¹⁶⁷ P. J. QUINONEZ, ⁶⁷ N. QUTOB, ⁵⁸ R. RADING, ²³² I. RAINHO, ¹⁴⁰ S. RAJA, ¹⁰⁵
 C. RAJAN, ¹⁰⁵ B. RAJBHANDARI ¹¹², K. E. RAMIREZ ⁶⁵, F. A. RAMIS VIDAL ¹⁰⁰, M. RAMOS AREVALO ¹⁶⁷,
 A. RAMOS-BUADES ^{100,37}, S. RANJAN ⁵⁸, K. RANSOM, ⁶⁵ P. RAPAGNANI ^{39,38}, B. RATTO, ⁶⁷ A. RAVICHANDRAN, ¹³⁵
 A. RAY ⁹⁸, V. RAYMOND ³³, M. RAZZANO ^{83,82}, J. READ, ⁵⁵ T. REGIMBAU, ³¹ S. REID, ⁵⁶ C. REISSEL, ³⁵
 D. H. REITZE ¹¹, A. I. RENZINI ^{11,128}, B. REVENU ^{295,41}, A. REVILLA PEÑA, ⁸⁴ R. REYES, ¹⁸² L. RICCA ¹⁵,
 F. RICCI ^{39,38}, M. RICCI ^{38,39}, A. RICCIARDONE ^{83,82}, J. RICE, ⁸⁰ J. W. RICHARDSON ²¹², M. L. RICHARDSON, ¹¹⁷
 A. RIJAL, ⁶⁷ K. RILES ⁹², H. K. RILEY, ³³ S. RINALDI ²⁷¹, J. RITTMAYER, ⁹⁹ C. ROBERTSON, ²³⁰ F. ROBINET, ⁴¹

- M. ROBINSON,² A. ROCCHI ,²² L. ROLLAND ,³¹ J. G. ROLLINS ,¹¹ A. E. ROMANO ,²⁹⁶ R. ROMANO ,^{3,4}
A. ROMERO ,³¹ I. M. ROMERO-SHAW,²²⁵ J. H. ROMIE,⁶⁵ S. RONCHINI ,⁷ T. J. ROOCKE ,¹¹⁷ L. ROSA,^{4,32}
T. J. ROSAUER,²¹² C. A. ROSE,⁵⁸ D. ROSIŃSKA ,¹²⁶ M. P. ROSS ,⁵³ M. ROSSELLO-SASTRE ,¹⁰⁰ S. ROWAN ,⁸⁸
S. K. ROY ,^{192,193} S. ROY ,¹⁵ D. ROZZA ,^{128,129} P. RUGGI,⁶⁴ N. RUHAMA,²⁴⁰ E. RUIZ MORALES ,^{297,209}
K. RUIZ-ROCHA,¹⁴⁶ S. SACHDEV ,⁵⁸ T. SADECKI,² P. SAFFARIEH ,^{37,109} S. SAFI-HARB ,¹⁷¹ M. R. SAH ,¹³
S. SAHA ,¹⁴⁴ T. SAINRAT ,⁶⁶ S. SAJITH MENON ,^{216,39,38} K. SAKAI,²⁹⁸ Y. SAKAI ,²⁷³ M. SAKELLARIADOU ,⁶⁹
S. SAKON ,⁷ O. S. SALAFIA ,^{161,129,128} F. SALCES-CARCOBA ,¹¹ L. SALCONI,⁶⁴ M. SALEEM ,¹⁵⁰ F. SALEMI ,^{39,38}
M. SALLÉ ,³⁷ S. U. SALUNKHE,⁸¹ S. SALVADOR ,^{176,175} A. SALVARESE,¹⁵⁰ A. SAMAJDAR ,^{73,37} A. SANCHEZ,²
E. J. SANCHEZ,¹¹ L. E. SANCHEZ,¹¹ N. SANCHIS-GUAL ,¹⁴⁰ J. R. SANDERS,¹⁸³ E. M. SÄNGER ,¹
F. SANTOLIUQUIDO ,^{44,45} F. SARANDREA,²⁸ T. R. SARAVANAN,⁸¹ N. SARIN,⁶ P. SARKAR,^{8,9} A. SASLI ,²⁵² P. SASSI ,^{51,78}
B. SASSOLAS ,¹⁷⁸ B. S. SATHYAPRAKASH ,^{7,33} R. SATO,²²⁸ S. SATO,¹⁵⁴ YUKINO SATO,¹⁵⁴ YU SATO,¹⁵⁴ O. SAUTER ,⁴⁶
R. L. SAVAGE ,² T. SAWADA ,⁵⁰ H. L. SAWANT,⁸¹ S. SAYAH,¹⁷⁸ V. SCACCO,^{21,22} D. SCHAETZL,¹¹ M. SCHEEL,¹⁵¹
A. SCHIEBELBEIN,¹⁹¹ M. G. SCHIWORSKI ,⁸⁰ P. SCHMIDT ,¹²⁰ S. SCHMIDT ,⁷³ R. SCHNABEL ,⁹⁹ M. SCHNEEWIND,^{8,9}
R. M. S. SCHOFIELD,⁷⁹ K. SCHOUTEDEN ,¹¹¹ B. W. SCHULTE,^{8,9} B. F. SCHUTZ,^{33,8,9} E. SCHWARTZ ,²⁹⁹ M. SCIALPI ,³⁰⁰
J. SCOTT ,⁸⁸ S. M. SCOTT ,³⁴ R. M. SEDAS ,⁶⁵ T. C. SEETHARAMU,⁸⁸ M. SEGLAR-ARROYO ,⁴³ Y. SEKIGUCHI ,³⁰¹
D. SELLERS,⁶⁵ N. SEMBO,²⁰⁶ A. S. SENGUPTA ,³⁰² E. G. SEO ,⁸⁸ J. W. SEO ,¹¹¹ V. SEQUINO,^{32,4} M. SERRA ,³⁸
A. SEVRIN,¹⁸⁹ T. SHAFFER,² U. S. SHAH ,⁵⁸ M. A. SHAIKH ,²⁶² L. SHAO ,³⁰³ A. K. SHARMA ,¹⁰⁰ PREETI SHARMA,¹²
PRIANKA SHARMA,¹⁰⁵ RITWIK SHARMA,¹⁸ S. SHARMA CHAUDHARY,¹⁰⁷ P. SHAWHAN ,¹²⁷ N. S. SHCHEBLANOV ,^{304,264}
E. SHERIDAN,¹⁴⁶ Z.-H. SHI,¹⁴⁴ M. SHIKAUCHI,⁴² R. SHIMOMURA,³⁰⁵ H. SHINKAI ,³⁰⁵ S. SHIRKE,⁸¹ D. H. SHOEMAKER ,³⁵
D. M. SHOEMAKER ,¹⁵⁰ R. W. SHORT,² S. SHYAMSUNDAR,¹⁰⁵ A. SIDER,¹⁶⁰ H. SIEGEL ,^{192,193} N. SIEMONSEN,³⁰⁶
D. SIGG ,² L. SILENZI ,^{36,37} L. SILVESTRI ,^{39,172} M. SIMMONDS,¹¹⁷ L. P. SINGER ,³⁰⁷ AMITESH SINGH,²¹⁷
ANIKA SINGH,¹¹ D. SINGH ,²⁰⁸ M. K. SINGH,²⁴ N. SINGH ,¹⁰⁰ S. SINGH,^{218,61} A. M. SINTES ,¹⁰⁰ V. SIPALA,^{173,158}
V. SKLIRIS ,³³ B. J. J. SLAGMOLEN ,³⁴ D. A. SLATER,²⁰¹ T. J. SLAVEN-BLAIR,⁷⁴ J. SMETANA,¹²⁰ J. R. SMITH ,⁵⁵
L. SMITH ,^{88,186,48} R. J. E. SMITH ,⁶ W. J. SMITH ,¹⁴⁶ S. SOARES DE ALBUQUERQUE FILHO,⁶² M. SOARES-SANTOS,¹⁹⁰
K. SOMIYA ,²¹⁸ I. SONG ,¹⁴⁴ S. SONI ,³⁵ V. SORDINI ,⁵⁷ F. SORRENTINO,²⁹ H. SOTANI ,³⁰⁸ F. SPADA ,⁸²
V. SPAGNUOLO ,³⁷ A. P. SPENCER ,⁸⁸ P. SPINICELLI ,⁶⁴ A. K. SRIVASTAVA,⁹⁵ F. STACHURSKI ,⁸⁸ C. J. STARK,¹²⁴
D. A. STEER ,³⁰⁹ N. STEINLE ,¹⁷¹ J. STEINLECHNER,^{36,37} S. STEINLECHNER ,^{36,37} N. STERGIOLAS ,²⁵² P. STEVENS,⁴¹
S. P. STEVENSON,¹⁵⁷ M. STPIERRE,¹⁶⁶ M. D. STRONG,¹² A. STRUNK,² A. L. STUVER,^{104,*} M. SUCHENEK,⁹⁷
S. SUDHAGAR ,⁹⁷ Y. SUDO,²³¹ N. SUELTMANN,⁹⁹ L. SULEIMAN ,⁵⁵ K. D. SULLIVAN,¹² J. SUN ,²⁴² L. SUN ,³⁴
S. SUNIL,⁹⁵ J. SURESH ,¹¹⁵ B. J. SUTTON,⁶⁹ P. J. SUTTON ,³³ K. SUZUKI,²¹⁸ M. SUZUKI,²⁰⁵ B. L. SWINKELS ,³⁷
A. SYX ,¹¹⁸ M. J. SZCZEPAŃCZYK ,³¹⁰ P. SZEWCZYK ,¹²⁶ M. TACCA ,³⁷ H. TAGOSHI ,²⁰⁵ K. TAKADA,²⁰⁵
H. TAKAHASHI ,²⁷³ R. TAKAHASHI ,²⁵ A. TAKAMORI ,⁴² S. TAKANO ,³¹¹ H. TAKEDA ,^{312,313} K. TAKESHITA,²¹⁸
I. TAKIMOTO SCHMIEGELOW,^{44,45} M. TAKOU-AYAHO,⁸⁰ C. TALBOT,¹³¹ M. TAMAKI,²⁰⁵ N. TAMANINI ,¹⁰² D. TANABE,¹⁴³
K. TANAKA,⁵⁰ S. J. TANAKA ,²³¹ S. TANIOKA ,³³ D. B. TANNER,⁴⁶ W. TANNER,^{8,9} L. TAO ,²¹² R. D. TAPIA,⁷
E. N. TAPIA SAN MARTÍN ,³⁷ C. TARANTO,^{21,22} A. TARUYA ,³¹⁴ J. D. TASSON ,¹⁵⁵ J. G. TAU ,¹¹² D. TELLEZ,⁵⁵
R. TENORIO ,¹⁰⁰ H. THEMANN,¹⁸² A. THEODOROPOULOS ,¹⁴⁰ M. P. THIRUGNANASAMBANDAM,⁸¹ L. M. THOMAS ,¹¹
M. THOMAS,⁶⁵ P. THOMAS,² J. E. THOMPSON ,²¹¹ S. R. THONDAPU,¹⁰⁵ K. A. THORNE,⁶⁵ E. THRANE ,⁶
J. TISSINO ,^{44,45} A. TIWARI,⁸¹ PAWAN TIWARI,⁴⁴ PRAVEER TIWARI,¹⁹⁶ S. TIWARI ,¹⁹⁰ V. TIWARI ,¹²⁰ M. R. TODD,⁸⁰
M. TOFFANO,⁹³ A. M. TOIVONEN ,¹⁸ K. TOLAND ,⁸⁸ A. E. TOLLEY ,⁷⁵ T. TOMARU ,²⁵ V. TOMMASINI,¹¹
T. TOMURA ,⁵⁰ H. TONG ,⁶ C. TONG-YU,¹⁴³ A. TORRES-FORNÉ ,^{140,141} C. I. TORRIE,¹¹ I. TOSTA E MELO ,³¹⁵
E. TOURNEFIER ,³¹ M. TRAD NERY,¹¹⁵ K. TRAN,¹²⁴ A. TRAPANANTI ,^{52,51} R. TRAVAGLINI ,¹⁷⁰ F. TRAVASSO ,^{52,51}
G. TRAYLOR,⁶⁵ M. TREVOR,¹²⁷ M. C. TRINGALI ,⁶⁴ A. TRIPATHEE ,⁹² G. TROIAN ,^{186,48} A. TROVATO ,^{186,48}
L. TROZZO,⁴ R. J. TRUDEAU,¹¹ T. TSANG ,³³ S. TSUCHIDA ,³¹⁶ L. TSUKADA ,²¹⁴ K. TURBANG ,^{189,23}
M. TURCONI ,¹¹⁵ C. TURSKI,⁹⁶ H. UBACH ,^{84,85} N. UCHIKATA ,²⁰⁵ T. UCHIYAMA ,⁵⁰ R. P. UDALL ,¹¹
T. UEHARA ,³¹⁷ K. UENO ,⁴² V. UNDHEIM ,²⁷⁸ L. E. URONEN,²²⁰ T. USHIBA ,⁵⁰ M. VACATELLO ,^{82,83}
H. VAHLBRUCH ,^{8,9} N. VAIDYA ,¹¹ G. VAJENTE ,¹¹ A. VAJPEYI,⁶ J. VALENCIA ,¹⁰⁰ M. VALENTINI ,^{109,37}
S. A. VALLEJO-PEÑA ,²⁹⁶ S. VALLERO,²⁸ V. VALSAN ,¹⁰ M. VAN DAEL ,^{37,318} E. VAN DEN BOSSCHE ,¹⁸⁹
J. F. J. VAN DEN BRAND ,^{36,109,37} C. VAN DEN BROECK,^{73,37} M. VAN DER SLUYS ,^{37,73} A. VAN DE WALLE,⁴¹
J. VAN DONGEN ,^{37,109} K. VANDRA,¹⁰⁴ M. VANDYKE,¹²¹ H. VAN HAEVERMAET ,²³ J. V. VAN HEIJNINGEN ,^{37,109}
P. VAN HOVE ,⁶⁶ J. VANIER,²⁶⁰ M. VANKEUREN,¹⁰⁶ J. VANOSKY,² N. VAN REMORTEL ,²³ M. VARDARO,^{36,37}
A. F. VARGAS ,¹²⁵ V. VARMA ,¹³⁵ A. N. VAZQUEZ,⁹¹ A. VECCHIO ,¹²⁰ G. VEDOVATO,⁹⁴ J. VEITCH ,⁸⁸
P. J. VEITCH ,¹¹⁷ S. VENIKOUDIS,¹⁵ R. C. VENTEREA ,¹⁸ P. VERDIER ,⁵⁷ M. VERECKEN,¹⁵ D. VERKINDT ,³¹
B. VERMA,¹³⁵ Y. VERMA ,¹⁰⁵ S. M. VERMEULEN ,¹¹ F. VETRANO,⁶² A. VEUTRO ,^{38,39} A. VICERÉ ,^{62,63}
S. VIDYANT,⁸⁰ A. D. VIETS ,⁹⁰ A. VIJAYKUMAR ,¹⁹¹ A. VILKHA,¹¹² N. VILLANUEVA ESPINOSA,¹⁴⁰
V. VILLA-ORTEGA ,⁵⁴ E. T. VINCENT ,⁵⁸ J.-Y. VINET,¹¹⁵ S. VIRET,⁵⁷ S. VITALE ,³⁵ H. VOCCA ,^{78,51} D. VOIGT ,⁹⁹

E. R. G. VON REIS,² J. S. A. VON WRANGEL,^{8,9} W. E. VOSSIUS,²³² L. VUJEVA ¹⁴² S. P. VYATCHANIN ¹¹⁰ J. WACK,¹¹
 L. E. WADE,¹⁰⁶ M. WADE ¹⁰⁶ K. J. WAGNER ¹¹² L. WALLACE,¹¹ E. J. WANG,⁹¹ H. WANG ²¹⁸ J. Z. WANG,⁹²
 W. H. WANG,¹⁶⁷ Y. F. WANG ¹ G. WARATKAR ¹⁹⁶ J. WARNER,² M. WAS ³¹ T. WASHIMI ²⁵
 N. Y. WASHINGTON,¹¹ D. WATARAI,⁴² B. WEAVER,² S. A. WEBSTER,⁸⁸ N. L. WEICKHARDT ⁹⁹ M. WEINERT,^{8,9}
 A. J. WEINSTEIN ¹¹ R. WEISS,³⁵ L. WEN ⁷⁴ K. WETTE ³⁴ J. T. WHELAN ¹¹² B. F. WHITING ⁴⁶
 C. WHITTLE ¹¹ E. G. WICKENS,⁷⁵ D. WILKEN ^{8,9,9} A. T. WILKIN,²¹² B. M. WILLIAMS,¹²¹ D. WILLIAMS ⁸⁸
 M. J. WILLIAMS ⁷⁵ N. S. WILLIAMS ¹ J. L. WILLIS ¹¹ B. WILLKE ^{9,8,9} M. WILS ¹¹¹ L. WILSON,¹⁰⁶
 C. W. WINBORN,¹⁰⁷ J. WINTERFLOOD,⁷⁴ C. C. WIPF,¹¹ G. WOAN ⁸⁸ J. WOEHLENER,^{36,37} N. E. WOLFE,³⁵
 H. T. WONG ¹⁴³ H. W. Y. WONG,²²⁰ I. C. F. WONG ^{220,111} K. WONG,¹⁹¹ T. WOUTERS,^{73,37} J. L. WRIGHT,²
 M. WRIGHT ^{88,73} B. WU,⁸⁰ C. WU ¹⁴⁴ D. S. WU ^{8,9} H. WU ¹⁴⁴ K. WU,¹²¹ Q. WU,⁵³ Y. WU,⁹⁸ Z. WU ¹⁰²
 E. WUCHNER,⁵⁵ D. M. WYSOCKI ¹⁰ V. A. XU ²⁰⁸ Y. XU ¹⁰⁰ N. YADAV ²⁸ H. YAMAMOTO ¹¹
 K. YAMAMOTO ¹⁵⁴ T. S. YAMAMOTO ⁴² T. YAMAMOTO ⁵⁰ R. YAMAZAKI ²³¹ T. YAN,¹²⁰ K. Z. YANG ¹⁸
 Y. YANG ¹⁴⁸ Z. YARBROUGH ¹² J. YEBANA,¹⁰⁰ S.-W. YEH,¹⁴⁴ A. B. YELIKAR ¹⁴⁶ X. YIN,³⁵ J. YOKOYAMA ^{319,42}
 T. YOKOZAWA,⁵⁰ S. YUAN,⁷⁴ H. YUZURIHARA ⁵⁰ M. ZANOLIN,⁶⁷ M. ZEESHAN ¹¹² T. ZELENKOVA,⁶⁴ J.-P. ZENDRI,⁹⁴
 M. ZEOLI ¹⁵ M. ZERRAD,⁴⁰ M. ZEVIN ⁹⁸ L. ZHANG,¹¹ N. ZHANG,⁵⁸ R. ZHANG ¹⁵² T. ZHANG,¹²⁰ C. ZHAO ⁷⁴
 YUE ZHAO,¹⁶⁴ YUHANG ZHAO,²⁰ Z.-C. ZHAO ³²⁰ Y. ZHENG ¹⁰⁷ H. ZHONG ¹⁸ H. ZHOU,⁸⁰ H. O. ZHU,⁷⁴
 Z.-H. ZHU ^{320,321} A. B. ZIMMERMAN ¹⁵⁰ L. ZIMMERMANN,⁵⁷ Y. ZLOCHOWER,¹¹² M. E. ZUCKER ^{35,11} J. ZWEIZIG ¹¹

THE LIGO SCIENTIFIC COLLABORATION, THE VIRGO COLLABORATION, AND THE KAGRA COLLABORATION

¹Max Planck Institute for Gravitational Physics (Albert Einstein Institute), D-14476 Potsdam, Germany

²LIGO Hanford Observatory, Richland, WA 99352, USA

³Dipartimento di Farmacia, Università di Salerno, I-84084 Fisciano, Salerno, Italy

⁴INFN, Sezione di Napoli, I-80126 Napoli, Italy

⁵University of Warwick, Coventry CV4 7AL, United Kingdom

⁶OzGrav, School of Physics & Astronomy, Monash University, Clayton 3800, Victoria, Australia

⁷The Pennsylvania State University, University Park, PA 16802, USA

⁸Max Planck Institute for Gravitational Physics (Albert Einstein Institute), D-30167 Hannover, Germany

⁹Leibniz Universität Hannover, D-30167 Hannover, Germany

¹⁰University of Wisconsin-Milwaukee, Milwaukee, WI 53201, USA

¹¹LIGO Laboratory, California Institute of Technology, Pasadena, CA 91125, USA

¹²Louisiana State University, Baton Rouge, LA 70803, USA

¹³Tata Institute of Fundamental Research, Mumbai 400005, India

¹⁴Centre de Physique Théorique, Aix-Marseille Université, Campus de Luminy, 163 Av. de Luminy, 13009 Marseille, France

¹⁵Université catholique de Louvain, B-1348 Louvain-la-Neuve, Belgium

¹⁶Queen Mary University of London, London E1 4NS, United Kingdom

¹⁷University of California, Davis, Davis, CA 95616, USA

¹⁸University of Minnesota, Minneapolis, MN 55455, USA

¹⁹Instituto Nacional de Pesquisas Espaciais, 12227-010 São José dos Campos, São Paulo, Brazil

²⁰Université Paris Cité, CNRS, Astroparticule et Cosmologie, F-75013 Paris, France

²¹Università di Roma Tor Vergata, I-00133 Roma, Italy

²²INFN, Sezione di Roma Tor Vergata, I-00133 Roma, Italy

²³Universiteit Antwerpen, 2000 Antwerpen, Belgium

²⁴International Centre for Theoretical Sciences, Tata Institute of Fundamental Research, Bengaluru 560089, India

²⁵Gravitational Wave Science Project, National Astronomical Observatory of Japan, 2-21-1 Osawa, Mitaka City, Tokyo 181-8588, Japan

²⁶Advanced Technology Center, National Astronomical Observatory of Japan, 2-21-1 Osawa, Mitaka City, Tokyo 181-8588, Japan

²⁷Theoretisch-Physikalisches Institut, Friedrich-Schiller-Universität Jena, D-07743 Jena, Germany

²⁸INFN Sezione di Torino, I-10125 Torino, Italy

²⁹INFN, Sezione di Genova, I-16146 Genova, Italy

³⁰Dipartimento di Fisica, Università degli Studi di Genova, I-16146 Genova, Italy

³¹Univ. Savoie Mont Blanc, CNRS, Laboratoire d'Annecy de Physique des Particules - IN2P3, F-74000 Annecy, France

³²Università di Napoli "Federico II", I-80126 Napoli, Italy

³³Cardiff University, Cardiff CF24 3AA, United Kingdom

³⁴OzGrav, Australian National University, Canberra, Australian Capital Territory 0200, Australia

³⁵LIGO Laboratory, Massachusetts Institute of Technology, Cambridge, MA 02139, USA

³⁶Maastricht University, 6200 MD Maastricht, Netherlands

- ³⁷ *Nikhef, 1098 XG Amsterdam, Netherlands*
- ³⁸ *INFN, Sezione di Roma, I-00185 Roma, Italy*
- ³⁹ *Università di Roma “La Sapienza”, I-00185 Roma, Italy*
- ⁴⁰ *Aix Marseille Univ, CNRS, Centrale Med, Institut Fresnel, F-13013 Marseille, France*
- ⁴¹ *Université Paris-Saclay, CNRS/IN2P3, IJCLab, 91405 Orsay, France*
- ⁴² *University of Tokyo, Tokyo, 113-0033, Japan*
- ⁴³ *Institut de Física d’Altes Energies (IFAE), The Barcelona Institute of Science and Technology, Campus UAB, E-08193 Bellaterra (Barcelona), Spain*
- ⁴⁴ *Gran Sasso Science Institute (GSSI), I-67100 L’Aquila, Italy*
- ⁴⁵ *INFN, Laboratori Nazionali del Gran Sasso, I-67100 Assergi, Italy*
- ⁴⁶ *University of Florida, Gainesville, FL 32611, USA*
- ⁴⁷ *Dipartimento di Scienze Matematiche, Informatiche e Fisiche, Università di Udine, I-33100 Udine, Italy*
- ⁴⁸ *INFN, Sezione di Trieste, I-34127 Trieste, Italy*
- ⁴⁹ *Tecnologico de Monterrey, Escuela de Ingeniería y Ciencias, 64849 Monterrey, Nuevo León, Mexico*
- ⁵⁰ *Institute for Cosmic Ray Research, KAGRA Observatory, The University of Tokyo, 238 Higashi-Mozumi, Kamioka-cho, Hida City, Gifu 506-1205, Japan*
- ⁵¹ *INFN, Sezione di Perugia, I-06123 Perugia, Italy*
- ⁵² *Università di Camerino, I-62032 Camerino, Italy*
- ⁵³ *University of Washington, Seattle, WA 98195, USA*
- ⁵⁴ *IGFAE, Universidad de Santiago de Compostela, E-15782 Santiago de Compostela, Spain*
- ⁵⁵ *California State University Fullerton, Fullerton, CA 92831, USA*
- ⁵⁶ *SUPA, University of Strathclyde, Glasgow G1 1XQ, United Kingdom*
- ⁵⁷ *Université Claude Bernard Lyon 1, CNRS, IP2I Lyon / IN2P3, UMR 5822, F-69622 Villeurbanne, France*
- ⁵⁸ *Georgia Institute of Technology, Atlanta, GA 30332, USA*
- ⁵⁹ *Chennai Mathematical Institute, Chennai 603103, India*
- ⁶⁰ *Royal Holloway, University of London, London TW20 0EX, United Kingdom*
- ⁶¹ *Astronomical course, The Graduate University for Advanced Studies (SOKENDAI), 2-21-1 Osawa, Mitaka City, Tokyo 181-8588, Japan*
- ⁶² *Università degli Studi di Urbino “Carlo Bo”, I-61029 Urbino, Italy*
- ⁶³ *INFN, Sezione di Firenze, I-50019 Sesto Fiorentino, Firenze, Italy*
- ⁶⁴ *European Gravitational Observatory (EGO), I-56021 Cascina, Pisa, Italy*
- ⁶⁵ *LIGO Livingston Observatory, Livingston, LA 70754, USA*
- ⁶⁶ *Université de Strasbourg, CNRS, IPHC UMR 7178, F-67000 Strasbourg, France*
- ⁶⁷ *Embry-Riddle Aeronautical University, Prescott, AZ 86301, USA*
- ⁶⁸ *Dipartimento di Fisica “E.R. Caianiello”, Università di Salerno, I-84084 Fisciano, Salerno, Italy*
- ⁶⁹ *King’s College London, University of London, London WC2R 2LS, United Kingdom*
- ⁷⁰ *Korea Institute of Science and Technology Information, Daejeon 34141, Republic of Korea*
- ⁷¹ *International College, Osaka University, 1-1 Machikaneyama-cho, Toyonaka City, Osaka 560-0043, Japan*
- ⁷² *Accelerator Laboratory, High Energy Accelerator Research Organization (KEK), 1-1 Oho, Tsukuba City, Ibaraki 305-0801, Japan*
- ⁷³ *Institute for Gravitational and Subatomic Physics (GRASP), Utrecht University, 3584 CC Utrecht, Netherlands*
- ⁷⁴ *OzGrav, University of Western Australia, Crawley, Western Australia 6009, Australia*
- ⁷⁵ *University of Portsmouth, Portsmouth, PO1 3FX, United Kingdom*
- ⁷⁶ *Università di Trento, Dipartimento di Fisica, I-38123 Povo, Trento, Italy*
- ⁷⁷ *INFN, Trento Institute for Fundamental Physics and Applications, I-38123 Povo, Trento, Italy*
- ⁷⁸ *Università di Perugia, I-06123 Perugia, Italy*
- ⁷⁹ *University of Oregon, Eugene, OR 97403, USA*
- ⁸⁰ *Syracuse University, Syracuse, NY 13244, USA*
- ⁸¹ *Inter-University Centre for Astronomy and Astrophysics, Pune 411007, India*
- ⁸² *INFN, Sezione di Pisa, I-56127 Pisa, Italy*
- ⁸³ *Università di Pisa, I-56127 Pisa, Italy*
- ⁸⁴ *Institut de Ciències del Cosmos (ICCUB), Universitat de Barcelona (UB), c. Martí i Franquès, 1, 08028 Barcelona, Spain*
- ⁸⁵ *Departament de Física Quàntica i Astrofísica (FQA), Universitat de Barcelona (UB), c. Martí i Franquès, 1, 08028 Barcelona, Spain*
- ⁸⁶ *Institut d’Estudis Espacials de Catalunya, c. Gran Capità, 2-4, 08034 Barcelona, Spain*
- ⁸⁷ *Dipartimento di Medicina, Chirurgia e Odontoiatria “Scuola Medica Salernitana”, Università di Salerno, I-84081 Baronissi, Salerno, Italy*
- ⁸⁸ *IGR, University of Glasgow, Glasgow G12 8QQ, United Kingdom*
- ⁸⁹ *HUN-REN Wigner Research Centre for Physics, H-1121 Budapest, Hungary*
- ⁹⁰ *Concordia University Wisconsin, Mequon, WI 53097, USA*

- ⁹¹ *Stanford University, Stanford, CA 94305, USA*
- ⁹² *University of Michigan, Ann Arbor, MI 48109, USA*
- ⁹³ *Università di Padova, Dipartimento di Fisica e Astronomia, I-35131 Padova, Italy*
- ⁹⁴ *INFN, Sezione di Padova, I-35131 Padova, Italy*
- ⁹⁵ *Institute for Plasma Research, Bhat, Gandhinagar 382428, India*
- ⁹⁶ *Universiteit Gent, B-9000 Gent, Belgium*
- ⁹⁷ *Nicolaus Copernicus Astronomical Center, Polish Academy of Sciences, 00-716, Warsaw, Poland*
- ⁹⁸ *Northwestern University, Evanston, IL 60208, USA*
- ⁹⁹ *Universität Hamburg, D-22761 Hamburg, Germany*
- ¹⁰⁰ *IAC3-IEEC, Universitat de les Illes Balears, E-07122 Palma de Mallorca, Spain*
- ¹⁰¹ *Aix-Marseille Université, Université de Toulon, CNRS, CPT, Marseille, France*
- ¹⁰² *Laboratoire des 2 Infinis - Toulouse (L2IT-IN2P3), F-31062 Toulouse Cedex 9, France*
- ¹⁰³ *Università di Siena, Dipartimento di Scienze Fisiche, della Terra e dell'Ambiente, I-53100 Siena, Italy*
- ¹⁰⁴ *Villanova University, Villanova, PA 19085, USA*
- ¹⁰⁵ *RRCAT, Indore, Madhya Pradesh 452013, India*
- ¹⁰⁶ *Kenyon College, Gambier, OH 43022, USA*
- ¹⁰⁷ *Missouri University of Science and Technology, Rolla, MO 65409, USA*
- ¹⁰⁸ *Indian Institute of Technology Madras, Chennai 600036, India*
- ¹⁰⁹ *Department of Physics and Astronomy, Vrije Universiteit Amsterdam, 1081 HV Amsterdam, Netherlands*
- ¹¹⁰ *Lomonosov Moscow State University, Moscow 119991, Russia*
- ¹¹¹ *Katholieke Universiteit Leuven, Oude Markt 13, 3000 Leuven, Belgium*
- ¹¹² *Rochester Institute of Technology, Rochester, NY 14623, USA*
- ¹¹³ *Université libre de Bruxelles, 1050 Bruxelles, Belgium*
- ¹¹⁴ *Bar-Ilan University, Ramat Gan, 5290002, Israel*
- ¹¹⁵ *Université Côte d'Azur, Observatoire de la Côte d'Azur, CNRS, Artemis, F-06304 Nice, France*
- ¹¹⁶ *University of British Columbia, Vancouver, BC V6T 1Z4, Canada*
- ¹¹⁷ *OzGrav, University of Adelaide, Adelaide, South Australia 5005, Australia*
- ¹¹⁸ *Centre national de la recherche scientifique, 75016 Paris, France*
- ¹¹⁹ *Univ Rennes, CNRS, Institut FOTON - UMR 6082, F-35000 Rennes, France*
- ¹²⁰ *University of Birmingham, Birmingham B15 2TT, United Kingdom*
- ¹²¹ *Washington State University, Pullman, WA 99164, USA*
- ¹²² *Cornell University, Ithaca, NY 14850, USA*
- ¹²³ *Laboratoire Kastler Brossel, Sorbonne Université, CNRS, ENS-Université PSL, Collège de France, F-75005 Paris, France*
- ¹²⁴ *Christopher Newport University, Newport News, VA 23606, USA*
- ¹²⁵ *OzGrav, University of Melbourne, Parkville, Victoria 3010, Australia*
- ¹²⁶ *Astronomical Observatory Warsaw University, 00-478 Warsaw, Poland*
- ¹²⁷ *University of Maryland, College Park, MD 20742, USA*
- ¹²⁸ *Università degli Studi di Milano-Bicocca, I-20126 Milano, Italy*
- ¹²⁹ *INFN, Sezione di Milano-Bicocca, I-20126 Milano, Italy*
- ¹³⁰ *Université de Lyon, Université Claude Bernard Lyon 1, CNRS, Institut Lumière Matière, F-69622 Villeurbanne, France*
- ¹³¹ *University of Chicago, Chicago, IL 60637, USA*
- ¹³² *Williams College, Williamstown, MA 01267, USA*
- ¹³³ *University of Arizona, Tucson, AZ 85721, USA*
- ¹³⁴ *INFN, Sezione di Napoli, Gruppo Collegato di Salerno, I-80126 Napoli, Italy*
- ¹³⁵ *University of Massachusetts Dartmouth, North Dartmouth, MA 02747, USA*
- ¹³⁶ *Niels Bohr Institute, Copenhagen University, 2100 København, Denmark*
- ¹³⁷ *Universidad de Guadalajara, 44430 Guadalajara, Jalisco, Mexico*
- ¹³⁸ *Istituto di Astrofisica e Planetologia Spaziali di Roma, 00133 Roma, Italy*
- ¹³⁹ *Colorado State University, Fort Collins, CO 80523, USA*
- ¹⁴⁰ *Departamento de Astronomía y Astrofísica, Universitat de València, E-46100 Burjassot, València, Spain*
- ¹⁴¹ *Observatori Astronòmic, Universitat de València, E-46980 Paterna, València, Spain*
- ¹⁴² *Niels Bohr Institute, University of Copenhagen, 2100 København, Denmark*
- ¹⁴³ *National Central University, Taoyuan City 320317, Taiwan*
- ¹⁴⁴ *National Tsing Hua University, Hsinchu City 30013, Taiwan*
- ¹⁴⁵ *OzGrav, Charles Sturt University, Wagga Wagga, New South Wales 2678, Australia*
- ¹⁴⁶ *Vanderbilt University, Nashville, TN 37235, USA*
- ¹⁴⁷ *University of the Chinese Academy of Sciences / International Centre for Theoretical Physics Asia-Pacific, Beijing 100049, China*

- ¹⁴⁸ *Department of Electrophysics, National Yang Ming Chiao Tung University, 101 Univ. Street, Hsinchu, Taiwan*
- ¹⁴⁹ *Kamioka Branch, National Astronomical Observatory of Japan, 238 Higashi-Mozumi, Kamioka-cho, Hida City, Gifu 506-1205, Japan*
- ¹⁵⁰ *University of Texas, Austin, TX 78712, USA*
- ¹⁵¹ *CaRT, California Institute of Technology, Pasadena, CA 91125, USA*
- ¹⁵² *Northeastern University, Boston, MA 02115, USA*
- ¹⁵³ *Dipartimento di Ingegneria Industriale (DIIN), Università di Salerno, I-84084 Fisciano, Salerno, Italy*
- ¹⁵⁴ *Faculty of Science, University of Toyama, 3190 Gofuku, Toyama City, Toyama 930-8555, Japan*
- ¹⁵⁵ *Carleton College, Northfield, MN 55057, USA*
- ¹⁵⁶ *University of Szeged, Dóm tér 9, Szeged 6720, Hungary*
- ¹⁵⁷ *OzGrav, Swinburne University of Technology, Hawthorn VIC 3122, Australia*
- ¹⁵⁸ *INFN Cagliari, Physics Department, Università degli Studi di Cagliari, Cagliari 09042, Italy*
- ¹⁵⁹ *Università degli Studi di Cagliari, Via Università 40, 09124 Cagliari, Italy*
- ¹⁶⁰ *Université Libre de Bruxelles, Brussels 1050, Belgium*
- ¹⁶¹ *INAF, Osservatorio Astronomico di Brera sede di Merate, I-23807 Merate, Lecco, Italy*
- ¹⁶² *Departamento de Matemáticas, Universitat de València, E-46100 Burjassot, València, Spain*
- ¹⁶³ *Montana State University, Bozeman, MT 59717, USA*
- ¹⁶⁴ *The University of Utah, Salt Lake City, UT 84112, USA*
- ¹⁶⁵ *Johns Hopkins University, Baltimore, MD 21218, USA*
- ¹⁶⁶ *University of Rhode Island, Kingston, RI 02881, USA*
- ¹⁶⁷ *The University of Texas Rio Grande Valley, Brownsville, TX 78520, USA*
- ¹⁶⁸ *Université de Liège, B-4000 Liège, Belgium*
- ¹⁶⁹ *DIFA- Alma Mater Studiorum Università di Bologna, Via Zamboni, 33 - 40126 Bologna, Italy*
- ¹⁷⁰ *Istituto Nazionale Di Fisica Nucleare - Sezione di Bologna, viale Carlo Berti Pichat 6/2 - 40127 Bologna, Italy*
- ¹⁷¹ *University of Manitoba, Winnipeg, MB R3T 2N2, Canada*
- ¹⁷² *INFN-CNAF - Bologna, Viale Carlo Berti Pichat, 6/2, 40127 Bologna BO, Italy*
- ¹⁷³ *Università degli Studi di Sassari, I-07100 Sassari, Italy*
- ¹⁷⁴ *INFN, Laboratori Nazionali del Sud, I-95125 Catania, Italy*
- ¹⁷⁵ *Université de Normandie, ENSICAEN, UNICAEN, CNRS/IN2P3, LPC Caen, F-14000 Caen, France*
- ¹⁷⁶ *Laboratoire de Physique Corpusculaire Caen, 6 boulevard du maréchal Juin, F-14050 Caen, France*
- ¹⁷⁷ *The University of Sheffield, Sheffield S10 2TN, United Kingdom*
- ¹⁷⁸ *Université Claude Bernard Lyon 1, CNRS, Laboratoire des Matériaux Avancés (LMA), IP2I Lyon / IN2P3, UMR 5822, F-69622 Villeurbanne, France*
- ¹⁷⁹ *Università di Firenze, Sesto Fiorentino I-50019, Italy*
- ¹⁸⁰ *Dipartimento di Scienze Matematiche, Fisiche e Informatiche, Università di Parma, I-43124 Parma, Italy*
- ¹⁸¹ *INFN, Sezione di Milano Bicocca, Gruppo Collegato di Parma, I-43124 Parma, Italy*
- ¹⁸² *California State University, Los Angeles, Los Angeles, CA 90032, USA*
- ¹⁸³ *Marquette University, Milwaukee, WI 53233, USA*
- ¹⁸⁴ *Perimeter Institute, Waterloo, ON N2L 2Y5, Canada*
- ¹⁸⁵ *Corps des Mines, Mines Paris, Université PSL, 60 Bd Saint-Michel, 75272 Paris, France*
- ¹⁸⁶ *Dipartimento di Fisica, Università di Trieste, I-34127 Trieste, Italy*
- ¹⁸⁷ *Université Côte d'Azur, Observatoire de la Côte d'Azur, CNRS, Lagrange, F-06304 Nice, France*
- ¹⁸⁸ *National Center for Nuclear Research, 05-400 Świerk-Otwock, Poland*
- ¹⁸⁹ *Vrije Universiteit Brussel, 1050 Brussel, Belgium*
- ¹⁹⁰ *University of Zurich, Winterthurerstrasse 190, 8057 Zurich, Switzerland*
- ¹⁹¹ *Canadian Institute for Theoretical Astrophysics, University of Toronto, Toronto, ON M5S 3H8, Canada*
- ¹⁹² *Stony Brook University, Stony Brook, NY 11794, USA*
- ¹⁹³ *Center for Computational Astrophysics, Flatiron Institute, New York, NY 10010, USA*
- ¹⁹⁴ *Montclair State University, Montclair, NJ 07043, USA*
- ¹⁹⁵ *HUN-REN Institute for Nuclear Research, H-4026 Debrecen, Hungary*
- ¹⁹⁶ *Indian Institute of Technology Bombay, Powai, Mumbai 400 076, India*
- ¹⁹⁷ *Centro de Física das Universidades do Minho e do Porto, Universidade do Minho, PT-4710-057 Braga, Portugal*
- ¹⁹⁸ *Aix Marseille Univ, CNRS/IN2P3, CPPM, Marseille, France*
- ¹⁹⁹ *CNR-SPIN, I-84084 Fisciano, Salerno, Italy*
- ²⁰⁰ *Scuola di Ingegneria, Università della Basilicata, I-85100 Potenza, Italy*
- ²⁰¹ *Western Washington University, Bellingham, WA 98225, USA*
- ²⁰² *SUPA, University of the West of Scotland, Paisley PA1 2BE, United Kingdom*
- ²⁰³ *Barry University, Miami Shores, FL 33168, USA*

- ²⁰⁴ *Eötvös University, Budapest 1117, Hungary*
- ²⁰⁵ *Institute for Cosmic Ray Research, KAGRA Observatory, The University of Tokyo, 5-1-5 Kashiwa-no-Ha, Kashiwa City, Chiba 277-8582, Japan*
- ²⁰⁶ *Department of Physics, Graduate School of Science, Osaka Metropolitan University, 3-3-138 Sugimoto-cho, Sumiyoshi-ku, Osaka City, Osaka 558-8585, Japan*
- ²⁰⁷ *University of Sannio at Benevento, I-82100 Benevento, Italy and INFN, Sezione di Napoli, I-80100 Napoli, Italy*
- ²⁰⁸ *University of California, Berkeley, CA 94720, USA*
- ²⁰⁹ *Instituto de Física Teórica UAM-CSIC, Universidad Autónoma de Madrid, 28049 Madrid, Spain*
- ²¹⁰ *Laboratoire d'Acoustique de l'Université du Mans, UMR CNRS 6613, F-72085 Le Mans, France*
- ²¹¹ *University of Southampton, Southampton SO17 1BJ, United Kingdom*
- ²¹² *University of California, Riverside, Riverside, CA 92521, USA*
- ²¹³ *Dipartimento di Ingegneria Industriale, Elettrotecnica e Meccanica, Università degli Studi Roma Tre, I-00146 Roma, Italy*
- ²¹⁴ *University of Nevada, Las Vegas, Las Vegas, NV 89154, USA*
- ²¹⁵ *University of Nottingham NG7 2RD, UK*
- ²¹⁶ *Ariel University, Ramat HaGolan St 65, Ari'el, Israel*
- ²¹⁷ *The University of Mississippi, University, MS 38677, USA*
- ²¹⁸ *Graduate School of Science, Institute of Science Tokyo, 2-12-1 Ookayama, Meguro-ku, Tokyo 152-8551, Japan*
- ²¹⁹ *Institute of Physics, Academia Sinica, 128 Sec. 2, Academia Rd., Nankang, Taipei 11529, Taiwan*
- ²²⁰ *The Chinese University of Hong Kong, Shatin, NT, Hong Kong*
- ²²¹ *American University, Washington, DC 20016, USA*
- ²²² *Dipartimento di Fisica, Università degli studi di Milano, Via Celoria 16, I-20133, Milano, Italy*
- ²²³ *INFN, sezione di Milano, Via Celoria 16, I-20133, Milano, Italy*
- ²²⁴ *Department of Applied Physics, Fukuoka University, 8-19-1 Nanakuma, Jonan, Fukuoka City, Fukuoka 814-0180, Japan*
- ²²⁵ *University of Cambridge, Cambridge CB2 1TN, United Kingdom*
- ²²⁶ *University of Lancaster, Lancaster LA1 4YW, United Kingdom*
- ²²⁷ *College of Industrial Technology, Nihon University, 1-2-1 Izumi, Narashino City, Chiba 275-8575, Japan*
- ²²⁸ *Faculty of Engineering, Niigata University, 8050 Ikarashi-2-no-cho, Nishi-ku, Niigata City, Niigata 950-2181, Japan*
- ²²⁹ *Department of Physics, Tamkang University, No. 151, Yingzhuang Rd., Danshui Dist., New Taipei City 25137, Taiwan*
- ²³⁰ *Rutherford Appleton Laboratory, Didcot OX11 0DE, United Kingdom*
- ²³¹ *Department of Physical Sciences, Aoyama Gakuin University, 5-10-1 Fuchinobe, Sagami-hara City, Kanagawa 252-5258, Japan*
- ²³² *Helmut Schmidt University, D-22043 Hamburg, Germany*
- ²³³ *Nambu Yoichiro Institute of Theoretical and Experimental Physics (NITEP), Osaka Metropolitan University, 3-3-138 Sugimoto-cho, Sumiyoshi-ku, Osaka City, Osaka 558-8585, Japan*
- ²³⁴ *Directorate of Construction, Services & Estate Management, Mumbai 400094, India*
- ²³⁵ *Observatoire Astronomique de Strasbourg, 11 Rue de l'Université, 67000 Strasbourg, France*
- ²³⁶ *Faculty of Physics, University of Białystok, 15-245 Białystok, Poland*
- ²³⁷ *National Astronomical Observatories, Chinese Academy of Sciences, 20A Datun Road, Chaoyang District, Beijing, China*
- ²³⁸ *School of Astronomy and Space Science, University of Chinese Academy of Sciences, 20A Datun Road, Chaoyang District, Beijing, China*
- ²³⁹ *Sungkyunkwan University, Seoul 03063, Republic of Korea*
- ²⁴⁰ *Department of Physics, Ulsan National Institute of Science and Technology (UNIST), 50 UNIST-gil, Ulju-gun, Ulsan 44919, Republic of Korea*
- ²⁴¹ *Institute for Cosmic Ray Research, The University of Tokyo, 5-1-5 Kashiwa-no-Ha, Kashiwa City, Chiba 277-8582, Japan*
- ²⁴² *Chung-Ang University, Seoul 06974, Republic of Korea*
- ²⁴³ *University of Washington Bothell, Bothell, WA 98011, USA*
- ²⁴⁴ *Laboratoire de Physique et de Chimie de l'Environnement, Université Joseph KI-ZERBO, 9GH2+3V5, Ouagadougou, Burkina Faso*
- ²⁴⁵ *Ewha Womans University, Seoul 03760, Republic of Korea*
- ²⁴⁶ *National Institute for Mathematical Sciences, Daejeon 34047, Republic of Korea*
- ²⁴⁷ *Korea Astronomy and Space Science Institute, Daejeon 34055, Republic of Korea*
- ²⁴⁸ *Department of Astronomy and Space Science, Chungnam National University, 9 Daehak-ro, Yuseong-gu, Daejeon 34134, Republic of Korea*
- ²⁴⁹ *Institute of Particle and Nuclear Studies (IPNS), High Energy Accelerator Research Organization (KEK), 1-1 Oho, Tsukuba City, Ibaraki 305-0801, Japan*
- ²⁵⁰ *Division of Science, National Astronomical Observatory of Japan, 2-21-1 Osawa, Mitaka City, Tokyo 181-8588, Japan*
- ²⁵¹ *Nagoya University, Nagoya, 464-8601, Japan*
- ²⁵² *Department of Physics, Aristotle University of Thessaloniki, 54124 Thessaloniki, Greece*
- ²⁵³ *Bard College, Annandale-On-Hudson, NY 12504, USA*
- ²⁵⁴ *Technical University of Braunschweig, D-38106 Braunschweig, Germany*

- ²⁵⁵ *Institute of Mathematics, Polish Academy of Sciences, 00656 Warsaw, Poland*
- ²⁵⁶ *Astronomical Observatory, Jagiellonian University, 31-007 Cracow, Poland*
- ²⁵⁷ *Department of Physics and Astronomy, University of Padova, Via Marzolo, 8-35151 Padova, Italy*
- ²⁵⁸ *Sezione di Padova, Istituto Nazionale di Fisica Nucleare (INFN), Via Marzolo, 8-35131 Padova, Italy*
- ²⁵⁹ *Department of Physics, Nagoya University, ES building, Furocho, Chikusa-ku, Nagoya, Aichi 464-8602, Japan*
- ²⁶⁰ *Université de Montréal/Polytechnique, Montreal, Quebec H3T 1J4, Canada*
- ²⁶¹ *Indian Institute of Science Education and Research, Kolkata, Mohanpur, West Bengal 741252, India*
- ²⁶² *Seoul National University, Seoul 08826, Republic of Korea*
- ²⁶³ *Department of Computer Simulation, Inje University, 197 Inje-ro, Gimhae, Gyeongsangnam-do 50834, Republic of Korea*
- ²⁶⁴ *NAVIER, École des Ponts, Univ Gustave Eiffel, CNRS, Marne-la-Vallée, France*
- ²⁶⁵ *Gravitational Wave Science Project, National Astronomical Observatory of Japan (NAOJ), Mitaka City, Tokyo 181-8588, Japan*
- ²⁶⁶ *Department of Physics, National Cheng Kung University, No.1, University Road, Tainan City 701, Taiwan*
- ²⁶⁷ *St. Thomas University, Miami Gardens, FL 33054, USA*
- ²⁶⁸ *Scuola Normale Superiore, I-56126 Pisa, Italy*
- ²⁶⁹ *Institució Catalana de Recerca i Estudis Avançats, E-08010 Barcelona, Spain*
- ²⁷⁰ *Institut de Física d'Altes Energies, E-08193 Barcelona, Spain*
- ²⁷¹ *Institut fuer Theoretische Astrophysik, Zentrum fuer Astronomie Heidelberg, Universitaet Heidelberg, Albert Ueberle Str. 2, 69120 Heidelberg, Germany*
- ²⁷² *Institucio Catalana de Recerca i Estudis Avançats (ICREA), Passeig de Lluís Companys, 23, 08010 Barcelona, Spain*
- ²⁷³ *Research Center for Space Science, Advanced Research Laboratories, Tokyo City University, 3-3-1 Ushikubo-Nishi, Tsuzuki-Ku, Yokohama, Kanagawa 224-8551, Japan*
- ²⁷⁴ *Tsinghua University, Beijing 100084, China*
- ²⁷⁵ *Institut des Hautes Etudes Scientifiques, F-91440 Bures-sur-Yvette, France*
- ²⁷⁶ *Faculty of Law, Ryukoku University, 67 Fukakusa Tsukamoto-cho, Fushimi-ku, Kyoto City, Kyoto 612-8577, Japan*
- ²⁷⁷ *Phenikaa Institute for Advanced Study (PIAS), Phenikaa University, Yen Nghia, Ha Dong, Hanoi, Vietnam*
- ²⁷⁸ *University of Stavanger, 4021 Stavanger, Norway*
- ²⁷⁹ *Physics Program, Graduate School of Advanced Science and Engineering, Hiroshima University, 1-3-1 Kagamiyama, Higashihiroshima City, Hiroshima 739-8526, Japan*
- ²⁸⁰ *GRAPPA, Anton Pannekoek Institute for Astronomy and Institute for High-Energy Physics, University of Amsterdam, 1098 XH Amsterdam, Netherlands*
- ²⁸¹ *University College London, London WC1E 6BT, United Kingdom*
- ²⁸² *Observatoire de Paris, 75014 Paris, France*
- ²⁸³ *Laboratoire Univers et Théories, Observatoire de Paris, 92190 Meudon, France*
- ²⁸⁴ *Graduate School of Science and Technology, Niigata University, 8050 Ikarashi-2-no-cho, Nishi-ku, Niigata City, Niigata 950-2181, Japan*
- ²⁸⁵ *University of Maryland, Baltimore County, Baltimore, MD 21250, USA*
- ²⁸⁶ *CSIR-Central Glass and Ceramic Research Institute, Kolkata, West Bengal 700032, India*
- ²⁸⁷ *Consiglio Nazionale delle Ricerche - Istituto dei Sistemi Complessi, I-00185 Roma, Italy*
- ²⁸⁸ *Department of Astronomy, Yonsei University, 50 Yonsei-Ro, Seodaemun-Gu, Seoul 03722, Republic of Korea*
- ²⁸⁹ *Department of Physics, University of Guadalajara, Av. Revolucion 1500, Colonia Olimpica C.P. 44430, Guadalajara, Jalisco, Mexico*
- ²⁹⁰ *Hobart and William Smith Colleges, Geneva, NY 14456, USA*
- ²⁹¹ *INAF, Osservatorio Astronomico di Padova, I-35122 Padova, Italy*
- ²⁹² *Dipartimento di Ingegneria, Università del Sannio, I-82100 Benevento, Italy*
- ²⁹³ *Museo Storico della Fisica e Centro Studi e Ricerche "Enrico Fermi", I-00184 Roma, Italy*
- ²⁹⁴ *Kennesaw State University, Kennesaw, GA 30144, USA*
- ²⁹⁵ *Subatech, CNRS/IN2P3 - IMT Atlantique - Nantes Université, 4 rue Alfred Kastler BP 20722 44307 Nantes CÉDEX 03, France*
- ²⁹⁶ *Universidad de Antioquia, Medellín, Colombia*
- ²⁹⁷ *Departamento de Física - ETSIDI, Universidad Politécnica de Madrid, 28012 Madrid, Spain*
- ²⁹⁸ *Department of Electronic Control Engineering, National Institute of Technology, Nagaoka College, 888 Nishikatagai, Nagaoka City, Niigata 940-8532, Japan*
- ²⁹⁹ *Trinity College, Hartford, CT 06106, USA*
- ³⁰⁰ *Dipartimento di Fisica e Scienze della Terra, Università Degli Studi di Ferrara, Via Saragat, 1, 44121 Ferrara FE, Italy*
- ³⁰¹ *Faculty of Science, Toho University, 2-2-1 Miyama, Funabashi City, Chiba 274-8510, Japan*
- ³⁰² *Indian Institute of Technology, Palaj, Gandhinagar, Gujarat 382355, India*
- ³⁰³ *Kavli Institute for Astronomy and Astrophysics, Peking University, Yiheyuan Road 5, Haidian District, Beijing 100871, China*
- ³⁰⁴ *Laboratoire MSME, Cité Descartes, 5 Boulevard Descartes, Champs-sur-Marne, 77454 Marne-la-Vallée Cedex 2, France*
- ³⁰⁵ *Faculty of Information Science and Technology, Osaka Institute of Technology, 1-79-1 Kitayama, Hirakata City, Osaka 573-0196, Japan*

³⁰⁶*Department of Physics, Princeton University, Princeton, NJ 08544, USA*

³⁰⁷*NASA Goddard Space Flight Center, Greenbelt, MD 20771, USA*

³⁰⁸*Faculty of Science and Technology, Kochi University, 2-5-1 Akebono-cho, Kochi-shi, Kochi 780-8520, Japan*

³⁰⁹*Laboratoire de Physique de l'École Normale Supérieure, ENS, (CNRS, Université PSL, Sorbonne Université, Université Paris Cité), F-75005 Paris, France*

³¹⁰*Faculty of Physics, University of Warsaw, Ludwika Pasteura 5, 02-093 Warszawa, Poland*

³¹¹*Laser Interferometry and Gravitational Wave Astronomy, Max Planck Institute for Gravitational Physics, Callinstrasse 38, 30167 Hannover, Germany*

³¹²*The Hakubi Center for Advanced Research, Kyoto University, Yoshida-honmachi, Sakyou-ku, Kyoto City, Kyoto 606-8501, Japan*

³¹³*Department of Physics, Kyoto University, Kita-Shirakawa Oiwake-cho, Sakyou-ku, Kyoto City, Kyoto 606-8502, Japan*

³¹⁴*Yukawa Institute for Theoretical Physics (YITP), Kyoto University, Kita-Shirakawa Oiwake-cho, Sakyou-ku, Kyoto City, Kyoto 606-8502, Japan*

³¹⁵*University of Catania, Department of Physics and Astronomy, Via S. Sofia, 64, 95123 Catania CT, Italy*

³¹⁶*National Institute of Technology, Fukui College, Geshi-cho, Sabae-shi, Fukui 916-8507, Japan*

³¹⁷*Department of Communications Engineering, National Defense Academy of Japan, 1-10-20 Hashirimizu, Yokosuka City, Kanagawa 239-8686, Japan*

³¹⁸*Eindhoven University of Technology, 5600 MB Eindhoven, Netherlands*

³¹⁹*Kavli Institute for the Physics and Mathematics of the Universe (Kavli IPMU), WPI, The University of Tokyo, 5-1-5 Kashiwa-no-Ha, Kashiwa City, Chiba 277-8583, Japan*

³²⁰*Department of Astronomy, Beijing Normal University, Xijiekouwai Street 19, Haidian District, Beijing 100875, China*

³²¹*School of Physics and Technology, Wuhan University, Bayi Road 299, Wuchang District, Wuhan, Hubei, 430072, China*

(Compiled: 3 November 2025)

ABSTRACT

We report the observation of gravitational waves from two binary black hole coalescences during the fourth observing run of the LIGO–Virgo–KAGRA detector network, GW241011 and GW241110. The sources of these two signals are characterized by rapid and precisely measured primary spins, non-negligible spin–orbit misalignment, and unequal mass ratios between their constituent black holes. These properties are characteristic of binaries in which the more massive object was itself formed from a previous binary black hole merger, and suggest that the sources of GW241011 and GW241110 may have formed in dense stellar environments in which repeated mergers can take place. As the third loudest gravitational-wave event published to date, with a median network signal-to-noise ratio of 36.0, GW241011 furthermore yields stringent constraints on the Kerr nature of black holes, the multipolar structure of gravitational-wave generation, and the existence of ultralight bosons within the mass range 10^{-13} – 10^{-12} eV.

1. INTRODUCTION

It has been a decade since the inception of practical gravitational-wave astronomy. In the years following the first direct observation of gravitational waves from a binary black hole coalescence in 2015 (Abbott et al. 2016a), the Advanced LIGO, Advanced Virgo, and KAGRA experiments (Aasi et al. 2015; Acernese et al. 2015; Akutsu et al. 2021) have operated in tandem to regularly identify an ever-increasing number of gravitational-wave signals (Abbott et al. 2024, 2023a). The recently-released fourth Gravitational-Wave Transient Catalog (GWTC-4.0), including signals discovered through January 2024, contains hundreds of gravitational-wave signals (Abac et al. 2025a), and the rate of discoveries

continues to accelerate as further upgrades improve broadband instrumental sensitivity to gravitational waves (Ganapathy et al. 2023; Jia et al. 2024; Capote et al. 2025; Soni et al. 2025; Acernese et al. 2023; Abac et al. 2025b). The growing collection of observed gravitational-wave sources includes binary neutron stars (Abbott et al. 2017a, 2020a), one of which was accompanied by transient multimessenger emission seen across the electromagnetic spectrum (e.g., Abbott et al. 2017b,a; Goldstein et al. 2017; Coulter et al. 2017; Hallinan et al. 2017; Margutti et al. 2017), as well as likely neutron star–black hole binaries (Abbott et al. 2021a, 2023a; Abac et al. 2024, 2025a). And it includes a growing number of black holes whose masses, whether unexpectedly large, unexpectedly small, or unexpectedly unequal, challenge present understanding of

* Deceased, September 2024.

compact binary formation and evolution (Abbott et al. 2016b, 2020b,c; Abac et al. 2024, 2025c).

Here, we report a pair of gravitational-wave events discovered in late 2024, GW241011.233834 and GW241110.124123, arising from binary black hole coalescences that each contain at least one rapidly rotating black hole. As illustrated in Fig. 1, the primary (more massive) source black hole of GW241011.233834 (hereafter abbreviated GW241011) exhibits one of the most rapid and precisely measured spins observed to date, with $\chi_1 = 0.78_{-0.09}^{+0.09}$. This event provides a larger lower bound on both spin magnitude and $\vec{\chi}_1 \cdot \hat{L}_N$, the spin projected parallel to a binary’s Newtonian orbital angular momentum \vec{L}_N , than any other binary previously published in GWTC-4.0 (Abac et al. 2025a). The primary spin of GW241011’s source is tilted by ~ 30 deg with respect to \hat{L}_N , and the gravitational-wave signal confidently exhibits relativistic spin-orbit precession. In contrast, the primary component of GW241110.124123 (hereafter GW241110) is measured to be spinning in a direction antiparallel to its orbital angular momentum vector, the most confidently antiparallel spin observed. Despite the opposite character of their spins, the sources of GW241011 and GW241110 possess similar masses. Each is inferred to contain a primary mass between approximately 15–20 M_\odot and both favor unequal component black hole masses, with GW241011 in particular requiring an approximately 3:1 mass ratio.

The rapid primary spins, significant spin–orbit misalignment, and unequal mass ratios of GW241011 and GW241110 are in tension with expectations from isolated evolution of massive stellar binaries (Kalogera 2000; Belczynski et al. 2016a; de Mink & Mandel 2016; Marchant et al. 2016; Rodriguez et al. 2016; Callister et al. 2021; Broekgaarden et al. 2022; Zevin & Bavera 2022). The source properties of GW241011 and GW241110 are consistent, however, with those expected from hierarchical mergers in dense stellar clusters. Binary black hole mergers yield remnant black holes that are rapidly rotating, with spin magnitudes of $\chi \approx 0.7$ (Pretorius 2005; Buonanno et al. 2008; Berti & Volonteri 2008). Asymmetric gravitational-wave emission can cause these remnant black holes to receive large kicks, with velocities that can reach thousands of kilometers per second (Fitchett 1983; Favata et al. 2004; Schnittman & Buonanno 2007; Campanelli et al. 2007; Gonzalez et al. 2007). In environments with sufficiently high escape velocities, however, remnant black holes may remain gravitationally bound, capture new partners, and participate in subsequent binary mergers (Lee 1995; O’Leary et al. 2006; Giersz et al. 2015; Antonini & Rasio 2016; Gerosa & Berti 2017; Fishbach et al. 2017;

Rodriguez et al. 2018b; Antonini et al. 2019; Rodriguez et al. 2019; Baibhav et al. 2020; Fragione & Silk 2020; Kimball et al. 2021; Baibhav et al. 2021; Doctor et al. 2021; Fragione et al. 2022; Gerosa & Fishbach 2021; Mahapatra et al. 2021; Mapelli et al. 2021; Antonini et al. 2023; Arca Sedda et al. 2023; Mahapatra et al. 2025b; Chattopadhyay et al. 2023). Under this hypothesis, the primary black holes of GW241011 and GW241110 may themselves each be a product of a previous binary black hole merger.

The rapid spins and unequal mass ratios of GW241011 and GW241110 furthermore make them prime laboratories with which to test fundamental physics. GW241011, in particular, exhibits both significant relativistic spin precession (Apostolatos et al. 1994; Kidder 1995) and gravitational radiation from higher-order multipole moments (Thorne 1980). By virtue of these features, GW241011 offers one of the most precise confirmations to date of the Kerr nature of spinning black holes (Kerr 1963; Carter 1971; Hansen 1974) and the multipolar emission pattern of gravitational waves.

The rest of this paper is organized as follows. In Section 2, we describe the low-latency identification and subsequent validation of GW241011 and GW241110. In Section 3, we discuss the measured properties of these two events. In Section 4, we describe the possible astrophysical interpretation and implications of GW241011 and GW241110, and in Section 5 present tests of general relativity (GR) using GW241011. We conclude in Section 6. Additional details and results are provided in the Appendices.

2. DETECTION AND SIGNIFICANCE

2.1. GW241011

GW241011 passed through the Earth’s geocenter on October 11, 2024 at 23:38:34.9 UTC. It was detected in low latency in LIGO Hanford and Virgo data (LIGO Scientific Collaboration et al. 2024a) by the GSTLAL matched-filter search pipeline (Messick et al. 2017; Sachdev et al. 2019; Hanna et al. 2020; Cannon et al. 2021; Sakon et al. 2024; Ewing et al. 2024; Tsukada et al. 2023; Ray et al. 2023; Joshi et al. 2025a,b). The signal was measured with optimized signal-to-noise ratios (SNRs) of 35.4 and 9.1 in LIGO Hanford and Virgo, respectively, and a false alarm rate (FAR) of $< 10^{-5}$ yr. LIGO Livingston was not operating at the time of the event. Significant candidates were also identified by the MBTA (Adams et al. 2016; Aubin et al. 2021; All  n   et al. 2025) and PyCBC (Allen 2005; Allen et al. 2012; Usman et al. 2016; Nitz 2018; Nitz et al. 2017; Dalton et al. 2021; Davies et al. 2020) pipelines at the time of GW241011, but fell outside the mass range for which

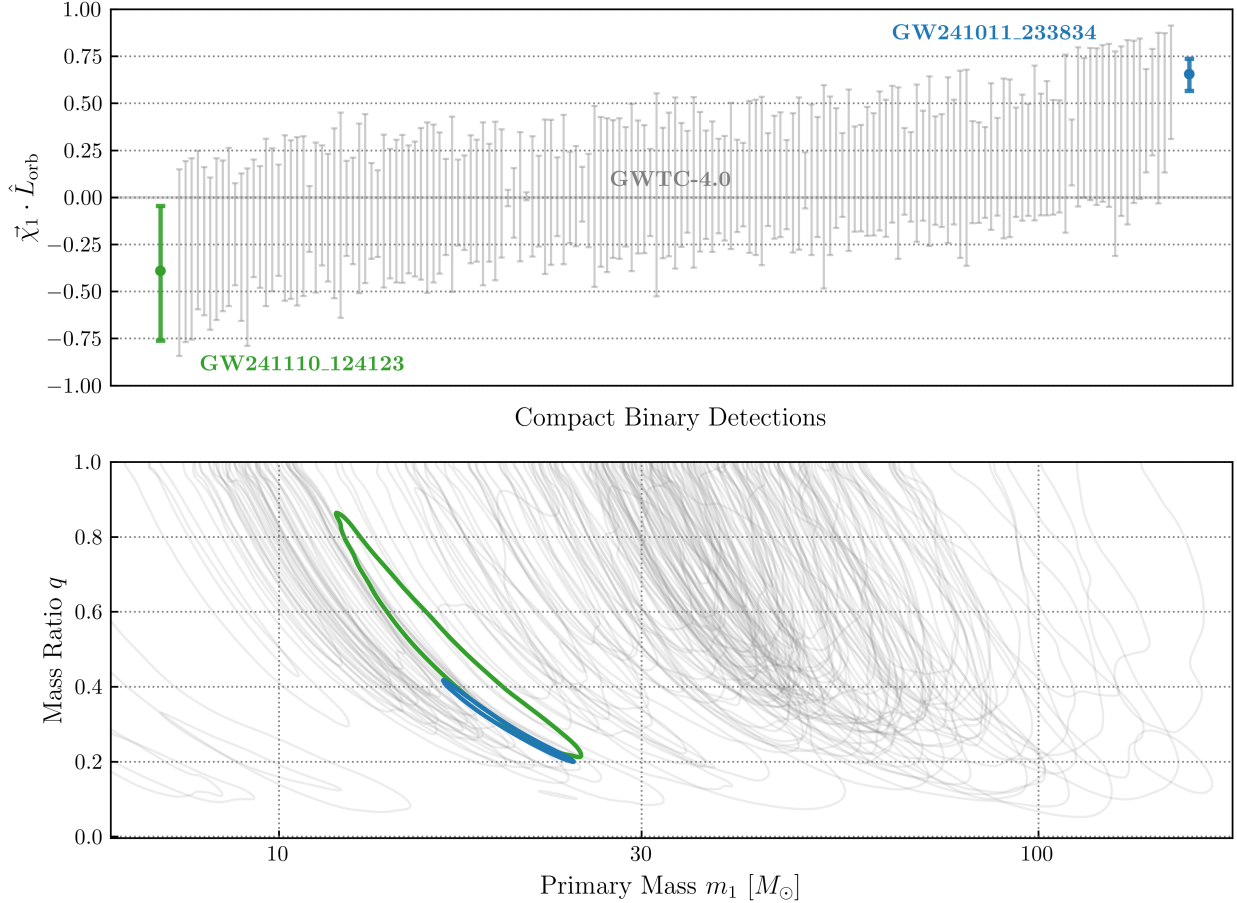


Figure 1. *Top:* Central 90% credible bounds on the dimensionless primary spins $\bar{\chi}_1$ of GW241011 (blue) and GW241110 (green), projected parallel to the direction \hat{L}_N of each binary’s Newtonian orbital angular momentum. Shown in grey for comparison are 90% credible bounds on the projected primary spins of previously-published compact binary coalescences in the fourth Gravitational-Wave Transient Catalog (GWTC-4.0; Abac et al. 2025a), sorted by their median posterior values of $\chi_{1,z} \equiv \bar{\chi}_1 \cdot \hat{L}_N$. We specifically show events with false alarm rates (FARs) below 1 yr^{-1} , consistent with the significance threshold adopted for compact binary population studies in GWTC-3.0 and GWTC-4.0 (Abbott et al. 2023b; Abac et al. 2025d). The source of GW241011 contains one of the most rapidly spinning black holes observed by LIGO–Virgo–KAGRA to date, possessing the largest lower limit on both its primary spin magnitude and projected spin $\bar{\chi}_{1,z}$. GW241110, conversely, yields the most confident measurement to date of a black hole spinning retrograde with respect to its orbit, with $\chi_{1,z} < 0$ at 97.7% credibility. *Bottom:* 90% credible posterior bounds on the primary masses and mass ratios of GW241011 and GW241110, together with all binary mergers in GWTC-4.0 with FAR < 1 yr^{-1} . Despite the opposite nature of their spins, GW241011 and GW241110 are likely to have very similar masses, each favoring a primary of $15\text{--}20 M_\odot$ and unequal mass ratios.

these searches report candidates in low latency seen in only one LIGO instrument (Abac et al. 2025e). LIGO Hanford and Virgo were each operating normally at the time of detection, with stable angle-averaged binary neutron star inspiral ranges of approximately 160 and 50 Mpc, respectively (Finn & Chernoff 1993; Chen et al. 2021). In subsequent high-latency searches, for which more comprehensive data quality assessment and precise background estimates were available, GSTLAL, MBTA, and PyCBC each detected GW241011 with false alarm rates below $3 \times 10^{-5} \text{ yr}^{-1}$. GW241011’s high network SNR makes it the third-loudest gravitational-wave event

published to date, behind GW230814.230901 (Abac et al. 2025a) and GW250114.082203 (Abac et al. 2025f).

2.2. GW241110

GW241110 arrived at Earth on November 10, 2024 at 12:41:23.6 UTC. It was identified in low latency in LIGO Hanford, LIGO Livingston, and Virgo data (Ligo Scientific Collaboration et al. 2024b), assigned FAR = 0.15 yr^{-1} by the GSTLAL search pipeline and lower significances by MBTA and PyCBC. At the time of GW241110, the LIGO instruments had angle-averaged binary neutron star inspiral ranges of approximately 160 Mpc, while Virgo’s inspiral range was near 50 Mpc.

High-latency analyses with the PyCBC, GstLAL, and MBTA pipelines later re-identified GW241110 with false alarm rates of $6.3 \times 10^{-4} \text{yr}^{-1}$, 0.099yr^{-1} , and 0.85yr^{-1} respectively.

For several hours around the arrival time of GW241110, microseismic ground motion near LIGO Livingston was elevated. Elevated microseism is known to increase the rate of scattered light glitches in detector strain data, particularly below 30 Hz (Soni et al. 2020, 2024). Between 0.3 and 2 s after the coalescence time, three noise transients are observed in the data, all below 30 Hz. Two are low-SNR transients, while the third is a high-SNR scattered-light glitch occurring below 15 Hz. Although these transients are not expected to affect the observation and analysis of GW241110 (Macas et al. 2022; Hourihane & Chatziioannou 2025), all further studies of GW241110’s properties (see Section 3) use LIGO Livingston data only above 30 Hz.

3. SOURCE PROPERTIES

Bayesian parameter estimation is performed on GW241011 and GW241110 following the methodology described in Abac et al. (2025e). Noise power spectral densities are obtained with the BAYESWAVE algorithm (Cornish & Littenberg 2015; Littenberg & Cornish 2015; Littenberg et al. 2016; Cornish et al. 2021; Gupta & Cornish 2024) and astrophysical parameter inference is performed using the RIFT (Pankow et al. 2015; Lange et al. 2017; Wysocki et al. 2019) and BILBY (Ashton et al. 2019; Romero-Shaw et al. 2020b) code packages, the latter of which invokes the DYNESTY (Speagle 2020) nested sampler. Analysis of GW241011 includes 32 s of data between 20–1792 Hz from LIGO Hanford and Virgo. Analysis of GW241110 incorporates 16 s of data from all three LIGO and Virgo instruments; data between 20–1792 Hz are used from LIGO Hanford and Virgo, whereas LIGO Livingston data are used only at frequencies above 30 Hz due to the presence of nonstationary low-frequency noise. We adopt priors that are uniform in detector-frame component masses, uniform and isotropic in component spin magnitudes and orientations, and uniform in comoving volume and source-frame time (Abac et al. 2025e). Black hole spin orientations evolve over the course of an inspiral due to relativistic spin-orbit precession; we present spin measurements corresponding to the asymptotic values in the limit of infinite binary separation (Mould & Gerosa 2022; Johnson-McDaniel et al. 2022; Gerosa et al. 2023).

The inferred source properties of GW241011 and GW241110 are summarized in Table 1. Posteriors on the primary black hole’s spin vectors of each binary are shown in Figure 2, while posteriors on a

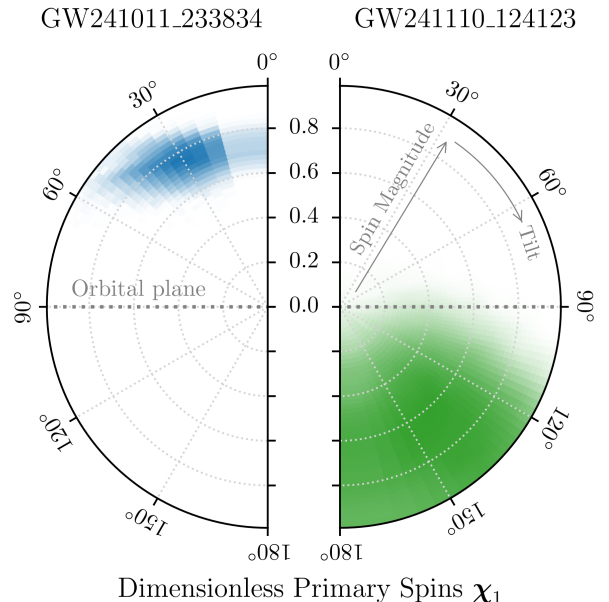


Figure 2. Posterior on the primary spin vector of GW241011 (left) and GW241110 (right). Within each subplot, radial coordinates span the range 0 to 1 and correspond to dimensionless spin magnitudes. The polar angles, spanning 0 to 180 deg, correspond to spin-orbit misalignment angles. Color saturation indicates posterior probability as a function of spin magnitude and orientation. Pixels are spaced linearly in spin magnitude and cosine tilt angle such that they each contain equal prior probability; a completely uninformative spin measurement would therefore yield a uniformly colored disk. GW241011 has a precisely measured spin magnitude of $\chi_1 = 0.78_{-0.09}^{+0.09}$ that is misaligned by 31_{-14}^{+11} degrees with respect to its orbital angular momentum. The primary spin of GW241110, in contrast, is constrained to be misaligned by more than 110 deg from its orbital angular momentum.

subset of other binary parameters appear in Figure 3. These results comprise the union of posterior samples obtained using three different waveform models, SEOBNRV5PHM (Ramos-Buades et al. 2023a), IMRPHENOMXPHM-SPINTAYLOR (Colleoni et al. 2025) and IMRPHENOMXO4A (Thompson et al. 2024), that each include the effects of spin-orbit precession and higher-order spherical harmonic modes. Further details about parameter inference, including source properties inferred with each individual waveform model, are presented in Appendix A.

3.1. Properties of GW241011

The source of GW241011 is inferred to possess a $19.6_{-2.5}^{+3.6} M_\odot$ primary mass and a confidently unequal mass ratio, $q = 0.30_{-0.08}^{+0.09}$. It has a large and precisely measured primary spin magnitude, $\chi_1 = 0.78_{-0.09}^{+0.09}$, and

Table 1. Inferred source properties of GW241011 and GW241110. Shown are each source’s primary mass (m_1), secondary mass (m_2), mass ratio (q), chirp mass (\mathcal{M}), and luminosity distance D_L , with mass parameters defined in the rest-frame of the source binary. We additionally quote a variety of spin measurements: primary dimensionless spin magnitude (χ_1) and spin–orbit misalignment angle (θ_1), primary spin components projected parallel ($\chi_{1,z} = \chi_1 \cos \theta_1$) and perpendicular ($\chi_{1,\perp} = \chi_1 \sin \theta_1$) to the binaries’ Newtonian orbital angular momenta, the effective inspiral spin χ_{eff} (Racine 2008; Ajith et al. 2011; Santamaria et al. 2010), and the effective precessing spin χ_p (Hannam et al. 2014; Schmidt et al. 2015). We do not obtain informative constraints on the secondary spins of each source; see Appendix A for secondary spin measurements. We follow parameter conventions as defined in Table 3 of (Abac et al. 2025b). For all but one parameter, we quote posterior medians and central 90% credible uncertainties. For θ_1 alone, uncertainties instead correspond to values containing the 90% credible highest posterior density interval for $\cos \theta_1$. This is done to minimize the influence of the uniform-in- $\cos \theta$ priors, which exclude $\theta_1 = 0$. Spin parameters are quoted at infinite binary separation.

Event	$m_1 [M_\odot]$	$m_2 [M_\odot]$	q	$\mathcal{M} [M_\odot]$	$D_L [\text{Mpc}]$	χ_1	$\theta_1 [\text{deg}]$	$\chi_{1,z}$	$\chi_{1,\perp}$	χ_{eff}	χ_p
GW241011	$19.6^{+3.6}_{-2.5}$	$5.9^{+0.8}_{-0.8}$	$0.30^{+0.09}_{-0.08}$	$9.1^{+0.1}_{-0.1}$	214^{+44}_{-48}	$0.78^{+0.09}_{-0.09}$	31^{+11}_{-14}	$0.66^{+0.08}_{-0.09}$	$0.39^{+0.19}_{-0.14}$	$0.49^{+0.06}_{-0.07}$	$0.39^{+0.19}_{-0.14}$
GW241110	$17.2^{+5.0}_{-4.4}$	$7.7^{+2.2}_{-1.5}$	$0.45^{+0.32}_{-0.17}$	$9.8^{+0.5}_{-0.4}$	736^{+270}_{-267}	$0.61^{+0.33}_{-0.40}$	133^{+47}_{-25}	$-0.39^{+0.34}_{-0.37}$	$0.40^{+0.34}_{-0.30}$	$-0.28^{+0.23}_{-0.20}$	$0.42^{+0.33}_{-0.27}$

its primary spin is inferred to be misaligned with respect to its Newtonian orbital angular momentum by $\theta_1 = 31^{+11}_{-14}$ deg. The spin of GW241011’s secondary black hole is unconstrained, as expected for an unequal-mass systems in which the primary’s spin angular momentum dominates. The inferred geometry of the spin vector of GW241011’s primary black hole is depicted in the left-hand side of Figure 2. Within this plot, the radial distance depicts the magnitude of GW241011’s primary spin vector, while the polar coordinate denotes its spin–orbit misalignment angle; color saturation indicates posterior probability. GW241011 is, furthermore, probably the closest binary black hole merger observed to date, with a luminosity distance of $D_L < 248$ Mpc at 90% credibility.

The primary of GW241011 is among the most rapidly rotating black holes observed to date. At 95% credibility, GW241011 has the largest lower limit obtained thus far on the spin of any merging black hole, with $\chi_1 > 0.69$. Figure 4 compares this primary spin measurement to two signals with similar spin magnitude limits, GW190517 (Abbott et al. 2023a) and the recently-announced GW231123 (Abac et al. 2025c), whose sources have $\chi_1 > 0.52$ and $\chi_1 > 0.63$ at 95% credibility, respectively. GW190403_051519 favors similarly rapid spins, but this candidate does not meet the significance threshold adopted for population analyses. Additionally, both the primary aligned spin $\chi_{1,z}$ and the effective inspiral spin of GW241011 (Racine 2008; Ajith et al. 2011; Santamaria et al. 2010), defined as

$$\chi_{\text{eff}} = \frac{(m_1 \vec{\chi}_1 + m_2 \vec{\chi}_2) \cdot \hat{L}_N}{m_1 + m_2}, \quad (1)$$

are bounded higher than any other gravitational-wave source. Among black holes that are confidently rotating, the primary spin magnitude of GW241011 is also the most precisely measured, with a 90% cred-

ible region that is half as wide as the next-most-precise measurement, made using GW190412 (Abbott et al. 2020d). The binary neutron star source of GW170817 (Abbott et al. 2017c), the lower mass gap binary source of GW190814 (Abbott et al. 2020c), and the low-significance neutron star-black hole candidate GW191219_163120 each have more precisely measured spins, but these spins are consistent with zero. GW241011 is therefore the gravitational-wave event that, taken individually, provides the strongest evidence to date that at least some component black holes in merging binaries spin rapidly, with dimensionless spins with magnitudes ~ 0.7 or greater.

GW241011 additionally exhibits strong signatures of orbital plane precession and radiation in higher spherical harmonic modes. Orbital plane precession occurs due to relativistic spin–orbit coupling, an effect that is maximized by the large and misaligned primary spin of GW241011. The degree of spin-orbit precession may be parametrized using the effective precessing spin (Hannam et al. 2014; Schmidt et al. 2015),

$$\chi_p = \text{Max} \left[\chi_1 \sin \theta_1, \frac{3 + 4q}{4 + 3q} q \chi_2 \sin \theta_2 \right], \quad (2)$$

related to the in-plane spin components $\chi_{i,\perp} = \chi_i \sin \theta_i$. The source of GW241011 has confidently non-zero effective precessing spin, with $\chi_p = 0.39^{+0.19}_{-0.14}$, and we obtain a log-Bayes factor of $\log_{10} \mathcal{B} = 5.4$ in favor of a precessing source over a model in which spins are restricted to be co-aligned with their orbit. As Bayes factors may, in general, be sensitive to one’s choice of prior, we additionally quantify evidence for precession via the precession SNR ρ_p (Fairhurst et al. 2020a,b), the posterior distribution of which is shown in Figure 5. We find $\rho_p = 5.3^{+2.1}_{-1.9}$. In the absence of precession, ρ_p is expected to follow the null distribution indicated in Fig. 5. Random draws from GW241011’s ρ_p posterior

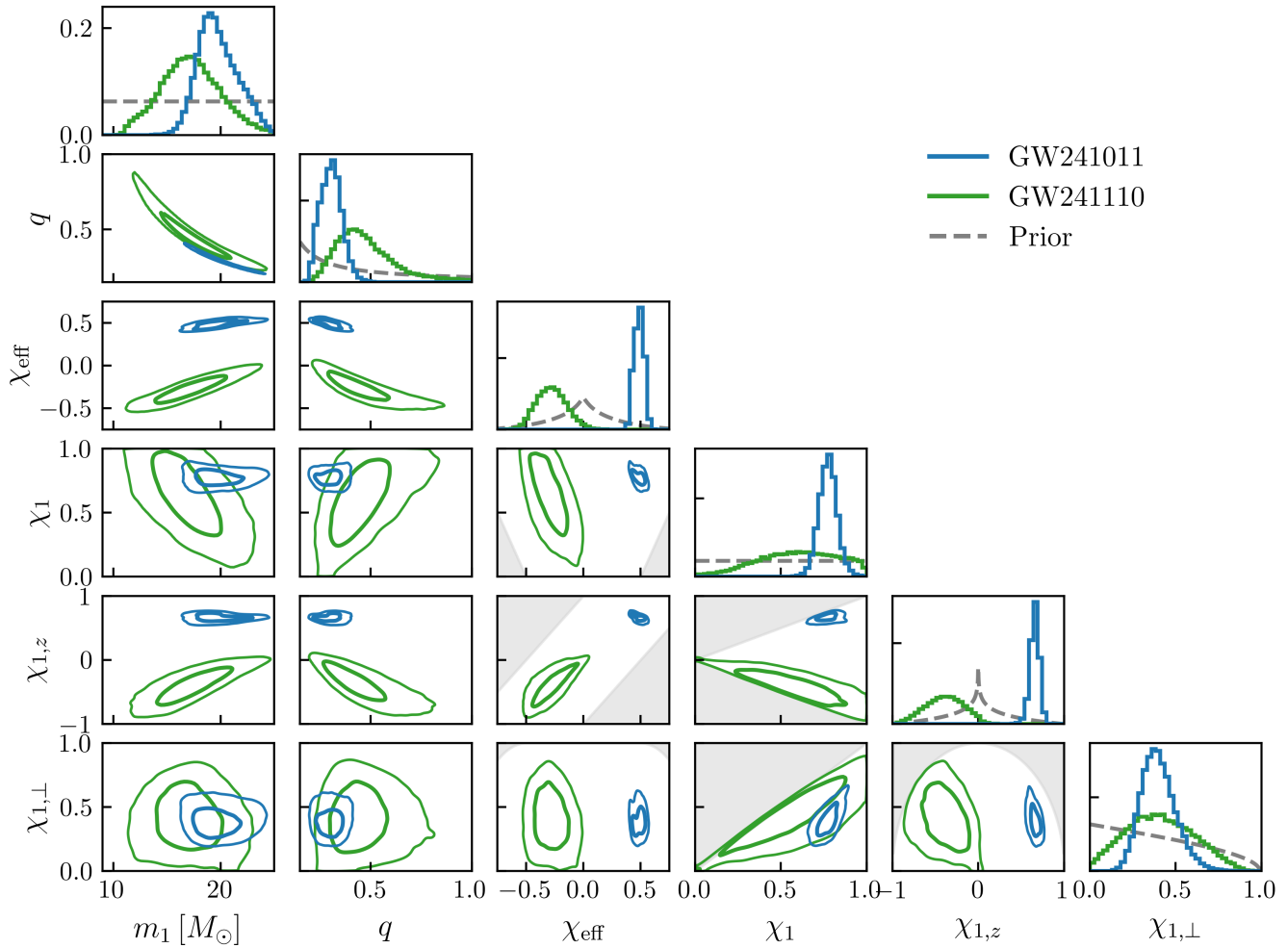


Figure 3. Posterior probabilities on selected properties of GW241011 (blue) and GW241110 (green): their primary masses m_1 , mass ratios q , effective inspiral spins χ_{eff} , primary spin magnitudes χ_1 , and components of their primary spins projected parallel ($\chi_{1,z}$) and perpendicular ($\chi_{1,\perp}$) to each binary’s Newtonian orbital angular momentum. Panels along the diagonal show marginalized posteriors on each parameter; the dashed histograms correspond to the prior probability distributions adopted during parameter estimation. Off-diagonal panels illustrate joint two-dimensional posteriors on each pair of parameters; thick and thin contours denote central 50% and 90% credible bounds. Shaded grey regions indicate to parts of parameter space that the constraint that spin magnitudes be less than or equal to one. Despite their extreme and opposite spins, GW241011 and GW241110 have consistent component mass measurements, each favoring a 15–20 M_\odot primary and an unequal mass ratio.

exceed random draws from this null distribution 99.5% of the time.

The significant mass asymmetry of GW241011 also yields significant radiation in higher-order spherical harmonic modes. Whereas gravitational-wave radiation is typically dominated by $(\ell, m) = (2, \pm 2)$ spherical harmonics, subdominant modes, such as $(\ell, m) = (2, \pm 1)$ or $(3, \pm 3)$, become increasingly important for systems with considerable mass asymmetry (Thorne 1980; Berti et al. 2007; Blanchet 2014; Mills & Fairhurst 2021). GW241011 exhibits significant radiation in the $(\ell, m) = (3, \pm 3)$ spherical harmonics, here assuming symmetric contributions from $m = 3$ and -3 modes thus neglecting small asymmetries arising from source precession.

We find a log-Bayes factor of $\log_{10} \mathcal{B} = 5.2$ in favor of a signal model including higher-order spherical harmonics, compared to a model including only contributions from $(\ell, m) = (2, \pm 2)$ modes. A posterior distribution on the SNR ρ_{33} measured in higher-order modes is shown in Figure 5, with $\rho_{33} = 5.9_{-1.1}^{+1.0}$. Random draws from the posterior on ρ_{33} exceed draws from the null distribution over 99.9% of the time. No detection is made of other spherical harmonic modes.

3.2. Properties of GW241110

GW241110 is inferred to have component masses consistent with those of GW241011, albeit with larger uncertainties due to its lower SNR: the primary mass and

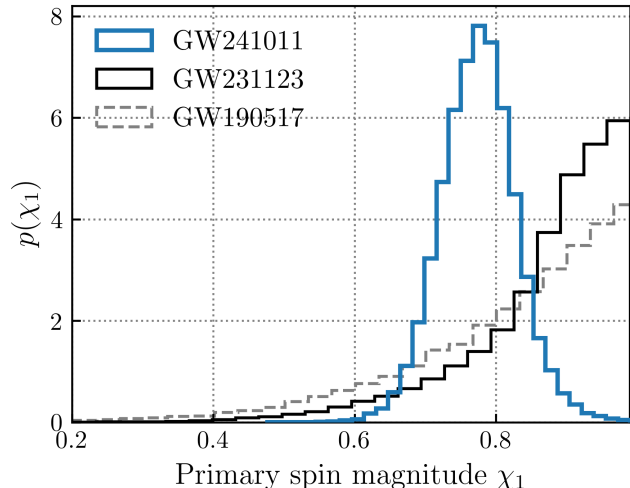


Figure 4. Posterior on the primary spin magnitude of GW241011 (blue). The spin of GW241011’s primary black hole has the largest lower bound than that of all other merging compact objects observed to date. We obtain $\chi_1 > 0.69$ at 95% credibility. For comparison, also shown are the primary spin measurements from GW231123 (black; [Abac et al. 2025c](#)) and GW190517 ([Abbott et al. 2023a](#), dashed grey), which provide the two next-largest lower limits of $\chi_1 > 0.63$ and $\chi_1 > 0.52$, respectively.

mass ratio of GW241110 are measured to be $m_1 = 17.2^{+5.0}_{-4.4} M_\odot$ and $q = 0.45^{+0.32}_{-0.17}$ (see Figure 3). Although GW241110 favors unequal component masses, mass ratios of $q \approx 1$ cannot be fully excluded.

In contrast to GW241011, though, GW241110 is measured to have a primary spin that is likely significantly misaligned with respect to its orbital angular momentum. The angle between the binary’s orbital angular momentum and the spin vector of its more massive black hole is $\theta_1 = 133^{+47}_{-25}$ degrees, with $\theta_1 > 108$ degrees at 90% credibility and $\theta_1 > 90$ degrees at 97.7% credibility. The spin of GW241110’s secondary black hole is unconstrained. GW241110 favors negative effective spin, with $\chi_{\text{eff}} < 0$ at 98.1% credibility. As illustrated in Figure 3, GW241110 inferred mass ratio is strongly anticorrelated with its inferred χ_{eff} and $\chi_{1,z}$. This effect arises from a degeneracy in the post-Newtonian expansion of a compact binary’s phase evolution ([Cutler & Flanagan 1994](#); [Poisson & Will 1995](#); [Baird et al. 2013](#); [Pürrer et al. 2013](#); [Ng et al. 2018](#)). Thus, if one requires GW241110 to have positive χ_{eff} (1.9% probability), it must also be the case that its mass ratio is $q \lesssim 0.3$. If GW241110’s mass ratio is above $q = 0.3$, then the event must have negative χ_{eff} at 99.9% credibility.

GW241110 offers the most significant, although not necessarily conclusive, direct evidence to date that at least some merging black holes have spins antialigned

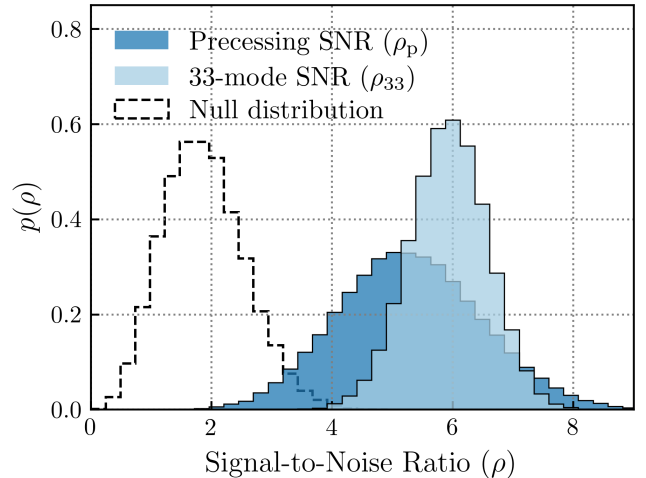


Figure 5. Posterior distribution on GW241011’s precession SNR ratio and its SNR in $(\ell, m) = (3, \pm 3)$ spherical harmonic modes. The precession SNR quantifies the observational strength of spin-orbit precession, while $(\ell, m) = (3, \pm 3)$ mode radiation arises from source multipoles beyond the leading-order mass quadrupole. The unequal mass ratio and large, misaligned primary spin of GW241011 together yield $\rho_p = 5.3^{+2.1}_{-1.9}$ and $\rho_{33} = 5.9^{+1.0}_{-1.1}$. For comparison, the dashed histogram illustrates the expected null distribution (a χ -distribution with four degrees of freedom, two per detector active during GW241011) of ρ_p and ρ_{33} in the absence of spin-orbit precession or higher-order radiation modes ([Prix 2007](#); [Harry & Fairhurst 2011](#)). This null distribution is conservative; in some cases the null distribution may take alternative forms (such as a χ -distribution with fewer degrees of freedom) concentrated towards smaller SNRs ([Fairhurst et al. 2020b](#); [Hoy et al. 2022, 2025](#)).

with their orbital angular momentum. A growing number of binary black holes have been observed with large spin-orbit misalignment angles (with, e.g., $\theta \gtrsim 50$ degrees at high credibility). Several detections, including, e.g., GW231230_170116, GW230723_101834, and GW230609_064958, furthermore favor misalignment angles greater than 90 degrees, but only at $\sim 80\%$ credibilities. ([Abac et al. 2025a](#)). Analysis of the binary black hole GW191109_010717 (GW191109; [Abbott et al. 2023a](#)) with a numerical-relativity surrogate waveform model, meanwhile, found a negative effective inspiral spin at $> 99\%$ credibility ([Islam et al. 2025](#)). The robustness of GW191109’s spin measurement is uncertain, however, due to significant contamination by noise transients ([Abbott et al. 2023a](#)); reanalyses that simultaneously seek to model and subtract these glitches are inconclusive ([Udall et al. 2025](#)). The spin measurement with GW241110, in contrast, is not believed to be subject to data-quality concerns. Under uniform and isotropic spin priors and standard waveform mod-

els, there does remain a 1.9% probability that the source possesses zero or positive effective inspiral spin. The confidence in GW241110’s spin anti-alignment is further bolstered when adopting an astrophysically-informed prior (see Appendix C.2), but we cannot completely exclude the possibility that the source has zero or positive primary spin.

3.3. Relationship with the binary black hole population

Although GW241011 and GW241110 are remarkable for their large and well-measured black hole spins, we do not conclude that they are outliers with respect to the known binary black hole population; see Appendix C for details. These events do, however, individually reinforce conclusions that have been previously drawn only on statistical grounds. Past studies of the binary black hole spin distribution have concluded (*i*) that merging black holes are usually, but not exclusively, slowly rotating, (*ii*) that black hole spins are unlikely to be isotropic, statistically favoring spin–orbit alignment and positive effective spins, but that (*iii*) black hole spins nevertheless exhibit a wide range of spin–orbit misalignment angles, with some component black holes misaligned by nearly or greater than 90 deg with respect to their orbit (Farr et al. 2017, 2018; Abbott et al. 2019; Roulet & Zaldarriaga 2019; Miller et al. 2020; Abbott et al. 2020d, 2023b; Callister et al. 2022; Tong et al. 2022; Vitale et al. 2022; Callister & Farr 2024; Banagiri et al. 2025; Abac et al. 2025d). GW241110 offers the strongest confirmation to date of this latter conclusion. The tension between population-level conclusions and the paucity of individual binary black holes favoring anti-aligned spins can be understood as a confluence of three factors: the large uncertainties typically inherent in spin measurements (van der Sluys et al. 2008; Vitale et al. 2014; Ghosh et al. 2016; Vitale et al. 2017; Chatziioannou et al. 2018; Pratten et al. 2020; Biscoveanu et al. 2021), a degeneracy between mass ratio and spins that asymmetrically biases χ_{eff} measurements towards larger positive values (Cutler & Flanagan 1994; Poisson & Will 1995; Baird et al. 2013; Pürrer et al. 2013; Ng et al. 2018), and selection effects that cause events with larger, positive χ_{eff} to be more readily detected and more precisely characterized (Flanagan & Hughes 1998; Campanelli et al. 2006; Ng et al. 2018). These effects together have been shown to resolve the apparent inconsistency between individual binary black hole properties and statistical population-level conclusions (Hoy et al. 2025; Payne et al. 2024).

While we do not conclude that GW241011 and GW241110 are outliers, it is possible that they are members of an emerging subpopulation of binary black

holes, characterized by low primary masses, unequal mass ratios, and a wide range of spin–orbit misalignment angles. It remains unknown, however, whether such a subpopulation exists and can be formally characterized. This question will be further explored in future work involving additional observations from LIGO–Virgo–KAGRA’s fourth observing run.

4. ASTROPHYSICAL INTERPRETATION AND IMPLICATIONS

4.1. GW241011 and GW241110 through isolated binary evolution

The primary spins of GW241011 and GW241110 are difficult to explain via isolated binary evolution. Efficient angular momentum transport from stellar interiors is predicted to yield black holes that are born slowly rotating (Spruit 1999, 2002; Qin et al. 2018; Fuller & Ma 2019), and torques exerted via mass transfer or tides are expected to coalign residual spin with a binary’s orbital angular momentum (Zaldarriaga et al. 2018; Gerosa et al. 2018; Qin et al. 2018; Bavera et al. 2020, 2021; Ma & Fuller 2023). The natal spins of black holes do remain highly uncertain, however, with the prediction of small spins due to the Spruit–Tayler dynamo being only one of many possibilities (Miller & Miller 2014). Models predicting larger natal spins may better accommodate the observed source properties of GW241011 and GW241110.

Alternative scenarios can also potentially explain the spin properties of GW241011 and GW241110 in the context of isolated binary evolution. Stochastic spin-up of stellar cores immediately preceding core collapse could impart large and misaligned birth spins to black holes (Fuller et al. 2014, 2015; Gilkis & Soker 2016; Ma & Fuller 2019; McNeill & Müller 2020; Antoni & Quataert 2022, 2023; Baibhav & Kalogera 2024). Although black hole progenitors are generally predicted to experience small natal kicks due to near-complete fallback accretion (e.g., Fryer et al. 2012; Zevin et al. 2017; Mandel & Müller 2020; Vigna-Gómez et al. 2024), stronger-than-expected natal kicks and/or asymmetric fallback might misalign spins either by tilting a binary’s orbital plane or by torquing of a black hole’s spin vector (Wongwathanarat et al. 2013; Chan et al. 2020; Janka et al. 2022; Tauris 2022; Burrows et al. 2024); spin–orbit misalignment among some black hole X-ray binaries may provide evidence for such effects (Zdziarski et al. 2018; Salvesen & Pokawanvit 2020; Poutanen et al. 2022; Zdziarski et al. 2023). Finally, the von Zeipel–Lidov–Kozai mechanism (von Zeipel 1910; Lidov 1962; Kozai 1962) due to a tertiary companion can, when coupled to relativistic spin–orbit precession and gravitational-wave emis-

sion, tilt the orbital plane as well as component spins to yield a large spin-orbit misalignment (Liu & Lai 2017; Antonini et al. 2018; Liu & Lai 2018; Fragione & Kocsis 2020; Liu et al. 2019; Yu et al. 2020; Stegmann & Klencki 2025); however, this mechanism does not explain large spin *magnitudes*.

4.2. *GW241011 and GW241110 as hierarchical mergers*

A more natural interpretation for GW241011 and GW241110 is that they involve the mergers of second-generation black holes in dense stellar environments, such as globular, nuclear, and young massive star clusters (Portegies Zwart et al. 2010; Neumayer et al. 2020). Compact binaries merging within clusters yield remnants that may be retained by the cluster, continue to interact dynamically, and themselves participate in subsequent mergers driven by gravitational wave emission (e.g., Lee 2001; O’Leary et al. 2006; Miller & Lauburg 2009; Giersz et al. 2015; Antonini & Rasio 2016; Rodriguez et al. 2019; Doctor et al. 2021; Fragione et al. 2022; Mahapatra et al. 2021; Rizzuto et al. 2022; Atallah et al. 2023; Mahapatra et al. 2025b; Arca Sedda et al. 2023). Such second-generation black holes are systematically more massive than their first-generation ancestors and are expected to be rapidly rotating; the spin distribution of remnant black holes is generically and robustly concentrated about $\chi \approx 0.7$ (Pretorius 2005; Buonanno et al. 2008; Berti & Volonteri 2008). A remnant black hole’s spin arises from the total remaining angular momentum of its ancestral binary at merger, which, for approximately equal-mass mergers, is dominated by the orbital angular momentum. The spin angular momenta of the ancestral black holes do affect the remnant’s spin, but their contribution is, in part, countered by the relationship between spin and inspiral duration. Binaries with larger aligned spins undergo longer inspirals and radiate away more orbital angular momentum, while binaries with small or anti-aligned spins merge more promptly and thus retain more orbital angular momentum (Campanelli et al. 2006).

Observationally, mergers involving second-generation objects (often called hierarchical mergers) would distinguish themselves via their large spin magnitudes, statistically isotropic spin orientations, and mass ratios that are typically less than unity. The spin magnitudes, spin-orbit misalignments, and unequal mass ratios of GW241011 and GW241110 therefore make these signals prime candidates for arising from a hierarchical origin. Figure 6, for example, illustrates predictions for the possible primary spin magnitudes (upper row) and mass ratios (lower row) among binary black hole merg-

ers in dense star clusters. Dashed contours indicate predicted properties of mergers in which both components are first generation black holes, while solid contours correspond to systems in which at least one component is the product of a previous merger. We show data from two models, the CLUSTER MONTE CARLO catalog (CMC; Kremer et al. 2020; Rodriguez et al. 2022) and the CLUSTERBHBDYNAMICS model (CBHBD; Antonini & Gieles 2020a; Antonini et al. 2023); further details regarding both models are provided in Appendix D. The spin magnitude and mass ratio of GW241011, in particular, are inconsistent with the properties predicted of first-generation mergers, but lie within ranges predicted by both models for higher-generation hierarchical mergers. Figure 6 does not, however, convey relative numbers of first-generation and higher-generation mergers; both models predict approximately one higher-generation merger per five first-generation mergers.

Hierarchical black hole mergers are often associated with massive black holes. At sub-solar metallicities, black holes masses are thought to be limited by (pulsational)-pair-instability processes (Barkat et al. 1967; Woosley et al. 2007), preventing the formation of first-generation black holes with masses between ~ 50 and $\sim 120 M_{\odot}$ (e.g., Spera & Mapelli 2017; Woosley & Heger 2021; Hendriks et al. 2023). Hierarchical mergers may yield second-generation remnants with masses situated in this range, and are therefore a possible evolutionary origin for massive systems like the sources of GW190521 (Abbott et al. 2020b) and GW231123_135430 (Abac et al. 2025c). The sources of GW241011 and GW241110 are, in contrast, relatively light. These masses are not inconsistent with a hierarchical origin, however. The three columns of Figure 6 correspond to predictions for clusters of differing stellar metallicities. At high metallicities, stellar winds increasingly strip massive stars of their envelopes, preventing the formation of massive carbon-oxygen cores and reducing the final masses of black holes (e.g., Belczynski et al. 2001; Fryer et al. 2012; Belczynski et al. 2016b; Spera et al. 2016). Therefore, although hierarchical mergers in low-metallicity environments predominantly involve high primary masses, clusters with stellar metallicities $Z \approx 0.1 Z_{\odot}$ and above are predicted to readily yield hierarchical mergers with $\sim 20 M_{\odot}$ primaries, consistent with the sources of GW241011 and GW241110 (Ye et al. 2025).

4.3. *The ancestors of GW241011 and GW241110*

If the primaries of GW241011 and GW241110 are second-generation remnants of previous mergers, we can indirectly constrain the masses, spins, and recoil kicks

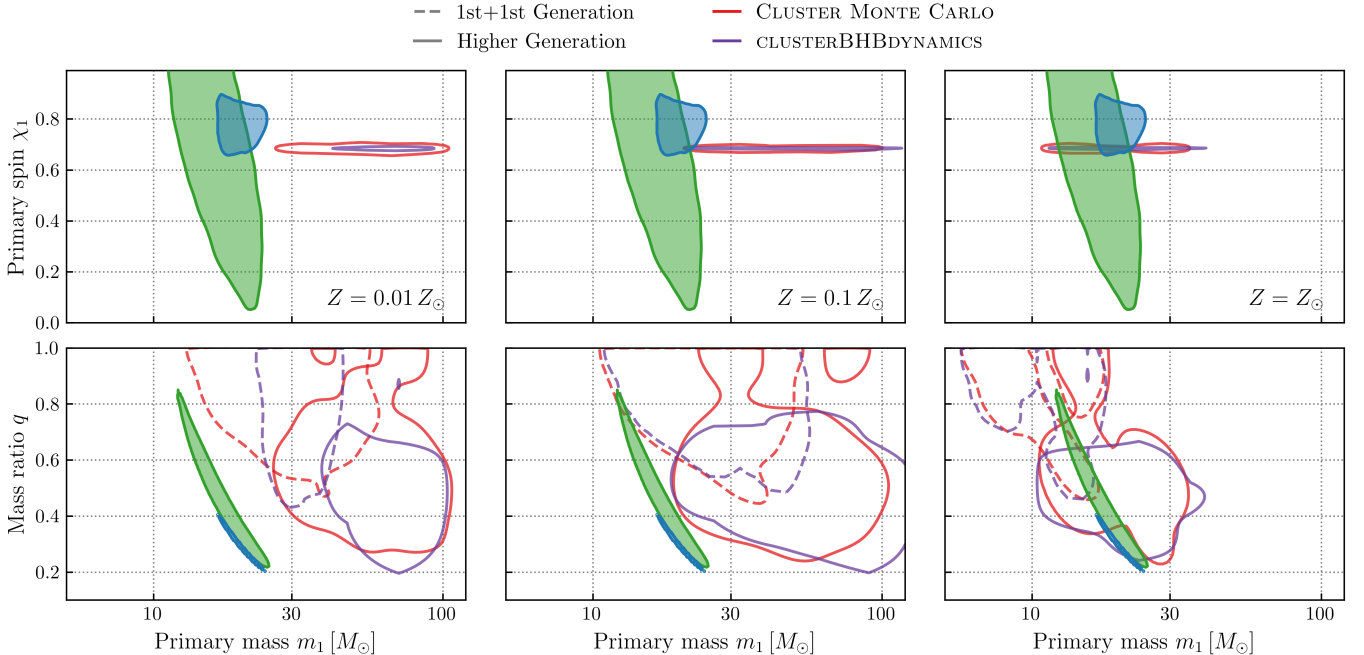


Figure 6. 90% credible bounds on the primary masses, mass ratios, spins of GW241011 (blue) and GW241110 (green), compared to predicted properties of merging black holes in dense star clusters from the CLUSTER MONTE CARLO catalog (Kremer et al. 2020; Rodriguez et al. 2022), and CLUSTERBHB DYNAMICS models (Antonini et al. 2023). Dashed contours correspond to merging first-generation black holes, while solid contours correspond to higher-generation binaries containing remnants from previous mergers. Both models assume black holes to be born non-rotating. The three columns correspond to star cluster simulations with stellar populations at three different metallicities: $Z = 0.01 Z_{\odot}$, $0.1 Z_{\odot}$, and Z_{\odot} . Under the modeling assumptions, the masses of GW241011 and GW241110 appear inconsistent with those predicted in low-metallicity stellar clusters with $Z = 0.01 Z_{\odot}$. Their masses and spins may be consistent, though, with those predicted among hierarchical binary black hole mergers that are formed in clusters of moderate or near-solar metallicities.

associated with their first-generation ancestors (e.g., Baibhav et al. 2021; Barrera & Bartos 2022; Paynter & Thrane 2023; Mahapatra et al. 2024; Araújo-Álvarez et al. 2024; Mahapatra et al. 2025a). We explore this question using two complementary methods. In the first method (the *Forward* approach), we adopt astrophysically-informed priors on the ancestral masses and spins of GW241011 and GW241110’s hypothesized first-generation ancestors. Priors are chosen to follow closely the results from stellar cluster simulations presented in Figure 6, strongly preferring equal masses and first-generation black hole spins near zero; these priors are described in more detail in Appendix E. We then proceed via a hierarchical Bayesian approach, using observed strain data to obtain posteriors on ancestral properties, marginalized over the source properties of GW241011 and GW241110 (Mahapatra et al. 2024). In the second method (the *Backward* approach), we proceed more agnostically. Beginning with the source masses and spins of GW241011 and GW241110’s primaries from Section 3, for each posterior sample we identify an ancestral binary whose remnant mass and spin are consistent, within a small tolerance, with this poste-

rior sample. This approach allows us to construct posteriors on required ancestral properties while preserving the astrophysically-agnostic priors and posteriors on the source properties of GW241011 and GW241110 themselves (Araújo-Álvarez et al. 2024). In both cases, numerical-relativity simulations are used to map between ancestral binaries and remnant properties (Varma et al. 2019).

Figure 7 illustrates the required properties of GW241011 and GW241110’s ancestors estimated in the more agnostic *Backward* approach. We infer a first-generation ancestor of GW241011 to have had masses $13.3^{+4.8}_{-3.2} M_{\odot}$ and $7.5^{+3.2}_{-3.9} M_{\odot}$. A first generation ancestor to GW241110 likely possessed similar masses: $12.3^{+5.6}_{-4.2} M_{\odot}$ and $5.1^{+3.6}_{-1.9} M_{\odot}$. The effective inspiral spin of GW241011’s ancestor is constrained to $\chi_{\text{eff}} = 0.23^{+0.29}_{-0.28}$; larger or smaller values would over- or under-predict, respectively, the observed primary spin χ_1 . The primary spin of GW241110 is measured less precisely and so allows for a broader range of ancestral effective spins: $\chi_{\text{eff}} = -0.04^{+0.65}_{-0.57}$. For both binaries, the remnant recoil kicks are inferred to lie between approximately $100\text{--}2000 \text{ km s}^{-1}$. Constraints on recoil kicks are, how-

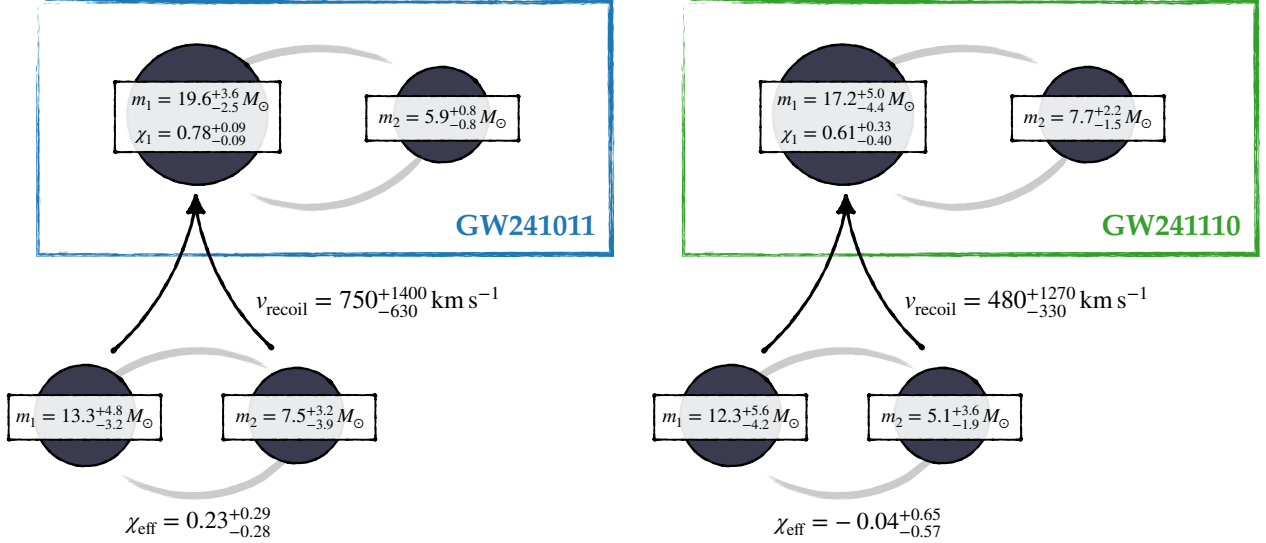


Figure 7. Inferred properties of the first-generation ancestors to the more massive black holes in GW241011 and GW241110, under the hypothesis that these black holes were formed hierarchically from a previous merger. Shown are median and 90% credible bounds inferred on ancestral component masses and effective inspiral spins, as well as the recoil kicks imparted to each remnant black hole due to asymmetric gravitational-wave-emission. We compute ancestral properties in two manners: one (the *Backward* approach) that agnostically retains the same priors and posteriors on GW241011 and GW241110’s source properties as presented in Section 3, and one (the *Forward* approach) that adopts an astrophysically-informed prior on possible ancestral properties. This figure includes results from the agnostic *Backward* approach; constraints obtained under the astrophysically-informed *Forward* approach are described in the text.

ever, almost entirely prior dominated, and it is therefore unclear if they yield meaningful constraints on environmental escape velocities required for successful remnant retention.

In the *Forward* approach, the astrophysically-informed yields posteriors favoring more equal-mass ancestors. The ancestor of GW241011 is inferred to have component masses $11.0^{+1.9}_{-1.6} M_\odot$ and $9.6^{+1.7}_{-1.8} M_\odot$, while GW241110’s ancestor is inferred to have masses $9.6^{+3.1}_{-2.0} M_\odot$ and $8.0^{+2.1}_{-2.3} M_\odot$. The global maximum of the binary black hole mass function is situated at approximately $10 M_\odot$ (Tiwari & Fairhurst 2021; Abbott et al. 2023b; Farah et al. 2023; Abac et al. 2025d); the ancestral black holes of both GW241011 and GW241110 are inferred to lie near this peak. Because the astrophysical prior adopted in the *Forward* approach requires ancestral spins to be near zero, inferred recoil kicks are systematically lower, ranging between approximately $10\text{--}300 \text{ km s}^{-1}$. As in the *Backward* approach above, this range is a consequence of our prior.

A more detailed presentation of both sets of results and additional methodological detail is provided in Appendix E.

4.4. No evidence for eccentricity

Binary black hole coalescences arising dynamically in dense stellar environments may bear unique signatures of orbital eccentricity in their gravitational-wave emission. Gravitational-wave emission rapidly circularizes initially eccentric orbits (Peters 1964), and binaries evolving in isolation are expected to be nearly perfectly quasi-circular by the time their gravitational-wave emission enters the sensitivity band of ground-based detectors. Following many-body encounters in dense clusters, however, binaries can be placed on nearly-hyperbolic trajectories and merge promptly. Several percent of these binaries may retain observable eccentricity in the frequency band of ground-based detectors. In old, metal-poor globular clusters, 5–10% of binary black hole mergers in the local universe are predicted to have eccentricities measurable by the LIGO, Virgo, and KAGRA experiments (Wen 2003; Gültekin et al. 2006; O’Leary et al. 2006; Antonini & Perets 2012; Antonini et al. 2014; Samsing et al. 2018; Samsing & Ramirez-Ruiz 2017; Samsing 2018; Rodriguez et al. 2018a; Zevin et al. 2019), although this may decrease by a factor of a couple when assuming higher initial cluster densities (Antonini & Gieles 2020b). The non-secular evolution of isolated triple systems may yield $\gtrsim 10\%$ of systems with measurable eccentricities, and potentially

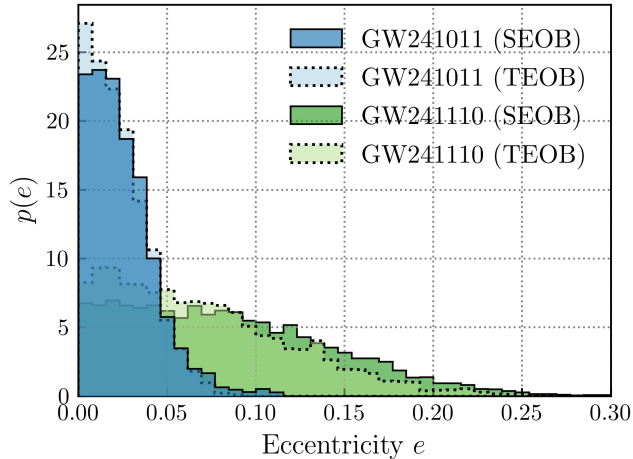


Figure 8. Posteriors on the orbital eccentricity of GW241011 and GW241110. Results are obtained using the SEOBNRv5EHM (Gamboa et al. 2025) and TEOBRESUMS-DALÍ (Nagar et al. 2024) waveform models, and eccentricities are quoted at a reference frequency of 13.33 Hz, when higher-order spherical harmonic modes first enter the observable frequency band. Neither event exhibits evidence for residual eccentricity. We bound $e < 0.05$ at 90% credibility for GW241011 under both waveform models. GW241110, meanwhile, yields 90% credible upper limits of $e < 0.17$ and $e < 0.14$ under the SEOBNRv5EHM and TEOBRESUMS-DALÍ models, respectively.

have a higher merger rate of eccentric sources in the local universe (Dorozsmai et al. 2025). The total merger rate in active galactic nuclei is uncertain with predictions that span multiple orders of magnitude (Gröbner et al. 2020), with predictions for measurably eccentric fraction ranging from $\gtrsim 10\%$ (Tagawa et al. 2021) up to $\sim 70\%$ (Samsing et al. 2022). There exists growing evidence that at least some observed compact binary mergers may possess residual eccentricity (Gayathri et al. 2022; Romero-Shaw et al. 2020a; Gamba et al. 2023; Romero-Shaw et al. 2022; Iglesias et al. 2024; Gupte et al. 2024; Romero-Shaw et al. 2025; Planas et al. 2025; Morras et al. 2025), possibly indicating binary formation in one or more of these environments.

If GW241011 and GW241110 evolved dynamically in dense clusters, they may be prime candidates to exhibit measurable eccentricity. We reanalyze GW241011 and GW241110 using a pair of alternative waveform models, SEOBNRv5EHM (Gamboa et al. 2025) and TEOBRESUMS-DALÍ (Nagar et al. 2024), that describe gravitational-wave emission from eccentric compact binaries through binary inspiral, merger, and ring-down. These waveform models are valid under restricted spin geometries, requiring component spins to be purely parallel or antiparallel to a binary’s orbital

angular momentum. The gravitational-wave signatures of orbital eccentricity and spin-orbit misalignment are known to be degenerate (e.g., Calderón Bustillo et al. 2021; Romero-Shaw et al. 2020a, 2023; Divyajyoti et al. 2024b; Planas et al. 2025). Degeneracies between spin misalignment and eccentricity are weakest for binaries like GW241011 and GW241110 (Romero-Shaw et al. 2023; Divyajyoti et al. 2024b) with low chirp masses, which complete many observable cycles. Nevertheless, eccentricity measurements that neglect effects of spin-orbit precession (or, conversely, spin measurements that neglect eccentricity, as in Section 3) may be biased.

Constraints on the orbital eccentricity of GW241011 and GW241110 are presented in Figure 8. Orbital eccentricity is an evolving function of time; results are quoted at the instant when the binaries’ orbit-averaged quadrupole emission is observed at 13.33 Hz, corresponding to the time at which $\ell = 3$ spherical harmonic modes enter the observable band at 20 Hz. Neither event possesses measurable eccentricity. Under both waveform models, GW241011 is bounded to have $e < 0.05$ at 90% credibility, while GW241110 has $e < 0.17$ and $e < 0.14$ under the SEOBNRv5EHM and TEOBRESUMS-DALÍ models, respectively. This is not inconsistent with a dynamical origin; the vast majority of mergers in clusters are expected to have eccentricities $e \lesssim 0.1$ at frequencies accessible to Advanced LIGO, Advanced Virgo, and KAGRA (Gultekin et al. 2006; O’Leary et al. 2006; Samsing et al. 2014; Samsing 2018; Rodriguez et al. 2018b; Gondán et al. 2018; Zevin et al. 2019; Dall’Amico et al. 2024). On the basis of eccentricity alone, though, we cannot rule out any individual formation scenarios for GW241011 and GW241110. Further details are presented in Appendix B.

5. TESTS OF FUNDAMENTAL PHYSICS

Gravitational waveforms from compact binary coalescences encode detailed information about the nature and internal structure of the merging objects, enabling rigorous tests of general relativity (GR) and fundamental physics. The large primary spin and significant mass asymmetry of GW241011, in particular, makes this event a uniquely powerful probe of the Kerr nature of black holes and the multipolar structure of gravitational-wave emission.

5.1. Black hole spin-induced quadrupole moment

Within GR, rotating and charge-neutral black holes are uniquely described by the Kerr solution (Kerr 1963; Carter 1971). In Kerr spacetime, the black hole spin-induced quadrupole moment, the leading contribution of spin to a black hole spacetime’s multipolar expansion, is

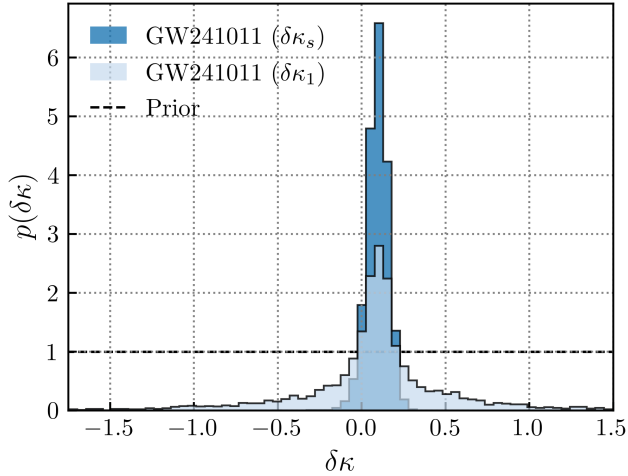


Figure 9. Deviations from the Kerr prediction for the spin-induced quadrupole moment of GW241011’s primary black hole, $\delta\kappa_1$, as well as the deviation $\delta\kappa_s$ in the symmetric combination $\kappa_s = (\kappa_1 + \kappa_2)/2$ (Krishnendu et al. 2017, 2019; Abbott et al. 2021b). We bound $\delta\kappa_1 = 0.10^{+0.82}_{-0.82}$ and $\delta\kappa_s = 0.10^{+0.09}_{-0.11}$, consistent with expectations from GR. The next-most informative event, GW190412 (Abbott et al. 2020d), yielded a constraint $\delta\kappa_s = 0^{+2}_{-91}$ (Divyajyoti et al. 2024a).

given by $Q = -\kappa S^2/(mc^2)$. Here, m is the black hole’s mass, S is its spin angular momentum, c is the speed of light, and $\kappa = 1$ exactly (Hansen 1974). Non-black hole spacetimes, including neutron stars (Laarakkers & Poisson 1999; Pappas & Apostolatos 2012a,b; Harry & Hinderer 2018), boson stars (Ryan 1997; Herdeiro & Radu 2014; Baumann et al. 2019; Chia & Edwards 2020), and other exotic compact objects, may in contrast exhibit significantly different values of κ owing to differences in internal structure and composition. Gravitational-wave sources containing rapidly-spinning black holes enable direct measurements of the spin-induced quadrupole moment and tests of the Kerr hypothesis (Arun et al. 2009; Mishra et al. 2016); any measured deviation from $\kappa = 1$ would strongly suggest the presence of non-black hole constituents or indicate new physics beyond the predictions of GR.

We define $\kappa_1 = 1 + \delta\kappa_1$ and $\kappa_2 = 1 + \delta\kappa_2$ as the spin-induced quadrupole coefficients of each compact object in GW241011’s source binary. We repeat parameter estimation with a modified IMRPHENOMXPHM waveform model (Pratten et al. 2021), allowing for non-zero $\delta\kappa_1$ and $\delta\kappa_2$ (Divyajyoti et al. 2024a). The resulting posterior is shown in Fig. 9. The spin-induced quadrupole coefficient of GW241011’s primary deviates from the Kerr prediction by $\delta\kappa_1 = 0.10^{+0.82}_{-0.82}$, consistent with GR (constraints on $\delta\kappa_2$ are uninformative). This is the most stringent constraint to date on the spin-induced

quadrupole of a compact object. The constraints offered by GW241011 on $\delta\kappa_1$ are unusual, enabled by the event’s high SNR, large primary spin, and unequal mass ratio. Typically, gravitational-wave signals primarily constrain only the symmetric combination $\kappa_s = (\kappa_1 + \kappa_2)/2$ (Krishnendu et al. 2017, 2019; Abbott et al. 2021b; Divyajyoti et al. 2024a). GW241011 constrains this symmetric combination to be within $\delta\kappa_s = 0.10^{+0.09}_{-0.11}$ of the Kerr hypothesis, under the assumption that $\kappa_1 = \kappa_2$. The previous best constraint on κ_s was obtained from the binary black hole GW190412 (Divyajyoti et al. 2024a), which gave $\delta\kappa_s = 0^{+2}_{-91}$. GW241011 improves on this constraint by approximately three orders of magnitude. A different implementation for the estimation of the spin-induced quadrupole moment, utilizing the SEOBNRv5HM_ROM (Pompili et al. 2023) waveform model, yields consistent results and is discussed in Appendix F.1.

Measurement of GW241011’s spin-induced quadrupole moment may rule out a wide range of exotic compact objects or black hole mimickers. Massive boson star models (Ryan 1997; Pacilio et al. 2020) predict spin-induced quadrupole moment parameters of order ~ 10 – 150 for self-interacting spinning boson stars with quadratic coupling. The measurement of $\delta\kappa_s \leq 0.17$ at 90% credibility from GW241011 likely rules out all the massive boson star models described in e.g. Pacilio et al. (2020). Other models, such as minimal boson stars (Kaup 1968; Ruffini & Bonazzola 1969; Vaglio et al. 2022) and solitonic boson stars (Friedberg et al. 1987), remain poorly understood in terms of their spin-induced multipole moments (Cardoso et al. 2017; Cardoso & Pani 2019). Another class of exotic compact objects are the gravastars (Mottola 2023), where the spin-induced multipole moments can take negative values due to the prolate deformation induced by their spinning motion. Although spin-induced quadrupole moment values have been predicted for thin-shell gravastar models (Uchikata & Yoshida 2016), the GW241011 data is insufficient to make definitive conclusions.

5.2. Radiation beyond the quadrupole approximation

Gravitational-wave radiation may be generically decomposed into an expansion over spin-weight -2 spherical harmonics, $_{-2}Y_{lm}$. The gravitational waves from merging compact binaries are dominated by the $(\ell, m) = (2, \pm 2)$ spherical harmonic, sourced by a binary’s mass quadrupole moment. As discussed in Section 3, however, GW241011 exhibits significant radiation in the $(\ell, m) = (3, \pm 3)$ mode sourced by the current quadrupole and mass octupole moments. General relativity fixes the relative amplitudes of gravitational radiation received

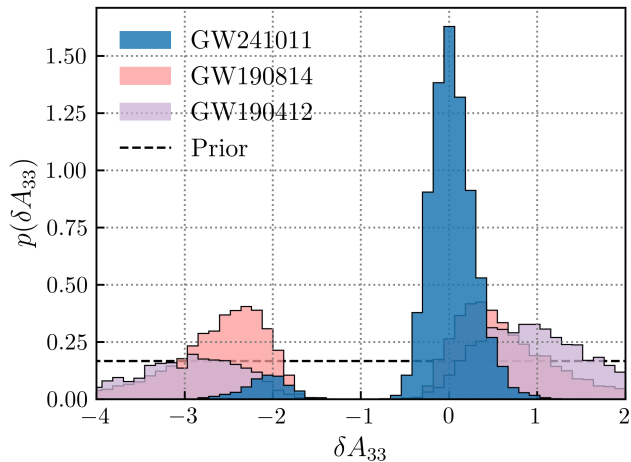


Figure 10. Posterior constraints on the amplitude of GW241011’s gravitational radiation in $(\ell, m) = (3, \pm 3)$ spherical harmonic modes, relative to the prediction from GR. GW241011 is consistent with expectation, with deviations from the GR limited to the interval $-1.9 \leq \delta A_{33} \leq 0.5$ at 90% credibility. Degeneracy with orbital inclination yields a strongly bimodal structure in the posterior for δA_{33} . The dominant mode has $\delta A_{33} = 0.0^{+0.5}_{-0.3}$, consistent with GR, while the subdominant mode has $\delta A_{33} = -2.1^{+0.4}_{-0.5}$. For comparison, also shown are the posteriors obtained from the next-most-informative gravitational-wave events, GW190814 and GW190412 (Abbott et al. 2020d,c; Puecher et al. 2022; Abac et al. 2025g).

in different spherical harmonic modes. The strong detection of multiple modes in a gravitational-wave signal, as in GW241011, offers an opportunity to test these predictions (Capano & Nitz 2020; Puecher et al. 2022; Mahapatra 2024; Abac et al. 2025g).

We repeat inference on the properties of GW241011, but now introduce a parameter δA_{33} that allows for deviations in the signal’s $(\ell, m) = (3, \pm 3)$ mode amplitudes, relative to the $(2, \pm 2)$ mode content (Puecher et al. 2022; Abac et al. 2025g). Higher-order modes, such as $(4, \pm 4)$ spherical harmonics, are not detected in GW241011, and so are not tested here. The resulting posterior distribution on δA_{33} is shown in Figure 10. Posteriors on δA_{33} are characteristically bimodal, due to degeneracies between a binary’s inclination, orbital phase, and expected $(3, \pm 3)$ mode amplitude (Mills & Fairhurst 2021; Puecher et al. 2022). The dominant mode is consistent with GR, with $\delta A_{33} = 0.0^{+0.5}_{-0.3}$, while the subdominant mode has $\delta A_{33} = -2.1^{+0.4}_{-0.5}$. Taking both posterior modes together, we find $-1.9 \leq \delta A_{33} \leq 0.5$ at 90% credibility. This is the best measurement to date of δA_{33} . Among binaries in GWTC-4, the next-best constraints are provided by GW190814 and GW190412 (Abbott et al. 2020d,c; Puecher et al. 2022),

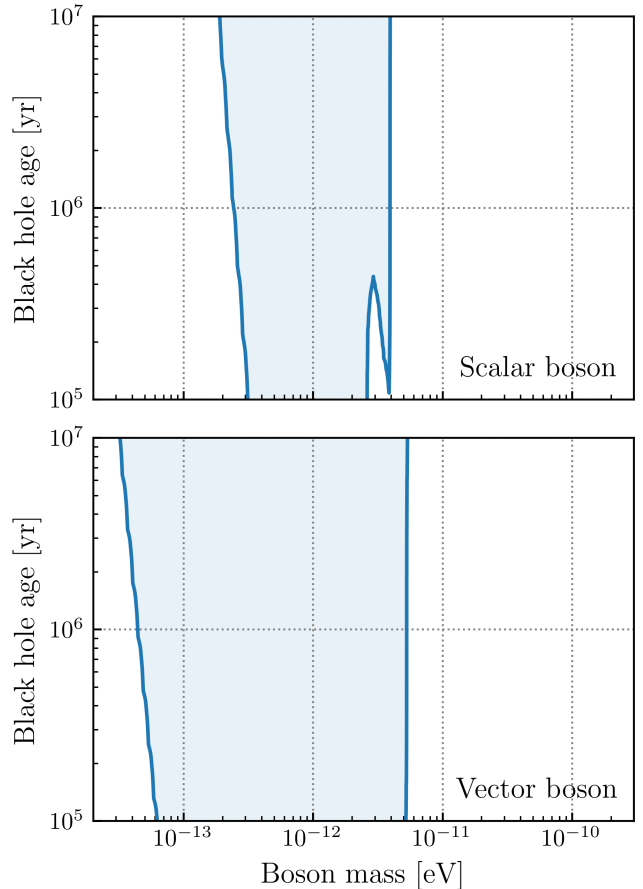


Figure 11. Masses of novel ultralight scalar (top) and vector (bottom) bosons that are excluded at 90% credibility by the non-zero spin measurements of GW241011. If bosons with masses lying in the shaded regions existed, then the primary black hole of GW241011 would have undergone the superradiance instability, spontaneously generating a cloud of bound boson particles and driving the black holes’ spins below their observed values. The superradiance instability can deplete a black hole’s spin over an astrophysically-brief timescale, but this timescale becomes significantly longer outside a narrow range of boson masses. The exclusion curves therefore depend on the presumed age of GW241011’s primary black hole.

which give $-3.6 \leq \delta A_{33} \leq 1.6$ and $-5.3 \leq \delta A_{33} \leq 4.0$, respectively (Abac et al. 2025g). GW241011 therefore confirms that gravitational waves radiated in $(3, \pm 3)$ spherical harmonic modes have amplitudes consistent with expectations from GR. Further details are elaborated in Appendix F.2.

5.3. Ultralight bosons

Spinning black holes may prodigiously and spontaneously source particle production through the superradiant instability mechanism (Press & Teukolsky 1972; Damour et al. 1976; Brito et al. 2015a). Ingoing waves

may acquire energy as they scatter off a rotating black hole. In the vicinity of a rotating black hole, an oscillating, gravitationally bound fluctuation in a bosonic field may grow exponentially, spontaneously turning an initially small perturbation into a macroscopic boson cloud surrounding the black hole. Cloud growth is powered at the expense of the black hole’s rotational energy and may occur on timescales as short as days or minutes. This superradiance instability is specifically relevant for bosons with Compton wavelengths comparable to the black hole’s size. If m_b is the boson mass, G is the gravitational constant, and M the black hole’s mass, then superradiance requires $m_b \sim \hbar c^2 / (GM)$. Thus, the observation of a rapidly-rotating black hole of mass M immediately excludes the existence of novel bosons with masses near m_b ; if such a particle existed, it should have long since depleted the black hole’s spin. Constraints can, in principle, be performed using both electromagnetic and gravitational-wave observations, and for both supermassive and stellar-mass black holes (e.g., Arvanitaki et al. 2010; Arvanitaki & Dubovsky 2011; Pani et al. 2012; Baryakhtar et al. 2017; Fernandez et al. 2019; Ng et al. 2021a,b; Stott 2020).

The confidently rapid primary spin of GW241011 excludes the existence of ultralight bosons with masses between approximately 10^{-13} and 3×10^{-12} eV. Figure 11 shows the boson masses excluded by the primary spin measurement of GW241011, as a function of the presumed age of each binary’s primary black hole and computed using the SUPERRAD package (Siemonsen et al. 2023; May et al. 2025); see Appendix F.3 for details. The top and bottom panels correspond to scalar and vector bosons, respectively. The filled contours indicate regions in which the primaries of both binaries should have undergone the superradiance instability, yielding final present-day spins that are inconsistent with observation at 90% credibility. Since all relevant azimuthal modes are included for the black hole ages considered, the narrow exclusion region near 4×10^{-12} eV in the scalar case arises from cloud growth with a higher azimuthal number $m = 3$. Conservatively assuming an age of 10^5 years for the primary black hole of GW241011, this signal excludes the existence of scalar bosons with masses in the interval $[0.3, 2.6] \times 10^{-12}$ eV. The signal excludes vector bosons, meanwhile, with masses in the $[0.1, 5.3] \times 10^{-12}$ eV interval. Due to its more uncertain spin measurements, GW241110 does not appreciably constrain the existence of ultralight bosons.

GW241011 rules out the existence of bosons at higher masses than those excluded by previous gravitational-wave observations. An analysis considering the population of black holes comprising the LIGO–Virgo–

KAGRA GWTC-2 catalog strongly disfavored scalar boson masses between $[2.2, 2.7] \times 10^{-13}$ eV when assuming 10^5 year old black holes (Ng et al. 2021b). Under the same age assumption, recent analysis using GW231123 and GW190517 excluded scalar and vector boson masses in the intervals $[0.6, 11] \times 10^{-13}$ and $[0.1, 18] \times 10^{-13}$ eV, respectively, at 90% credibility (Aswathi et al. 2025). A complementary analysis of GW231123 with a relativistic model for self-interacting scalars excludes axion masses in the interval $[0.6, 5] \times 10^{-13}$ eV with decay constants $\gtrsim 10^{14}$ GeV (Caputo et al. 2025).

6. CONCLUSIONS

In this paper, we have presented gravitational-wave signals from two binary black hole coalescences – GW241011 and GW241110 – discovered during the second part of the fourth observing run of the LIGO, Virgo, and KAGRA observatories. The measured properties of these events naturally suggest consideration as a pair. The spins of the more massive black holes in GW241011 and GW241110 are respectively situated at either extreme of the binary black hole population. The primary black hole of GW241011 possesses one of the largest and most precisely measured black hole spins observed via gravitational waves, and is spinning in a direction primarily (but not exactly) aligned with its orbital angular momentum. Conversely, the primary black hole of GW241110 is rapidly spinning in a direction confidently antiparallel to its orbit, the first confidently anti-aligned black hole spin measured to date. At the same time, these two binary black holes exhibit nearly identical masses, with each event favoring a primary mass in the range $15\text{--}20 M_\odot$ and an unequal mass ratio between their component black holes.

Taken together, the mass ratios, large primary spins, and significant spin-orbit misalignment angles of GW241011 and GW241110 are strongly suggestive of hierarchical binary black hole mergers in dense stellar environments, such as globular, nuclear, or young stellar clusters. Under this interpretation, the primary black holes of both binaries are themselves the remnants of past black hole mergers. However, although the properties of GW241011 and GW241110 are in strong tension with predictions from isolated binary evolution, from gravitational-wave data alone we cannot rule out formation by massive stellar binaries (or systems of higher multiplicity). GW241011 and GW241110 nevertheless suggest that at least some merging binary black holes merge dynamically in dense environments, and that these environments are sufficiently massive to retain remnant black holes and foster repeated mergers.

The large and precisely measured primary spin of GW241011 furthermore enables myriad tests of fundamental physics. In particular, we find that this event provides the best measurements to date of a black hole’s spin induced quadrupole moment, confirming the Kerr prediction to within a factor of two (or to within 10%, depending on the parametrization used, an improvement in precision by two orders of magnitude; see Section 5.1). The nature of this test is independent from and complementary to the ringdown spectroscopy performed on the extremely loud event GW250114; analysis of GW250114’s ringdown identified overtones with frequencies constrained to within 30% of their Kerr predictions (Abac et al. 2025f,h). GW241011’s strong radiation in multiple spherical harmonic modes furthermore enables the best constraint to date on the relative amplitudes of $(\ell, m) = (2, \pm 2)$ and $(3, \pm 3)$ modes, confirming the expected structure of gravitational-wave emission beyond the quadrupole approximation. Finally, the large spins of both GW241011 and GW241110 rule out the existence of novel boson particles with masses in the range 10^{-13} to 10^{-12} eV.

Growing gravitational-wave catalogs, enabled by the concurrent operation of increasingly sensitive gravitational-wave observatories, continue to yield individually-interesting sources that expand our knowledge of the compact binary landscape. Gravitational waves detected during the fourth observing run of the LIGO, Virgo, and KAGRA observatories have thus far enabled novel tests of relativity and gravitational-waveform models (Abac et al. 2025i,f,h) and provided sources in new and unexpected regions of parameter space (Abac et al. 2024, 2025c). We expect discoveries to continue through the remainder of the fourth LIGO–Virgo–KAGRA observing run and beyond.

ACKNOWLEDGMENTS

This material is based upon work supported by NSF’s LIGO Laboratory, which is a major facility fully funded by the National Science Foundation. The authors also gratefully acknowledge the support of the Science and Technology Facilities Council (STFC) of the United Kingdom, the Max-Planck-Society (MPS), and the State of Niedersachsen/Germany for support of the construction of Advanced LIGO and construction and operation of the GEO 600 detector. Additional support for Advanced LIGO was provided by the Australian Research Council. The authors gratefully acknowledge the Italian Istituto Nazionale di Fisica Nucleare (INFN), the French Centre National de la Recherche Scientifique (CNRS) and the Netherlands Organization for Scientific Research (NWO) for the construction and opera-

tion of the Virgo detector and the creation and support of the EGO consortium. The authors also gratefully acknowledge research support from these agencies as well as by the Council of Scientific and Industrial Research of India, the Department of Science and Technology, India, the Science & Engineering Research Board (SERB), India, the Ministry of Human Resource Development, India, the Spanish Agencia Estatal de Investigación (AEI), the Spanish Ministerio de Ciencia, Innovación y Universidades, the European Union NextGenerationEU/PRTR (PRTR-C17.I1), the ICSC - Centro Nazionale di Ricerca in High Performance Computing, Big Data and Quantum Computing, funded by the European Union NextGenerationEU, the Comunitat Autònoma de les Illes Balears through the Conselleria d’Educació i Universitats, the Conselleria d’Innovació, Universitats, Ciència i Societat Digital de la Generalitat Valenciana and the CERCA Programme Generalitat de Catalunya, Spain, the Polish National Agency for Academic Exchange, the National Science Centre of Poland and the European Union - European Regional Development Fund; the Foundation for Polish Science (FNP), the Polish Ministry of Science and Higher Education, the Swiss National Science Foundation (SNSF), the Russian Science Foundation, the European Commission, the European Social Funds (ESF), the European Regional Development Funds (ERDF), the Royal Society, the Scottish Funding Council, the Scottish Universities Physics Alliance, the Hungarian Scientific Research Fund (OTKA), the French Lyon Institute of Origins (LIO), the Belgian Fonds de la Recherche Scientifique (FRS-FNRS), Actions de Recherche Concertées (ARC) and Fonds Wetenschappelijk Onderzoek - Vlaanderen (FWO), Belgium, the Paris Île-de-France Region, the National Research, Development and Innovation Office of Hungary (NKFIH), the National Research Foundation of Korea, the Natural Sciences and Engineering Research Council of Canada (NSERC), the Canadian Foundation for Innovation (CFI), the Brazilian Ministry of Science, Technology, and Innovations, the International Center for Theoretical Physics South American Institute for Fundamental Research (ICTP-SAIFR), the Research Grants Council of Hong Kong, the National Natural Science Foundation of China (NSFC), the Israel Science Foundation (ISF), the US-Israel Binational Science Fund (BSF), the Leverhulme Trust, the Research Corporation, the National Science and Technology Council (NSTC), Taiwan, the United States Department of Energy, and the Kavli Foundation. The authors gratefully acknowledge the support of the NSF, STFC, INFN and CNRS for provision of computational resources. This work was supported by MEXT,

the JSPS Leading-edge Research Infrastructure Program, JSPS Grant-in-Aid for Specially Promoted Research 26000005, JSPS Grant-in-Aid for Scientific Research on Innovative Areas 2402: 24103006, 24103005, and 2905: JP17H06358, JP17H06361 and JP17H06364, JSPS Core-to-Core Program A. Advanced Research Networks, JSPS Grants-in-Aid for Scientific Research (S) 17H06133 and 20H05639, JSPS Grant-in-Aid for Transformative Research Areas (A) 20A203: JP20H05854, the joint research program of the Institute for Cosmic Ray Research, University of Tokyo, the National Research Foundation (NRF), the Computing Infrastructure Project of the Global Science experimental Data hub Center (GSDC) at KISTI, the Korea Astronomy and Space Science Institute (KASI), the Ministry of Science and ICT (MSIT) in Korea, Academia Sinica (AS), the AS Grid Center (ASGC) and the National Science and Technology Council (NSTC) in Taiwan under grants including the Science Vanguard Research Program, the Advanced Technology Center (ATC) of NAOJ, and the Mechanical Engineering Center of KEK.

We are grateful for the valuable feedback provided by anonymous reviewers. Additional acknowledgements for support of individual authors may be found in the following document:

<https://dcc.ligo.org/LIGO-M2300033/public>. For the purpose of open access, the authors have applied a Creative Commons Attribution (CC BY) license to any Author Accepted Manuscript version arising. We request that citations to this article use ‘A. G. Abac *et al.* (LIGO-Virgo-KAGRA Collaboration), ...’ or similar phrasing, depending on journal convention.

Software: Calibration of the LIGO strain data was performed with a GSTLAL-based calibration software pipeline (Viets *et al.* 2018). Data-quality products and event-validation results were computed using the DMT (Zweizig, J. 2006), DQR (LIGO Scientific Collaboration and Virgo Collaboration 2018), DQSEGDB (Fisher *et al.* 2021), gwdechar (Macleod *et al.* 2025), hveto (Smith *et al.* 2011), iDQ (Essick *et al.* 2020), Omicron (Robinet *et al.* 2020), and PythonVirgoTools (Virgo Collaboration 2021) software packages

and contributing software tools. Analyses in this catalog relied on software from the LVK Algorithm Library Suite (LIGO Scientific, Virgo, and KAGRA Collaboration 2018; Wette 2020). The detection of the signals and subsequent significance evaluations were performed with the GSTLAL-based inspiral software pipeline (Messick *et al.* 2017; Sachdev *et al.* 2019; Hanna *et al.* 2020; Cannon *et al.* 2021; Sakon *et al.* 2024; Ewing *et al.* 2024; Tsukada *et al.* 2023; Ray *et al.* 2023; Joshi *et al.* 2025a,b), with the MBTA pipeline (Adams *et al.* 2016; Aubin *et al.* 2021; All  n   *et al.* 2025), and with the PyCBC (Usman *et al.* 2016; Nitz 2018; Nitz *et al.* 2017; Dal Canton *et al.* 2021; Davies *et al.* 2020) packages. Estimates of the noise spectra and glitch models were obtained using BAYESWAVE (Cornish & Littenberg 2015; Littenberg & Cornish 2015; Littenberg *et al.* 2016; Cornish *et al.* 2021; Gupta & Cornish 2024). Low-latency source localization was performed using BAYESTAR (Singer & Price 2016). Source-parameter estimation was performed with the BILBY library (Ashton *et al.* 2019; Romero-Shaw *et al.* 2020b), using the DYNesty nested sampling package (Speagle 2020), and the RIFT (Pankow *et al.* 2015; Lange *et al.* 2017; Wysocki *et al.* 2019) package. SEOBNRv5PHM waveforms used in parameter estimation were generated using pySEOBNR (Mihaylov *et al.* 2023). PESummary was used to post-process and collate parameter estimation results (Hoy & Raymond 2021). The various stages of the parameter estimation analysis were managed with the Asimov library (Williams *et al.* 2023). Population inference was performed with the GWPOPULATION package (Talbot *et al.* 2025). The SUPERRAD package (Siemonsen *et al.* 2023; May *et al.* 2025) was used to characterize superradiance phenomena. Plots were prepared with MATPLOTLIB (Hunter 2007). NUMPY (Harris *et al.* 2020) and SCIPY (Virtanen *et al.* 2020) were used for analyses in the manuscript.

Data availability: Strain data from the LIGO and Virgo observatories associated with GW241011 and GW241110 are available from the Gravitational Wave Open Science Center. Datasets generated as part of this study, including posterior samples on the source properties of both events, are available on Zenodo, together with notebooks reproducing figures in this paper (LIGO Scientific, Virgo, and KAGRA Collaboration 2025).

APPENDIX

A. SOURCE PARAMETER ESTIMATION: FURTHER RESULTS AND DETAILS

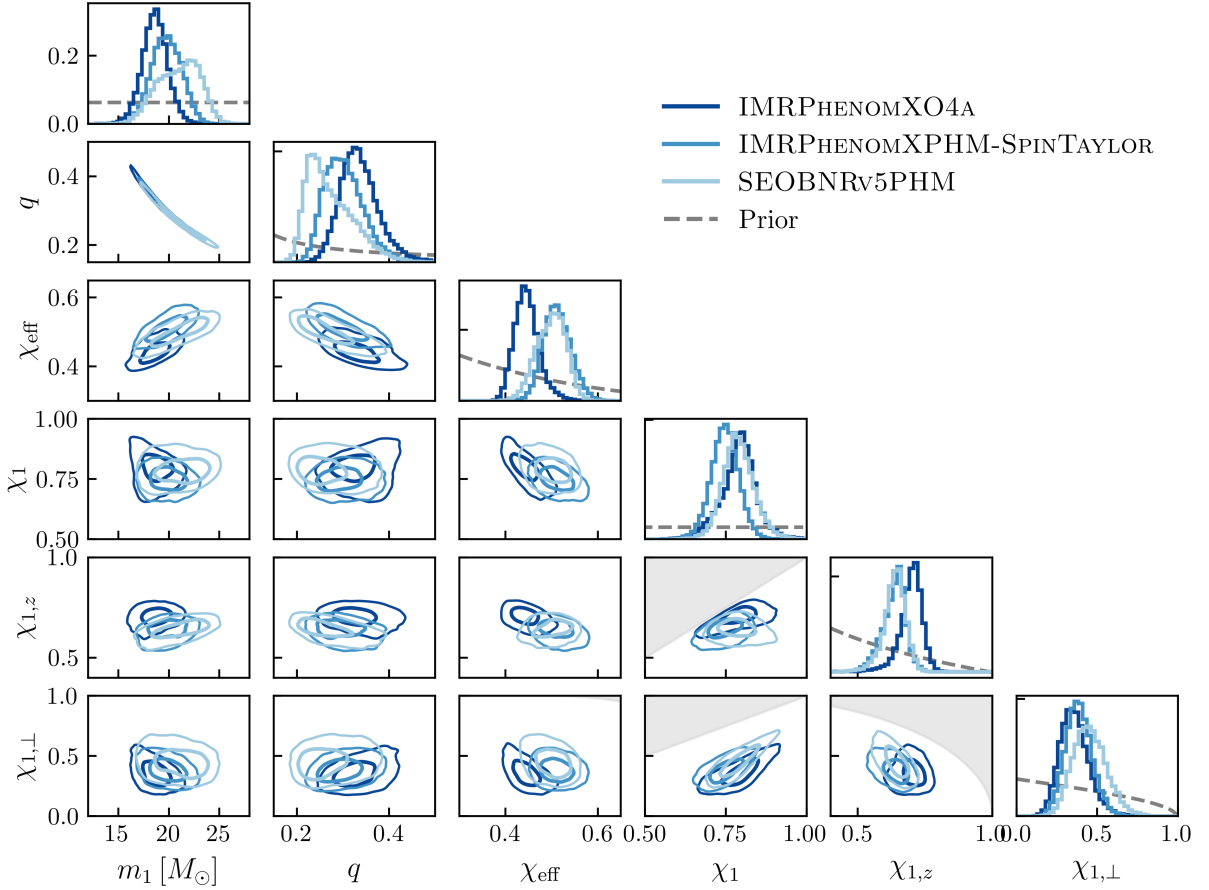
Results quoted in the main text are given by the union of posterior samples under three different gravitational waveform models: SEOBNRv5PHM (SEOBNR; Ramos-Buades *et al.* 2023a), IMRPHENOMXPHM-SPINTAYLOR (XPHM; Pratten *et al.* 2021; Colleoni *et al.* 2025) and IMRPHENOMXO4A (XO4A; Thompson *et al.*

Table 2. Inferred source properties of GW241011 under different waveform models.

Waveform	$m_1 [M_\odot]$	$m_2 [M_\odot]$	q	$\mathcal{M} [M_\odot]$	$D_L [\text{Mpc}]$	χ_1	$\theta_1 [\text{deg}]$	$\chi_{1,z}$	$\chi_{1,\perp}$	χ_{eff}	χ_{p}
SEOBNRv5PHM	$21.1^{+2.8}_{-3.6}$	$5.5^{+0.9}_{-0.5}$	$0.26^{+0.11}_{-0.05}$	$9.0^{+0.1}_{-0.1}$	225^{+39}_{-40}	$0.79^{+0.09}_{-0.08}$	35^{+11}_{-14}	$0.64^{+0.06}_{-0.08}$	$0.45^{+0.19}_{-0.15}$	$0.50^{+0.05}_{-0.06}$	$0.45^{+0.19}_{-0.15}$
IMRPHENOMXPHM-ST	$19.8^{+2.4}_{-2.4}$	$5.9^{+0.7}_{-0.5}$	$0.30^{+0.08}_{-0.06}$	$9.1^{+0.1}_{-0.1}$	214^{+41}_{-43}	$0.75^{+0.07}_{-0.07}$	31^{+10}_{-12}	$0.64^{+0.06}_{-0.09}$	$0.38^{+0.15}_{-0.13}$	$0.51^{+0.05}_{-0.04}$	$0.38^{+0.15}_{-0.13}$
IMRPHENOMXO4A	$18.6^{+2.1}_{-2.1}$	$6.2^{+0.7}_{-0.5}$	$0.33^{+0.08}_{-0.06}$	$9.1^{+0.1}_{-0.1}$	201^{+44}_{-46}	$0.79^{+0.08}_{-0.10}$	27^{+9}_{-12}	$0.70^{+0.05}_{-0.08}$	$0.35^{+0.17}_{-0.13}$	$0.44^{+0.05}_{-0.04}$	$0.35^{+0.17}_{-0.13}$

Table 3. Inferred source properties of GW241110 under different waveform models.

Waveform	$m_1 [M_\odot]$	$m_2 [M_\odot]$	q	$\mathcal{M} [M_\odot]$	$D_L [\text{Mpc}]$	χ_1	$\theta_1 [\text{deg}]$	$\chi_{1,z}$	$\chi_{1,\perp}$	χ_{eff}	χ_{p}
SEOBNRv5PHM	$17.4^{+5.1}_{-4.7}$	$7.7^{+2.3}_{-1.5}$	$0.44^{+0.33}_{-0.17}$	$9.8^{+0.5}_{-0.4}$	736^{+277}_{-280}	$0.59^{+0.34}_{-0.39}$	133^{+47}_{-26}	$-0.37^{+0.34}_{-0.38}$	$0.39^{+0.34}_{-0.29}$	$-0.27^{+0.23}_{-0.20}$	$0.40^{+0.33}_{-0.26}$
IMRPHENOMXPHM	$17.2^{+5.0}_{-4.5}$	$7.7^{+2.2}_{-1.5}$	$0.45^{+0.33}_{-0.17}$	$9.9^{+0.5}_{-0.4}$	738^{+263}_{-261}	$0.58^{+0.35}_{-0.39}$	132^{+48}_{-26}	$-0.37^{+0.33}_{-0.38}$	$0.39^{+0.34}_{-0.29}$	$-0.27^{+0.22}_{-0.20}$	$0.40^{+0.33}_{-0.26}$
IMRPHENOMXO4A	$16.9^{+4.9}_{-4.2}$	$7.8^{+2.1}_{-1.6}$	$0.46^{+0.31}_{-0.17}$	$9.8^{+0.5}_{-0.4}$	731^{+268}_{-260}	$0.65^{+0.30}_{-0.41}$	133^{+47}_{-22}	$-0.43^{+0.35}_{-0.35}$	$0.43^{+0.32}_{-0.32}$	$-0.30^{+0.22}_{-0.20}$	$0.45^{+0.31}_{-0.29}$

**Figure 12.** Posterior on the source properties of GW241011 under each individual waveform model considered. Different waveform models yield qualitatively similar conclusions, although waveforms exhibit non-negligible systematic differences due to the strong precession and unequal masses of the source binary.

2024). Although all of these models describe quasi-circular precessing binaries and include higher-order multipole moments, they differ in the approach used to model the waveforms. The SEOBNR, XPHM, and XO4A models are each constructed from a combination of analytical and numerical information. They offer a complete description of

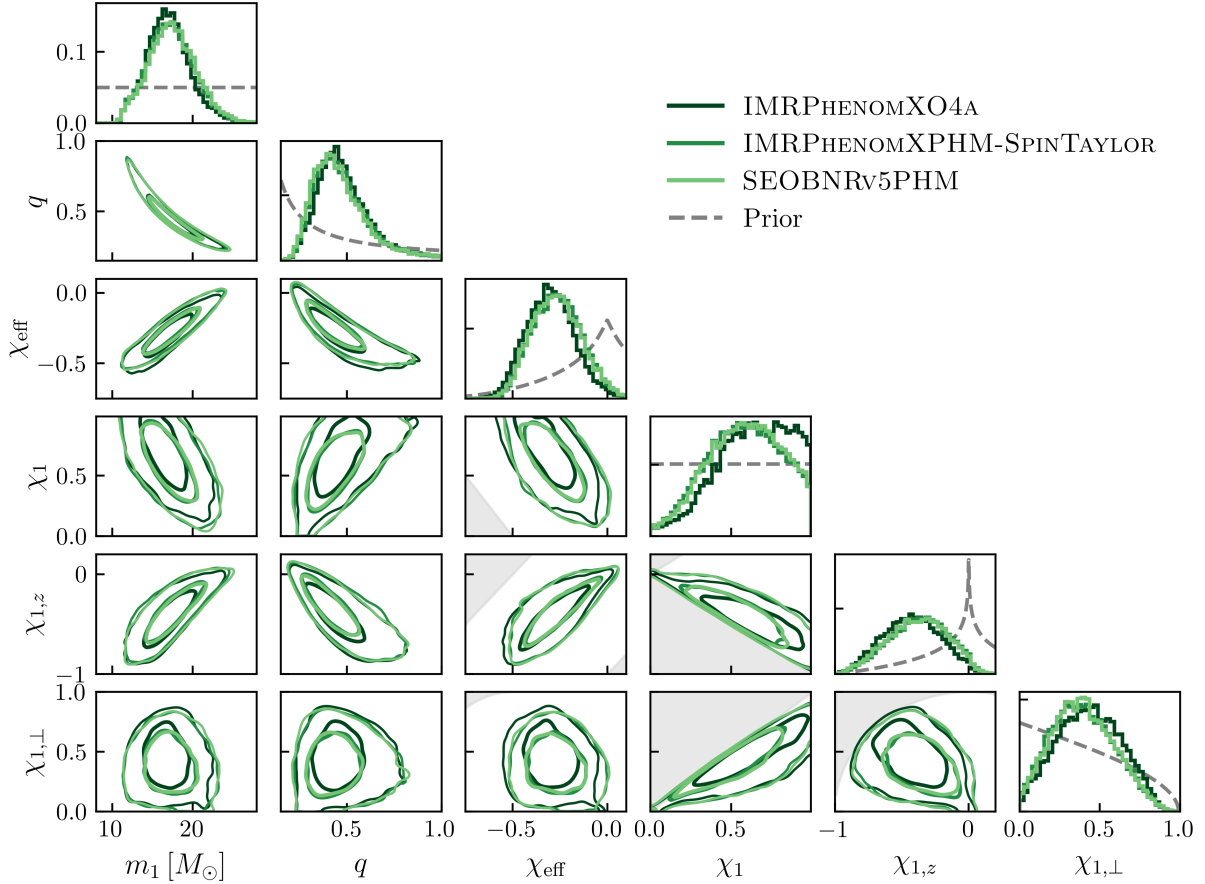


Figure 13. As in Figure 12, but for GW241110.

binary inspiral, merger, and ringdown, and are therefore applicable to systems of any mass. The SEOBNR model computes the signal in the time domain. The XPHM and XO4A models each calculate signals in the frequency domain, but differ in their treatment of spin precession. Whereas the XPHM model numerically solves the post-Newtonian spin-precession dynamics, the XO4A model adopts a phenomenological ansatz that is fit to numerical-relativity simulations, calibrating evolution of precession angles, the coprecessing frame, and modal asymmetries between positive and negative m modes.

The main text presented only primary spin measurements with GW241011 and GW241110. For completeness, in Figure 14 we present posteriors on both the primary and secondary dimensionless spin magnitude of each binary black hole. The magnitude and orientation of the events' secondary spin vectors are unconstrained; neither the secondary spin magnitudes, the secondary spin-orbit misalignment angles, nor the azimuthal angles between component spins constrained away from the boundaries of their respective priors.

In Table 2 and Figure 12, we present posteriors on the source properties of GW241011 obtained independently with each waveform. All models recover nearly identical binary chirp masses. At the same time, they each provide slightly different (although statistically consistent) estimates of the binary's primary mass, mass ratio, and primary spin. Such systematic differences between waveform models are not unexpected; the unequal mass ratio, high spin, significant spin precession, and high SNR of this source are likely to exacerbate differences between waveform models (Dhani et al. 2025; Mac Uilliam et al. 2024; Akçay et al. 2025). Table 3 and Figure 13, in turn, shows properties of GW241110 inferred under the previously listed waveform models. We recover good agreement between the different waveforms, with only small differences in the width and mean of the posterior for parameters like the chirp mass and the spin parameters.

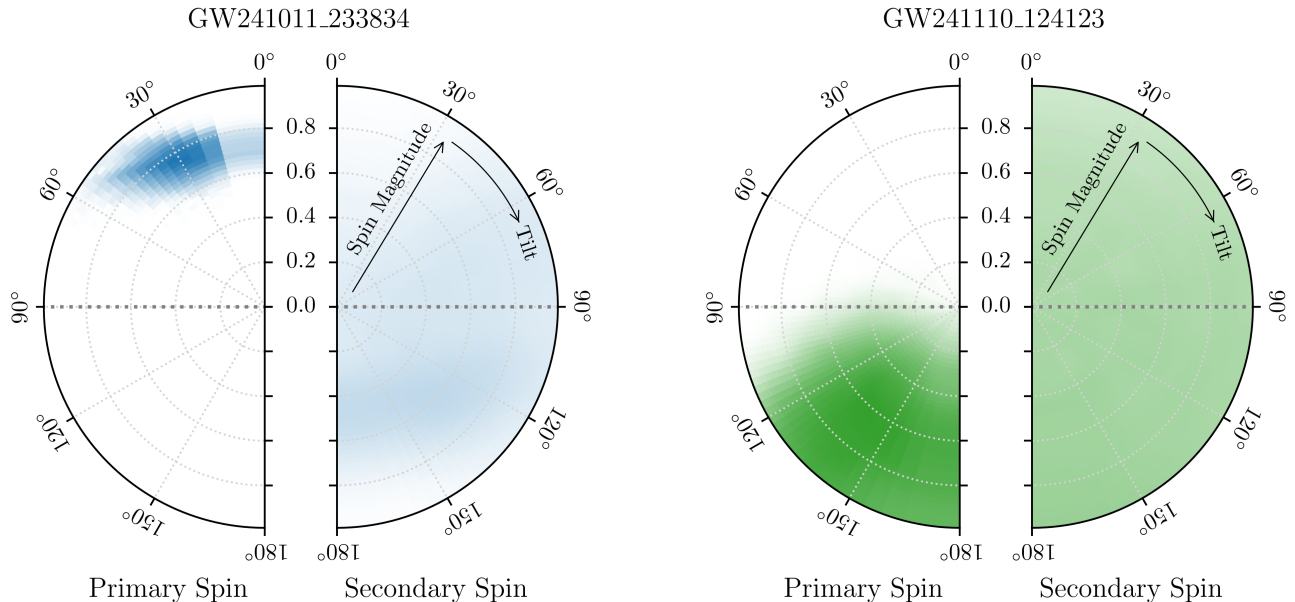


Figure 14. Posterior on both the primary and secondary spin vectors of GW241011 (left) and GW241110 (right). As in Fig. 2, radial and polar coordinates correspond to dimensionless spin magnitude vectors and spin-orbit misalignment angles, respectively. Pixels spaced uniformly in spin magnitude and in cosine-tilt angles, such that each pixel contains equal prior probability. For both events, the properties of the secondary spin vectors are unconstrained.

B. ECCENTRICITY MEASUREMENTS: FURTHER DETAILS

Gravitational-wave measurements of orbital eccentricity have long been challenging, as the dynamics of eccentric orbits vary rapidly on short orbital timescales and give rise to complex waveform morphologies. Recently, however, a number of mature models have been developed that describe gravitational-wave emission from eccentric compact binaries through binary inspiral, merger, and ringdown. We study the eccentricity of GW241011 and GW241110 using two waveform models: the SEOBNRv5EHM (Gamboa et al. 2025) and TEOBRESUMS-DALÍ (Nagar et al. 2024) waveforms. Both models define eccentricity based a Keplerian parametrization of the orbit (Darwin 1959), in which the deformation of the orbit is measured by the Keplerian eccentricity e and the relative position of the binary along the orbit at a specific reference frequency is determined by the relativistic anomaly (SEOBNRv5EHM) or mean anomaly (TEOBRESUMS-DALÍ). Each model restricts spin to lie parallel (or antiparallel) to a binary’s orbital angular momentum, and therefore neglects precessional effects due to in-plane spin components. We adopt Bayesian priors that are uniform in detector-frame component masses, uniform in comoving volume and detector-frame time, and isotropic in source position and orientation. The prior on aligned spin components is taken to be the projection of uniform-in-magnitude and isotropic spin priors, consistent with the prior adopted in Sec. 3. We adopt uniform priors on the relativistic anomaly and on the eccentricity at a reference frequency of 13.33 Hz (Ramos-Buades et al. 2023b). Sampling of the SEOBNRv5EHM waveform model is performed using both the BILBY (Ashton et al. 2019; Romero-Shaw et al. 2020b) and RIFT (Pankow et al. 2015; Lange et al. 2017; Wysocki et al. 2019) packages, the former invoking the DYNESTY (Speagle 2020) nested sampler; posterior samples from each software are combined in equal proportion. Sampling of the SEOBNRv5EHM waveform model is performed with RIFT.

Figure 15 shows more complete posteriors on the source properties of GW241011 and GW241110 using both waveform models. The component masses, effective inspiral spin, and primary aligned spin of both sources are consistent with results presented above using quasicircular and precessing waveform models, with little correlation between these parameters and orbital eccentricity. This suggests, although does not prove, that eccentricity limits for GW241011 and GW241110 are minimally biased by the lack of precessional effects, and conversely that measurements of spin-orbit precession are likely robust despite neglecting eccentricity.

Care must be taken when comparing eccentricities among waveform families and to predictions from the literature. First, the orbital eccentricity for inspiraling compact binaries is not uniquely defined; different waveform families

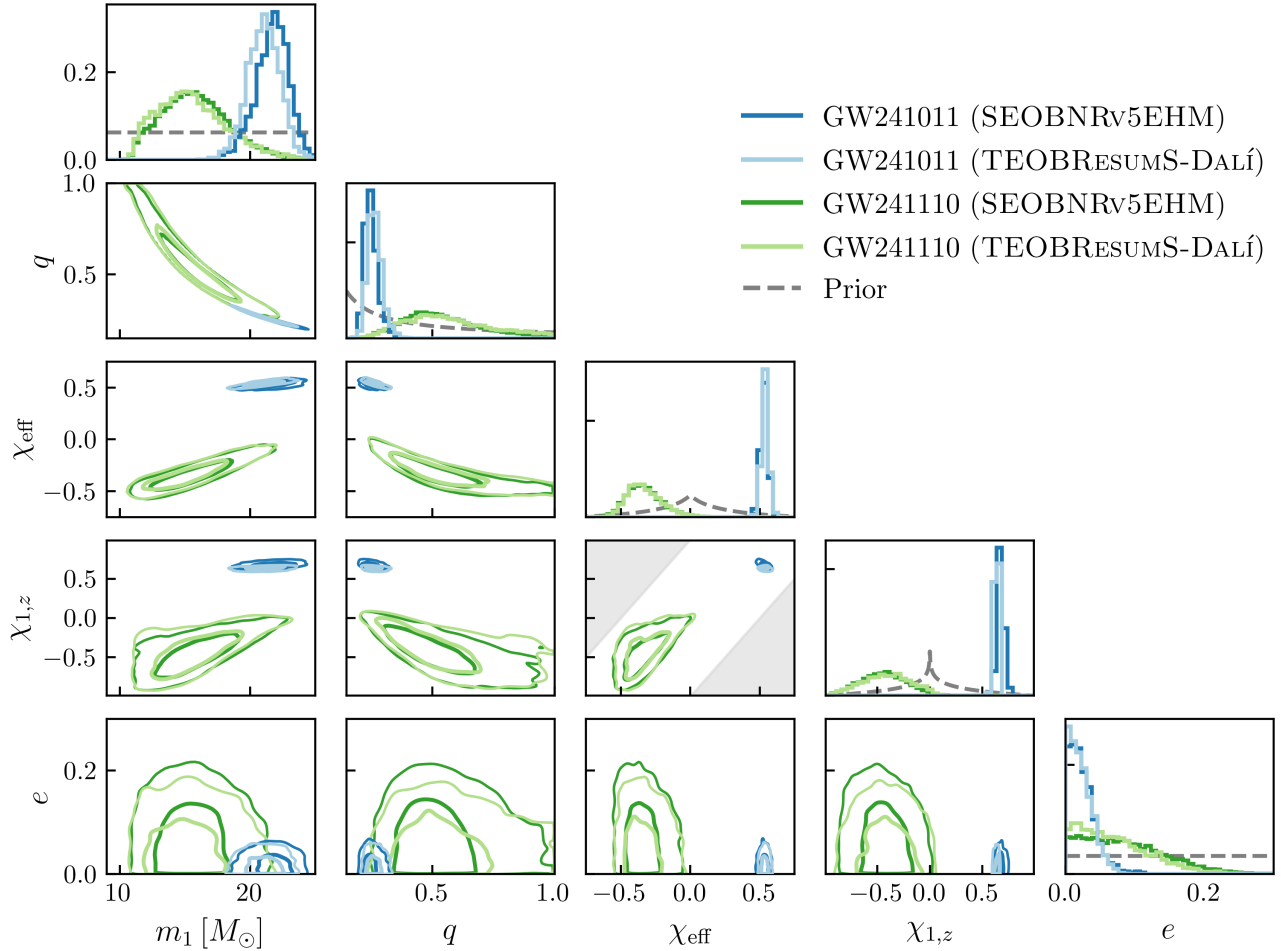


Figure 15. Posteriors on the source properties of GW241011 and GW241110, obtained using the eccentric and spin-aligned SEOBNRv5EHM (Gamboa et al. 2025) and TEOBRESUMS-DALÍ (Nagar et al. 2024) waveform models. Orbital eccentricities, quoted at a reference frequency of 13.33 Hz, are consistent with $e = 0$, while other source parameters are consistent with estimates obtained elsewhere using quasicircular and precessing waveform models.

may adopt distinct, gauge-dependent choices for e . Growing efforts exist to standardize the definition of compact binary eccentricity using waveform-based descriptions to remove gauge-ambiguity (Shaikh et al. 2023; Islam & Venumadhav 2025; Shaikh et al. 2025), but in this paper we have not attempted to unify the SEOBNRv5EHM and TEOBRESUMS-DALÍ definitions in this fashion. We nevertheless find strong consistency between eccentricity limits placed by both waveform models. Second, orbital eccentricity rapidly evolves under gravitational-wave radiation, and thus must be quoted at a specific time. As in our case above, orbital eccentricity is typically quoted at a fixed gravitational-wave reference frequency, to be taken as a proxy for time. The instantaneous frequency of an eccentric binary inspiral is not monotonic in time, however, and so there exist different conventions with which to define reference frequencies. In this work, we define the reference frequency as the orbit-averaged detector-frame frequency of a binary’s $(\ell, m) = (2, \pm 2)$ quadrupole radiation. Astrophysical predictions, in contrast, tend to adopt reference frequencies defined by the frequency of the *instantaneously loudest frequency harmonic* (Wen 2003). Eccentricities quoted at numerically identical reference frequencies can, under both prescriptions, correspond to eccentricities at very distinct times in a binary’s evolution (Vijaykumar et al. 2024).

C. BINARY BLACK HOLE POPULATION INFERENCE WITH GW241011 AND GW241110

In Section 3.3, we noted that GW241011 and GW241110 do not appear to be clear outliers with respect to the population of merging binary black holes. This appendix elaborates on this statement, presenting and discussing updated measurements of the binary black hole population using GW241011 and GW241110.

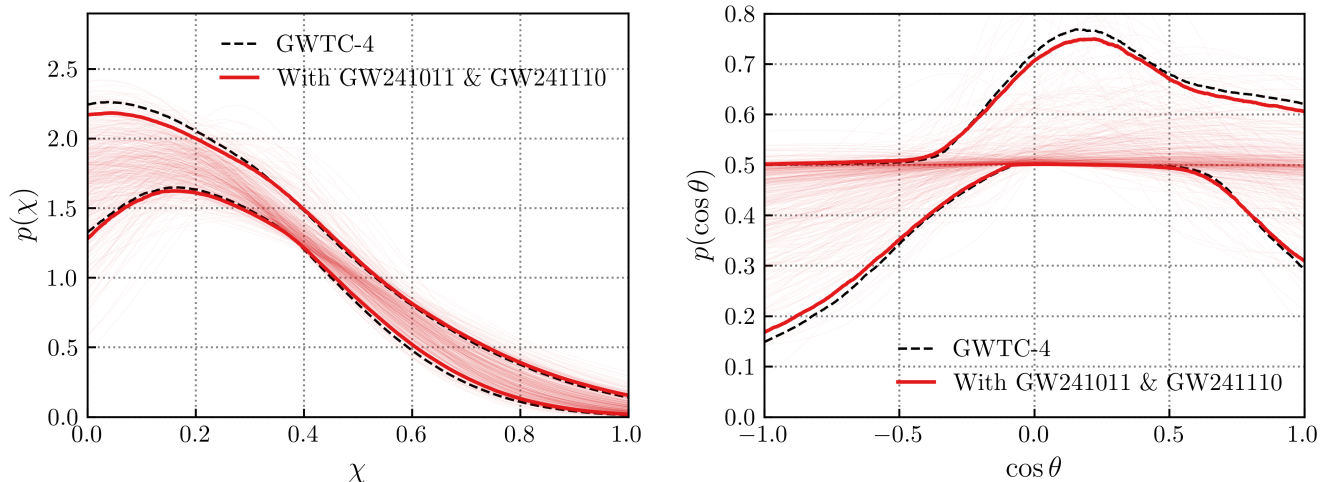


Figure 16. Inferred distribution of component spin magnitudes (left) and cosine spin-orbit misalignment angles (right) of merging binary black holes, with and without GW241011 and GW241110. We use the GAUSSIAN COMPONENT SPIN population model from Abac et al. (2025d), in which spin magnitudes are Gaussian-distributed, and cosine spin-orbit angles follow a mixture between Gaussian and uniform components. Dashed lines indicate 90% credible bounds on $p(\chi)$ and $p(\cos \theta)$ when using binary black holes from GWTC-4.0 (Abac et al. 2025a), while the thick red lines indicate updated bounds when additionally including GW241011 and GW241110. The ensemble of thin red lines shows the probability distributions corresponding to individual draws on our population posterior, when including GW241011 and GW241110. The inclusion of GW241011 and GW241110 negligibly affects the inferred spin magnitude and spin-orbit tilt distributions.

C.1. The binary black hole spin distribution

We hierarchically measure the population properties of binary black holes following the methodology described in Abac et al. (2025d). We select all binary black holes among GWTC-4.0 (Abac et al. 2025a), detected with a false-alarm rate below 1 yr^{-1} by at least one search algorithm, and exclude the events GW190814 (Abbott et al. 2020c), GW190917_114630 (Abbott et al. 2024), and GW230529 (Abac et al. 2024) that contain low-mass objects of unknown nature. This yields a total of 153 binary black hole coalescences, plus GW241011 and GW241110. Selection biases are estimated using a suite of simulated signals added to data from the first three observing runs (O1, O2, and O3) and the first part of the fourth LIGO-Virgo-KAGRA observing run (O4a; Essick et al. 2025; Abac et al. 2025d). We neglect the additional time-volume surveyed early in the second part of the fourth observing run (O4b), in which GW241011 and GW241110 were detected. This slightly biases our measurements of the binary black hole population, but the short duration and comparable sensitivity of early O4b render this bias negligible. We perform hierarchical inference using the GWPOPULATION package (Talbot et al. 2019, 2025) and the DYNESTY nested sampler (Speagle 2020).

Figure 16 illustrates the inferred distributions of spin magnitudes (left) and spin-orbit misalignment angles (right) among binary black holes, with and without GW241011 and GW241110. We use the GAUSSIAN COMPONENT SPIN model described in Abac et al. (2025d), in which component spin magnitudes are identically and independently drawn from a truncated normal distribution,

$$p(\chi_1, \chi_2) = N_{[0,1]}(\chi_1 | \mu_\chi, \sigma_\chi) N_{[0,1]}(\chi_2 | \mu_\chi, \sigma_\chi), \quad (\text{C1})$$

and cosine spin-orbit tilts are jointly distributed as a mixture between Gaussian and uniform components:

$$p(\cos \theta_1, \cos \theta_2) = \zeta N_{[-1,1]}(\cos \theta_1 | \mu_t, \sigma_t) N_{[-1,1]}(\cos \theta_2 | \mu_t, \sigma_t) + (1 - \zeta) U_{[-1,1]}(\cos \theta_1) U_{[-1,1]}(\cos \theta_2). \quad (\text{C2})$$

Here, $N_{[a,b]}$ and $U_{[a,b]}$ represent Gaussian and uniform distributions truncated and normalized on the interval $[a, b]$, and the means μ_χ and μ_t , standard deviations σ_χ and σ_t , and mixing fraction ζ are free parameters inferred from data. We assume that black hole masses and redshifts follow the default distributions adopted in Abac et al. (2025d) and adopt the same Bayesian priors. We see that the inclusion of events GW241011 and/or GW241110 yields a spin-tilt distribution marginally more consistent with isotropy, but that these events otherwise have negligible effects on the inferred spin distributions.

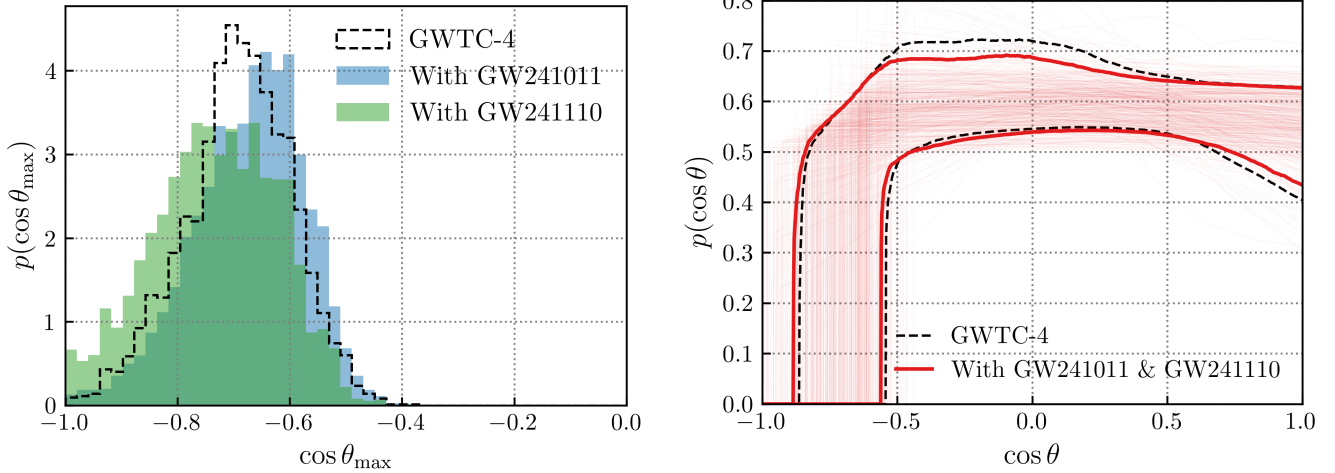


Figure 17. *Right:* Inferred distribution of cosine spin–orbit misalignment angles, when additionally inferring the maximum misalignment angle (minimum $\cos\theta$ value) among the binary black hole population (the MAX-TILT model). As in Figure 16, dashed lines indicate 90% credible bounds using black holes from GWTC-4.0 (Abac et al. 2025a), thick red lines indicate updated bounds when additionally including GW241011 and GW241110, and thin red lines illustrate individual draws from our updated population posterior. *Left:* Posterior obtained on the minimum value $\cos(\theta_{\max})$ below which the $\cos\theta$ distribution is truncated. The inclusion of GW241011 and GW241110 minimally affects inference of the maximum spin misalignment angle among the binary black hole population. Inference using GWTC-4.0 binary black holes requires $\cos\theta_{\max} < -0.57$ ($\theta_{\max} > 125$ degrees) at 90% credibility. Adding GW241011 and GW241110 gives $\cos(\theta_{\max}) \leq -0.55$ and -0.59 , respectively.

It is possible that the GAUSSIAN COMPONENT SPIN model, with unimodal spin magnitude and tilt distributions, may provide a poor description of events like GW241011 and GW241110. We therefore explore two extensions of this model to further study the implications of GW241011 and GW241110.

1. First, whereas the $\cos\theta$ distribution in Eq. (C2) was truncated on the interval $[-1, 1]$, we instead introduce a variable lower truncation bound $\cos(\theta_{\max})$ (Galaudage et al. 2021; Tong et al. 2022) (i.e. a maximum spin tilt angle θ_{\max}) with a prior uniform on the interval $[-1, 1]$, and ask how extreme spin–orbit misalignment angles must be to accommodate events like GW241110 (the MAX-TILT model),

$$p(\cos\theta_1, \cos\theta_2) = \zeta N_{[\cos(\theta_{\max}), 1]}(\cos\theta_1 | \mu_t, \sigma_t) N_{[\cos(\theta_{\max}), 1]}(\cos\theta_2 | \mu_t, \sigma_t) + (1 - \zeta) U_{[\cos(\theta_{\max}), 1]}(\cos\theta_1) U_{[\cos(\theta_{\max}), 1]}(\cos\theta_2). \quad (\text{C3})$$

2. Second, we allow for the existence of a distinct subpopulation of rapidly spinning black holes with large χ , designed to explore whether events like GW241011 require a multimodal spin distribution (HIGH-SPIN model). We extend the C1 model by introducing a high spin Gaussian,

$$p(\chi_1, \chi_2) = \left(\xi_\chi N_{[0, 1]}(\chi_1 | \mu_\chi, \sigma_\chi) + (1 - \xi_\chi) N_{[0, 1]}(\chi_1 | \mu_{\chi, \text{high}}, \sigma_{\chi, \text{high}}) \right) \times \left(\xi_\chi N_{[0, 1]}(\chi_2 | \mu_\chi, \sigma_\chi) + (1 - \xi_\chi) N_{[0, 1]}(\chi_2 | \mu_{\chi, \text{high}}, \sigma_{\chi, \text{high}}) \right), \quad (\text{C4})$$

where $\mu_{\chi, \text{high}}$ is the mean high spin Gaussian with a prior the uniform on the interval $[0.5, 1]$, $\sigma_{\chi, \text{high}}$ is the width of the high spin Gaussian with a prior the uniform on the interval $[0.005, 1]$, and finally ξ_χ is the mixing fraction between the low spin and high spin Gaussians with a uniform prior on the interval $[0, 1]$.

Figure 17 shows the measured distribution of spin–orbit misalignment angles θ when inferring the maximum misalignment angle θ_{\max} . The left-hand panel shows the posterior on $\cos(\theta_{\max})$. Binary black holes among GWTC-4.0 require

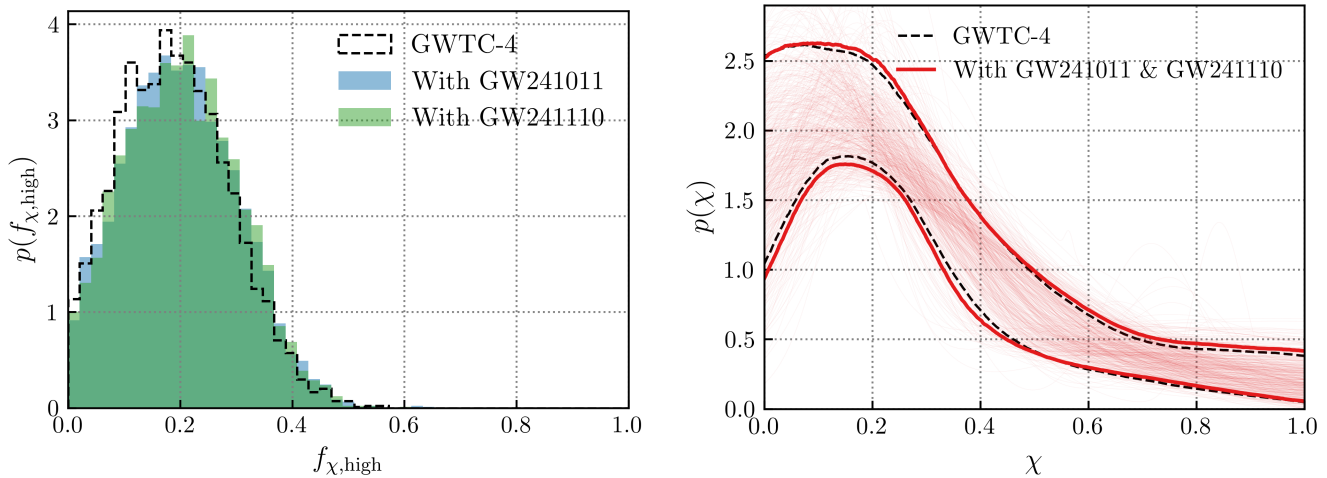


Figure 18. *Right:* Inferred distribution of black hole component spin magnitudes when allowing for a distinct subpopulation of rapidly spinning black holes where one or both black hole components occupy this high spin region (the HIGH-SPIN model). As above, the dashed lines and filled region span 90% credible bounds with and without GW241011 and GW241110, respectively. *Left:* Inferred fraction of black holes comprising a possible highly-spinning subpopulation. As above, results are negligibly affected by the inclusion or exclusion of GW241011 and GW241110. In both cases, current data do not require the existence of a distinct population of events with rapidly-spinning components. When including GW241011 and GW241110, we bound $f_{\chi,high} \leq 0.36$ at 90% credibility, consistent with zero.

maximum spin-orbit misalignment angles of $\theta_{max} \geq 125$ degrees ($\cos \theta_{max} \leq -0.57$) at 90% credibility. This result is only marginally affected by the inclusion of GW241011 or GW241110, which yield $\theta_{max} \geq 124$ degrees and 126 degrees, respectively. Figure 18, meanwhile, shows the inferred black hole spin-magnitude distribution when allowing for a distinct subpopulation of rapidly spinning black holes, together with the inferred fraction of events $f_{\chi,high}$ with one or both components occupying a possible high-spin population. When compared to Figure 16, it is clear that different models yield slight, systematic differences in the measured spin magnitude distribution; the HIGH-SPIN model gives a spin distribution more concentrated at small χ with an extended tail to high spin magnitudes. However, the addition or exclusion of GW241011 and GW241110 again result in negligible differences. Binary black holes among GWTC-4.0 do not require the existence of a distinct, high-spinning subpopulation, with $f_{\chi,high} < 0.32$ at 90% credibility. When including GW241011 and GW241110, the high-spin fraction remains consistent with zero, with $f_{\chi,high} < 0.36$.

Taken together, our results indicate that GW241011 and GW241110 are not evident population outliers, requiring neither greater spin-orbit misalignments nor larger spin magnitudes than already afforded by binary black holes among GWTC-4.0.

C.2. Population Reweighting

We reweight the parameter estimation samples using population-informed mass and spin distributions using the three population models. Reweighted posteriors are obtained with leave-one-out posterior predictive distributions (Galaudage et al. 2020; Callister 2021; Essick & Fishbach 2021), providing astrophysically motivated priors (such reweighting excludes the contribution of the event in question to the population inference, thus avoiding double-counting effects). The resulting posteriors for the GAUSSIAN COMPONENT SPIN population model, for example, are shown in Figure 19.

For the posterior on $\cos(\theta_1)$ of GW241110, reweighted by the population using the GAUSSIAN COMPONENT SPIN, MAX-TILT and HIGH-SPIN, the upper limit (or minimum misalignment) is given by -0.43 , -0.26 and -0.37 respectively at 90% credibility. The MAX-TILT fit gives the least misaligned result as the model has the flexibility to cut off at values of $\cos(\theta_1) > -1$ whereas the other two models require the fit to end at $\cos(\theta_1) = -1$. For the posterior on χ_1 of GW241011, reweighted by the population using the GAUSSIAN COMPONENT SPIN, MAX-TILT and HIGH-SPIN, the lower limit (or minimum spin magnitude) is given by 0.68 , 0.68 and 0.69 respectively. The lower limit on the spin magnitude is consistent under all three models.

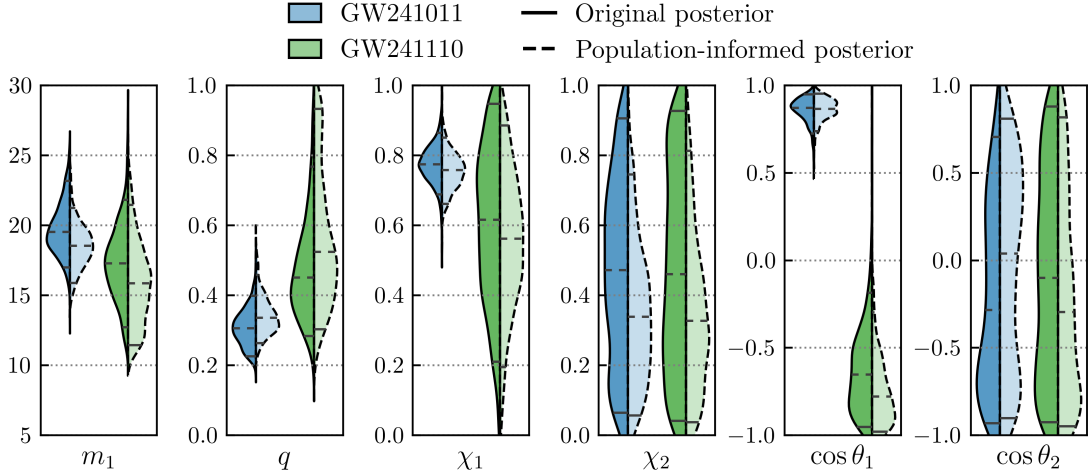


Figure 19. Comparison of original and population-informed (using the GAUSSIAN COMPONENT SPIN population model) posterior distributions for GW241011 and GW241110.

Table 4. Number of binary black hole mergers included in datasets from the CMC and cBHBD catalogs. We include the total numbers of first-generation and higher-generation black hole mergers in each catalog, as well as the number of mergers at each stellar metallicity as highlighted in Figure 6.

Model	Generation	$Z = 0.01 Z_{\odot}$	$Z = 0.1 Z_{\odot}$	$Z = Z_{\odot}$	Total
CLUSTER MONTE CARLO	First-generation	3681	3566	3758	11005
CLUSTER MONTE CARLO	Higher-generation	660	625	978	2263
CLUSTERBHBDYNAMICS	First-generation	1690	1761	1825	5276
CLUSTERBHBDYNAMICS	Higher-generation	316	351	638	1305

D. CLUSTER MODELS: FURTHER DETAILS

In this appendix, we provide further details regarding the astrophysical population models plotted alongside the properties of GW241011 and GW241110 in Figure 6. For a complete description of the stellar (binary) evolution and cluster dynamics models underlying these results, we direct the reader to [Kremer et al. \(2020\)](#), [Rodriguez et al. \(2022\)](#), and [Antonini et al. \(2023\)](#).

The CMC catalog ([Kremer et al. 2020](#); [Rodriguez et al. 2022](#)) contains a suite of 148 cluster simulations, primarily comprising a grid of 144 models with varying particle number ($N = \{2, 4, 8, 16\} \times 10^5$), virial radius ($r_v = \{0.5, 1, 2, 4\}$ pc), metallicity ($Z/Z_{\odot} = \{0.01, 0.1, 1\}$), and Galactocentric distance ($R_{\text{gc}} = \{2, 8, 20\}$ kpc). In addition, the CMC catalog include four more massive clusters with $N = 3.2 \times 10^6$ at $R_{\text{gc}} = 20$ kpc, spanning two metallicities (0.01 and $1 Z_{\odot}$). Compared to earlier CMC model suites ([Chatterjee et al. 2010, 2013](#); [Morscher et al. 2015](#)), this set extends the explored ranges of r_v and Z , and decouples metallicity from Galactocentric distance. Cluster models are evolved dynamically over one Hubble time, and binary black hole mergers are identified as those binaries that successfully coalesce over this timescale. The total numbers of available black hole mergers (both first-generation and hierarchical) are provided in Table 4. In Figure 6 we specifically show the direct union of binary black hole mergers obtained across all simulations at each given metallicity, in order to illustrate the range of binary black hole masses, mass ratios, and spins that can be achieved over a broad range of cluster conditions. A more detailed prediction for the merger population expected from clusters, in contrast, would likely adopt a weighted combination corresponding to assumptions about the distribution of cluster masses, metallicities, and formation histories.

The cBHBD code is a semi-analytical model that applies cluster dynamics and energy-balance theory to follow the coupled evolution of clusters and their black hole populations, yielding predictions for black hole binary merger rates and properties. We use the cBHBD catalog published in [Antonini et al. \(2023\)](#), containing 10^6 cluster models that are sampled uniformly in the mass range $10^2 M_{\odot}$ to $2 \times 10^7 M_{\odot}$. We select the subset of models with the same metallicities considered above ($Z/Z_{\odot} = \{0.01, 0.1, 1\}$) and with initial half-mass densities of $10^5 M_{\odot} \text{pc}^{-3}$, yielding a sample of 129

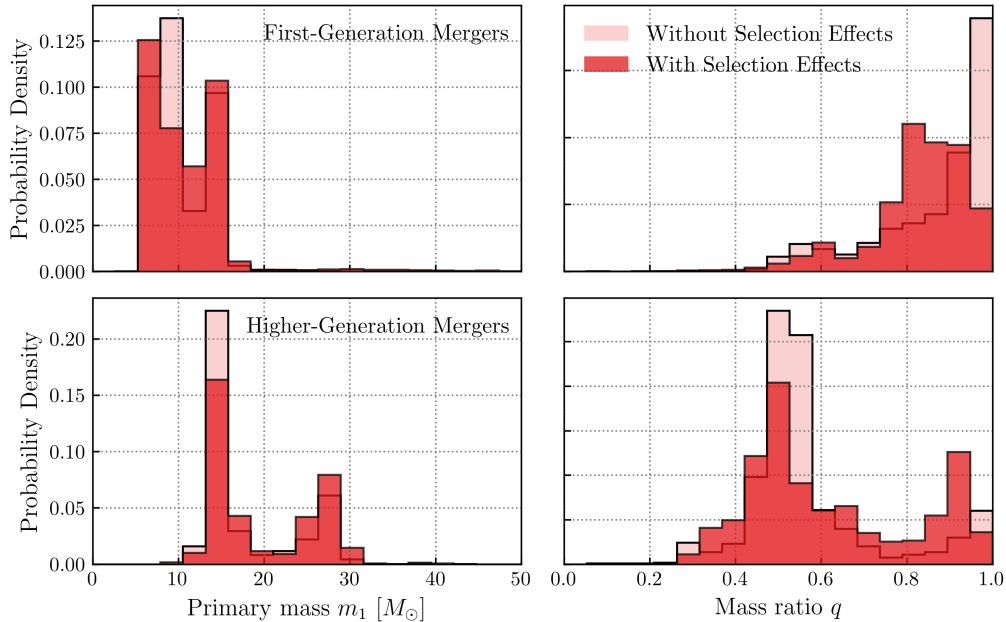


Figure 20. The impact of observational selection effects on the predicted properties of binary black hole mergers in dense stellar clusters. We specifically show the properties predicted in the CMC catalog for clusters of stellar metallicity $Z = Z_{\odot}$, corresponding to the right-hand column of Figure 6. The upper row corresponds to mergers in which both components are first-generation black holes, and the bottom row to mergers in which one or both components are formed from a previous binary black hole coalescence. Light red distributions correspond to predictions directly from CMC (and shown previously in Figure 6), while dark red distributions have been subjected to an observational selection cut calculated using a campaign of simulated signals injected into LIGO and Virgo data (Essick et al. 2025; Abac et al. 2025j).

cluster models with total masses up to $2 \times 10^6 M_{\odot}$. The cluster models are evolved over one Hubble time, and Figure 6 contains binary black holes that merge in this time. The total numbers of available mergers are given in Table 4. As with the CMC results above, we take the direct union of binary mergers across all cluster masses, in order to illustrate the range of possible binary properties.

Figure 6 illustrates the range of binary black hole properties predicted under two models of globular cluster evolution. It does not, however, account for observational selection effects, which may alter the range of binary properties that we expect to successfully detect. We verify that the inclusion of selection effects does not significantly affect the content of Figure 6 by using a suite of simulated signals injected into LIGO and Virgo data (Essick et al. 2025; Abac et al. 2025j). We reweight these simulated signals from their original proposal distribution to target distributions defined by the CMC and cBHBD. Selecting only successfully recovered signals then yields the expected distribution of detectable binaries arising from stellar clusters. The target distributions are themselves obtained by fitting Gaussian mixture models to CMC and cBHBD predictions at each stellar metallicity; the number of mixture components is determined by minimizing the Akaike information criterion (Akaike 1974) on reserved testing data. In order to establish detectability, it is necessary to assume a redshift distribution for binary black hole mergers. We choose a volumetric merger rate that grows with redshift z as $(1+z)^{2.6}$, following the low-redshift star formation rate of Madau & Fragos (2017). Our results do not depend strongly on this particular choice, however.

As an example, Figure 20 shows the original range (light red) of properties among first-generation (top row) and higher-generation (bottom row) black hole mergers, as predicted by CMC for a cluster of stellar metallicity $Z = Z_{\odot}$. Imposing an observational selection cut shifts the distributions of binary masses and mass ratios to higher values, at which expected SNRs are largest. The effect is small, however. The black hole spin distributions predicted by both CMC and cBHBD are sufficiently narrow (nearly delta functions at spin magnitudes of zero or ~ 0.7) that they are unaffected by a selection cut. Despite the slight shift to larger mass ratios, mergers at the highest mass ratios are conversely suppressed by observational selection effects. This is due to the fact that binaries with the largest total masses tend to be those with more unequal mass ratios. Thus, although measured SNR is maximized by increasing

Table 5. Properties of the ancestral binary black holes of GW241011 and GW241110, under the hypothesis that the primary mass of each observed merger is itself a remnant from a previous merger. Specifically, we include constraints on the primary and secondary masses of the hypothesized ancestors, the ancestors’ effective inspiral spins, and the recoil velocity experienced by the remnants following each merger. For each event, we show ancestral properties inferred under two different approaches. In the *Forward* approach, we place astrophysically-informed priors directly on the ancestral properties GW241011 and GW241110. In the *Backward* approach, we agnostically maintain the source parameters of GW241011 and GW241110 inferred in standard parameter estimation and identify ancestral binaries compatible with these measured parameters.

Event	Method	Ancestral $m_1 [M_\odot]$	Ancestral $m_2 [M_\odot]$	Ancestral χ_{eff}	$v_{\text{recoil}} [\text{km s}^{-1}]$
GW241011	<i>Forward</i>	$11.0^{+1.9}_{-1.6}$	$9.6^{+1.7}_{-1.8}$	$0.02^{+0.08}_{-0.06}$	100^{+190}_{-70}
GW241011	<i>Backward</i>	$13.3^{+4.8}_{-3.2}$	$7.5^{+3.2}_{-3.9}$	$0.23^{+0.29}_{-0.28}$	750^{+1400}_{-630}
GW241110	<i>Forward</i>	$9.6^{+3.1}_{-2.0}$	$8.0^{+2.1}_{-2.3}$	$-0.00^{+0.06}_{-0.06}$	100^{+160}_{-80}
GW241110	<i>Backward</i>	$12.3^{+5.6}_{-4.2}$	$5.1^{+3.6}_{-1.9}$	$-0.04^{+0.65}_{-0.57}$	480^{+1270}_{-330}

mass ratio at fixed total mass, in practice we see that large SNRs most commonly occur for massive sources with somewhat unequal mass ratios.

E. FURTHER DETAILS ON ESTIMATING PROGENITOR BINARY PARAMETERS

This appendix provides additional details regarding calculation of GW241011 and GW241110’s ancestral binaries, under the hypothesis that these events contain second-generation black holes born from a previous binary black hole merger. As discussed in the main text, we approach this calculation in two ways. In the *Forward* approach, we adopt a hierarchical Bayesian formalism, placing astrophysically-informed priors on the hypothesized ancestral binaries and marginalizing over the source properties of GW241011 and GW241110 to directly obtain posteriors on ancestral properties. In the *Backward* approach, we more agnostically adopt the same uninformative priors on the source properties of GW241011 and GW241110 used in standard parameter estimation. More details about each approach are described in Appendices E.1 and E.2 below.

E.1. The Forward Approach

Given the gravitational-wave data d due to a binary black hole merger containing a second-generation remnant, we wish to obtain a probability distribution $p(\vec{\theta}_{1g}|d)$ on the properties $\vec{\theta}_{1g}$ of that black hole’s first-generation ancestors. Rather than repeat Bayesian parameter estimation, we proceed using the results of standard parameter estimation performed directly on GW241011 and GW241110, constructing the posterior (Mahapatra et al. 2024)

$$p(\vec{\theta}_{1g}|d) = \frac{\pi(\vec{\theta}_{1g}) p(\vec{\theta}_{2g}|d)}{\mathcal{Z}_{1g}(d) \pi(\vec{\theta}_{2g})} \Big|_{\vec{\theta}_{2g}=\vec{F}(\vec{\theta}_{1g})}. \quad (\text{E5})$$

Here, $\pi(\vec{\theta}_{1g})$ is the prior distribution on $\vec{\theta}_{1g}$. The quantity $\vec{\theta}_{2g}$ denotes parameters of the observed binary merger (i.e. GW241011 and GW241110 themselves); $p(\vec{\theta}_{2g}|d)$ and $\pi(\vec{\theta}_{2g})$ are the posterior and prior probability distributions for these events obtained through ordinary parameter estimation. The normalization constant

$$\mathcal{Z}_{1g}(d) \equiv \int \pi(\vec{\theta}_{1g}) \frac{p(\vec{\theta}_{2g}|d)}{\pi(\vec{\theta}_{2g})} \Big|_{\vec{\theta}_{2g}=F(\vec{\theta}_{1g})} d\vec{\theta}_{1g} \quad (\text{E6})$$

is the evidence for d under the hierarchical merger hypothesis, while $F(\vec{\theta}_{1g}) = \vec{\theta}_{2g}$ is the function mapping the ancestral binary’s properties to the final mass and spin of its remnant black hole. We compute $F(\vec{\theta}_{1g})$ using the numerical-relativity remnant surrogate model NRSUR7DQ4REMNANT (Varma et al. 2019), valid for binary black holes in quasi-circular orbits. In practice, we reconstruct $p(\vec{\theta}_{2g}|d)$ and $\pi(\vec{\theta}_{2g})$ using a Gaussian kernel density estimator fit to samples from each distribution. To sample possible ancestral properties from $p(\vec{\theta}_{1g}|d)$, we employ BILBY (Ashton et al. 2019) using the DYNesty (Speagle 2020) nested sampler.

We choose a prior distribution $\pi(\vec{\theta}_{1g}|d)$ that is a close match to the properties of first-generation binary mergers, as predicted in the CMC catalog and shown in Figure 6. Upon combining successful mergers across all simulated clusters, the primary masses of first-generation mergers follow an approximately log-normal distribution, with best-fit mean

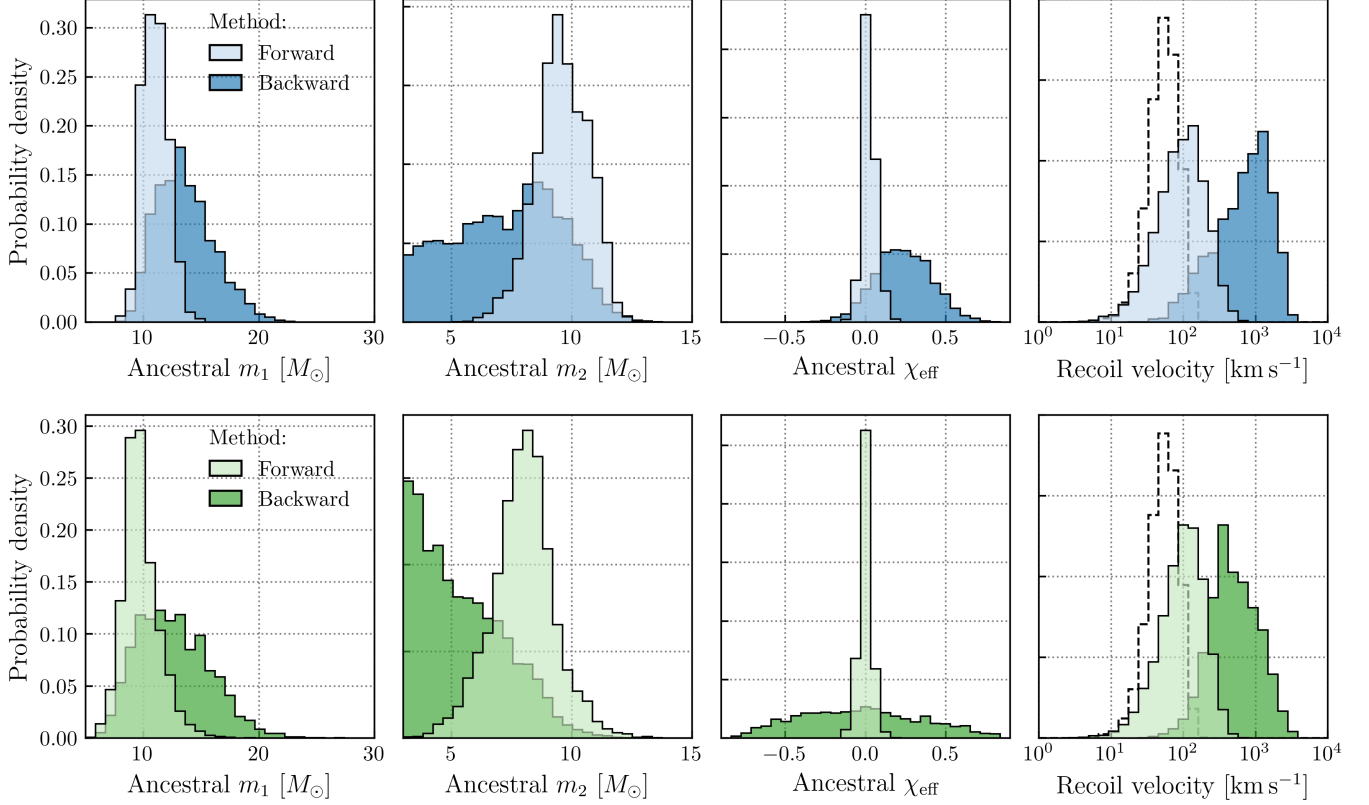


Figure 21. Inferred parameters on the ancestral binary black holes that previously merged to form the primary components of GW241011 (top row) and GW241110 (bottom row), under the hypothesis that each system contains a second-generation primary. We show results obtained under two sets of priors. Darker distributions correspond to an agnostic approach that leaves the priors on GW241011 and GW241110’s source properties unchanged, relative to standard parameter estimation. Lighter distributions correspond to an astrophysically-motivated approach, in which priors are placed on the ancestral binaries, inducing priors on GW241011 and GW241110’s primary masses and spins consistent with their hypothesized hierarchical origin. For comparison, the dashed histograms illustrate the distribution of cluster escape velocities predicted by CMC. In order for the sources of GW241011 and GW241110 to remain consistent with a hierarchical origin in globular clusters, their ancestral recoil velocities should not exceed these escape velocities.

$\mu_{\ln m_1} = 2.9$ and standard deviation $\sigma_{\ln m_1} = 0.6$, while mass ratios are well-described by a power law $p(q) \propto q^\beta$, with $\beta = 4.3$. We adopt these distributions as our priors on ancestral primary masses and mass ratios. In the CMC catalog, first-generation black holes are assumed to have identically zero spins. We accordingly limit spins to be small but non-zero, adopting a half-normal prior distribution with a standard deviation of 0.1 on both primary and secondary spin magnitudes.

E.2. The Backward Approach

The above method sets priors on ancestral black hole parameters which, in turn, lead to posterior distributions on the source properties of the observed gravitational waves that are modified with respect to those obtained in standard parameter estimation. As an alternative, the method presented in Araujo-Álvarez et al. (2024) preserves the agnostic priors on the source properties of GW241011 and GW241110 themselves, thereby preserving the original posteriors on the observed “child” binaries (provided that all child parameters can be realized with non-negligible probability from a chosen prior range of ancestral black holes). More precisely, this method yields a joint posterior $p(\vec{\theta}_{1g}, \vec{\theta}_{2g}|d)$ that, when marginalized over $\vec{\theta}_{1g}$, yields a posterior that is proportional to our original posterior $p(\vec{\theta}|d)$, for all $\vec{\theta}_{2g}$ satisfying $p(\vec{\theta}_{2g}|\vec{\theta}_{1g}) \neq 0$. Equality is achieved when every child parameter is compatible with at least one ancestral configuration under the proposed prior. This method differs from that of Appendix E.1 simply by replacing the term $\pi(\vec{\theta}_{2g})$ in Eq. (E5), which denotes the prior probability on the child parameters set by our original Bayesian parameter estimation, with $\pi(\vec{\theta}_{1g})$, the prior probability on the child parameters induced by the priors on the ancestral ones.

In practice, we proceed by drawing 2×10^6 random samples from a broad ancestral prior $p(\vec{\theta}_{1g})$. Ancestral component masses are drawn uniformly from the range $[3M_\odot, 300M_\odot]$, with the mass ratio constrained to lie between 1/6 and unity, and dimensionless spin magnitudes are sampled uniformly from the range $[0, 0.99]$. Remnant properties and a recoil kick are computed for each sample, yielding the induced prior distribution $p(\vec{\theta}_{2g})$ on possible remnant properties. For each primary mass and spin posterior sample $\{m_1, \chi_1\}$ obtained from $p(\vec{\theta}_{2g}|d)$ via the original parameter estimation, we draw random samples from $p(\vec{\theta}_{2g})$ satisfying $\{m_f, \chi_f\} = \{m_1 \pm \delta m_1, \chi_1 \pm \delta \chi_1\}$. We stress that, depending on the choice of ancestral prior $p(\vec{\theta}_{1g})$, this will only be possible for a fraction of the posterior samples. The usage of non-zero tolerances δm_1 and $\delta \chi_1$ is motivated by the fact that the discrete nature of our samples for $p(\vec{\theta}_{1g})$ would naturally prevent us from encountering samples exactly matching the remnant posterior samples. In our case, we choose $(\delta m_1, \delta \chi_1) = (1, 0.05)$, identified in Araújo-Álvarez et al. (2024) to yield stable results.

E.3. Progenitor Properties: Additional Results

Table 5 and Figure 21 present the posterior distributions on ancestral properties, as obtained through both the astrophysically-motivated *Forward* approach and the agnostic *Backward* approach. Both approaches yield similar estimates for the ancestral primary masses of GW241011 and GW241110. The *Forward* approach, with more stringent priors favoring equal mass ratios, yields more precise estimates of the ancestors' secondary masses. Under an agnostic prior, GW241011 is consistent with an ancestral binary with moderately large, positive effective spin, although both GW241011 and GW241110 are also consistent with non-spinning ancestors. Recoil velocities are almost entirely dominated by spin priors; the low ancestral spins required in the *Forward* approach limit recoil kicks to lower velocities, while the large spins allowed in the *Backward* approach yield more rapid recoils.

Despite recoil velocity posteriors being prior dominated, for self-consistency it is valuable to check that these posteriors are not inconsistent with expected cluster escape velocities. The dashed histograms in Fig. 21 show the distribution of cluster escape velocities predicted in the CMC catalog. If the sources of GW241011 and GW241110 are to be consistent with a hierarchical origin in dense clusters (or at least clusters with masses similar to those explored in the CMC catalog), their inferred ancestral recoil velocities must not be larger than these predicted escape velocities. The *Forward* approach yields recoil velocity posteriors consistent with the distribution of expected escape velocities. The *Backward* approach yields a posterior with support in the range of expected escape velocities, although the posterior also extends to much higher recoil velocities; this is expected, due to the deliberately agnostic prior allowing for rapidly spinning ancestors.

F. TESTS OF FUNDAMENTAL PHYSICS: FURTHER DETAILS

F.1. Spin-induced quadrupole moment

In this appendix we provide further detail regarding constraints on GW241011's spin-induced quadrupole moment, discussed in Sec. 5.1.

When testing for the spin-induced quadrupole moment, corrections are added to the inspiral phase of the gravitational waveform, with uniform priors adopted on the correction parameters. In addition to the results shown in Figure 9, based on corrections to the IMRPHEMOMXPHM waveform model (Pratten et al. 2021; Divyajyoti et al. 2024a), we additionally explored results using corrections to the SEOBNRv5HM_ROM (Pompili et al. 2023) waveform model under the Flexible Theory-Independent framework (Mehta et al. 2023). Besides relying on different base waveform models, these two approaches differ in the treatment of the binary's evolution from inspiral to merger and ringdown. Additionally, the IMRPHEMOMXPHM includes spin precession while SEOBNRv5HM_ROM assumes spin-aligned binaries. Given the significant spin precession effects in GW241011, the IMRPHEMOMXPHM-based results from Figure 9 should therefore be taken as the most physically-meaningful constraints on the spin-induced quadrupole, but the SEOBNRv5HM_ROM results are helpful in quantifying the degree of systematic uncertainties arising from missing waveform physics.

The SEOBNRv5HM_ROM-based test gives $\delta\kappa_1 = -0.44^{+1.66}_{-2.01}$ and $\delta\kappa_s = -0.45^{+0.39}_{-1.01}$. While $\delta\kappa_1$ is consistent with a Kerr black hole in GR, $\delta\kappa_s$ is shifted slightly towards negative values, with the Kerr value lying beyond the 95% credible interval. This bias, as well as the broadened posteriors relative to IMRPHEMOMXPHM RESULTS is due to the absence of relativistic spin-orbit precession noted above (Lyu et al. 2024; Divyajyoti et al. 2024a). To verify this, we analyzed simulated signals with source parameters consistent with those of GW241011. We considered both signals with misaligned precessing spins and with aligned spin configurations. When analyzing simulated aligned-spin

signals with SEOBNRv5HM_ROM, posteriors are unbiased and peak near zero. When instead analyzing simulated precessing signals, posteriors are instead biased towards negative values, as in the case of GW241011.

F.2. Subdominant mode amplitude consistency

The gravitational-wave strain emitted by compact binary mergers can be decomposed into spin-weighted spherical harmonics of weight -2 as:

$$h(t, \theta_{JN}, \boldsymbol{\lambda}) = \sum_{\ell \geq 2} \sum_{m=-\ell}^{\ell} h_{\ell m}(t, \boldsymbol{\lambda}) {}_{-2}Y_{\ell m}(\theta_{JN}, \phi_0), \quad (\text{F7})$$

where (θ_{JN}, ϕ_0) specify the observer's orientation in the source frame, and $\boldsymbol{\lambda}$ encodes intrinsic parameters such as masses and spins. Following common practice, we fix $\phi_0 = 0$ so that θ_{JN} denotes the angle between the binary's total angular momentum vector and the observer's line of sight (Pratten et al. 2021).

Typically, gravitational-wave signals are dominated by the quadrupole $(\ell, m) = (2, \pm 2)$ multipole. However, higher-order multipoles such as $(2, \pm 1)$ and $(3, \pm 3)$ become increasingly relevant for systems with unequal masses or for viewing angles away from face-on ($\theta_{JN} \neq 0$). To quantify potential deviations of these subdominant multipoles from GR, the subdominant multipole amplitude (SMA) test (Puecher et al. 2022) introduces amplitude deviations $\delta A_{\ell m}$ explicitly into the $(2, \pm 1)$ and the $(3, \pm 3)$ multipoles in the XPHM waveform model:

$$\begin{aligned} h(t, \theta_{JN}, \boldsymbol{\lambda}) = & \sum_{m=\pm 2} h_{2m}(t, \boldsymbol{\lambda}) {}_{-2}Y_{2m}(\theta_{JN}, 0) + \sum_{m=\pm 1} (1 + \delta A_{21}) h_{2m}(t, \boldsymbol{\lambda}) {}_{-2}Y_{2m}(\theta_{JN}, 0) \\ & + \sum_{m=\pm 3} (1 + \delta A_{33}) h_{3m}(t, \boldsymbol{\lambda}) {}_{-2}Y_{3m}(\theta_{JN}, 0) + \sum_{\text{other HOM}} h_{\ell m}(t, \boldsymbol{\lambda}) {}_{-2}Y_{\ell m}(\theta_{JN}, 0). \end{aligned} \quad (\text{F8})$$

The application of the SMA test requires sufficient SNR in the multipole of interest. For each $(\ell, \pm m)$ mode, the mode-specific SNR, $\rho_{\ell m}$, is computed by projecting $h_{\ell \pm m}$ onto the subspace orthogonal to the dominant $(2, \pm 2)$ mode and evaluating the optimal SNR of the residual (Mills & Fairhurst 2021). In the absence of the $(\ell, \pm m)$ multipole in signal, $\rho_{\ell m}$ follows a χ distribution with two degrees of freedom in Gaussian noise, portrayed as the null distribution in Figure 5. To ensure sufficient mode content, we adopt a conservative selection threshold: a given mode for an event is included in the SMA analysis only if the lower bound of the 68% credible interval of its $\rho_{\ell m}$ distribution exceeds 2.145, corresponding to the 90th percentile of the null distribution. Among the two considered events, only the $(3, \pm 3)$ mode in GW241011 satisfies this criterion. Accordingly, we perform parameter estimation for this mode with a uniform prior on δA_{33} in the range $[-10, 10]$.

F.3. Constraining ultralight bosons through superradiance

In the presence of an ultralight scalar or vector field, a spinning black hole is unstable to the superradiant instability (Brito et al. 2015a). Oscillating bosonic modes that satisfy the superradiant condition, $\omega_R < m\Omega_{\text{BH}}$, grow exponentially with time at the expense of the black hole's rotational energy. Here $\omega_R \sim m_b c^2 / \hbar$ is the angular frequency, m is the azimuthal number, and Ω_{BH} is the horizon frequency of the black hole. The growth of a mode and spindown of the black hole persist until the superradiant condition is saturated (Arvanitaki et al. 2010; Brito et al. 2015b; East & Pretorius 2017; East 2018). Typically, the lowest m mode that is superradiant grows the fastest, but with sufficient time multiple modes can grow and saturate, reducing the black hole's spin to ever smaller values. The vector boson instability rate is parametrically faster than the scalar rate, such that vector bosons spin down a black hole to lower values in a fixed time. For example, adopting the median mass and spin values for the primary black hole in GW241011 (Table 1), the shortest e -folding time for mass growth of a boson cloud is ~ 8 s for a vector boson and 9 hr for a scalar. This assumes a boson mass optimally matched to the black hole; for smaller boson masses the instability timescales lengthen—roughly as $\propto m_b^{-7}$ and $\propto m_b^{-9}$ for vector and scalar modes, respectively (Baryakhtar et al. 2017).

Given a boson mass and a time since black hole formation (or the time since the black hole gained angular momentum), there will be excluded regions of the black hole's mass-spin parameter space where the superradiant instability should have reduced the black hole's spin to lower values. We calculate this excluded region using the SUPERRAD package (Siemonsen et al. 2023; May et al. 2025), based on the linear superradiantly unstable modes and including all relevant azimuthal number modes, for both vectors and scalars. For the dominant modes, with $m \leq 2$, we use

the relativistic frequencies and instability rates. For higher azimuthal modes, we use a non-relativistic approximation, which in general underestimates the instability rate and is thus conservative.

Using the posteriors for the source primary masses and spins of GW241011 and GW241110, we determine the fraction P of each event's posterior samples lying in the region permitted by the given boson mass and black hole age (Aswathi et al. 2025). Sufficiently small P would disfavor this mass–age combination. It is important, however, to guard against prior effects; it is possible for uninformative data, with spin magnitude samples drawn randomly from a uniform prior, to yield small P for specific ultralight boson masses. Following Aswathi et al. (2025), we therefore also calculate a prior fraction P' , obtained by replacing the black hole spin posterior with samples drawn from a uniform distribution $[0, 1)$. The exclusion regions shown in Figure 11 correspond to the requirement that $P < 0.1 P'$; this corresponds to a 90% or better credible bound while also ensuring that constraints are strongly likelihood-driven.

This analysis assumes only a minimally coupled boson with gravitational interactions, but will also apply to scalar or vector bosons with sufficiently weak interactions so as to not disrupt the black hole spindown. We also neglect the impact of gravitational effects from the binary companion on the superradiant growth of the boson cloud, implicitly assuming the growth would occur at large enough separation for this to be negligible.

REFERENCES

- Aasi, J., et al. 2015, *Class. Quant. Grav.*, 32, 074001
- Abac, A. G., et al. 2024, *Astrophys. J. Lett.*, 970, L34
- . 2025a, arXiv:2508.18082
- . 2025b, arXiv:2508.18080
- . 2025c, arXiv:2507.08219
- . 2025d, arXiv:2508.18083
- . 2025e, arXiv:2508.18081
- . 2025f, *Phys. Rev. Lett.*, 135, 111403
- . 2025g, In prep., ,
- . 2025h, arXiv:2509.08099
- . 2025i, arXiv:2509.07348
- . 2025j, arXiv:2508.18083
- Abbott, B. P., et al. 2016a, *Phys. Rev. Lett.*, 116, 061102
- . 2016b, *Astrophys. J. Lett.*, 818, L22
- . 2017a, *Astrophys. J. Lett.*, 848, L13
- . 2017b, *Astrophys. J. Lett.*, 848, L12
- . 2017c, *Phys. Rev. Lett.*, 119, 161101
- . 2019, *Astrophys. J. Lett.*, 882, L24
- . 2020a, *Astrophys. J. Lett.*, 892, L3
- Abbott, R., et al. 2020b, *Phys. Rev. Lett.*, 125, 101102
- . 2020c, *Astrophys. J. Lett.*, 896, L44
- . 2020d, *Phys. Rev. D*, 102, 043015
- . 2021a, *Astrophys. J. Lett.*, 915, L5
- . 2021b, arXiv:2112.06861
- . 2023a, *Phys. Rev. X*, 13, 041039
- . 2023b, *Phys. Rev. X*, 13, 011048
- . 2024, *Phys. Rev. D*, 109, 022001
- Acernese, F., et al. 2015, *Class. Quant. Grav.*, 32, 024001
- . 2023, *J. Phys. Conf. Ser.*, 2429, 012040
- Adams, T., Buskulic, D., Germain, V., et al. 2016, *Class. Quant. Grav.*, 33, 175012
- Ajith, P., et al. 2011, *Phys. Rev. Lett.*, 106, 241101
- Akaike, H. 1974, *IEEE Transactions on Automatic Control*, 19, 716
- Akçay, S., Hoy, C., & Mac Uilliam, J. 2025, arXiv:2506.19990
- Akutsu, T., et al. 2021, *PTEP*, 2021, 05A101
- Allen, B. 2005, *Phys. Rev. D*, 71, 062001
- Allen, B., Anderson, W. G., Brady, P. R., Brown, D. A., & Creighton, J. D. E. 2012, *Phys. Rev. D*, 85, 122006
- Alléné, C., et al. 2025, *Class. Quant. Grav.*, 42, 105009
- Antoni, A., & Quataert, E. 2022, *Mon. Not. Roy. Astron. Soc.*, 511, 176
- . 2023, *Mon. Not. Roy. Astron. Soc.*, 525, 1229
- Antonini, F., & Gieles, M. 2020a, *Mon. Not. Roy. Astron. Soc.*, 492, 2936
- . 2020b, *Phys. Rev. D*, 102, 123016
- Antonini, F., Gieles, M., Dosopoulou, F., & Chattopadhyay, D. 2023, *Mon. Not. Roy. Astron. Soc.*, 522, 466
- Antonini, F., Gieles, M., & Gualandris, A. 2019, *Mon. Not. Roy. Astron. Soc.*, 486, 5008
- Antonini, F., Murray, N., & Mikkola, S. 2014, *Astrophys. J.*, 781, 45
- Antonini, F., & Perets, H. B. 2012, *Astrophys. J.*, 757, 27
- Antonini, F., & Rasio, F. A. 2016, *Astrophys. J.*, 831, 187
- Antonini, F., Rodriguez, C. L., Petrovich, C., & Fischer, C. L. 2018, *Mon. Not. Roy. Astron. Soc.*, 480, L58
- Apostolatos, T. A., Cutler, C., Sussman, G. J., & Thorne, K. S. 1994, *Phys. Rev. D*, 49, 6274
- Araújo-Álvarez, C., Wong, H. W. Y., Liu, A., & Bustillo, J. C. 2024, *Astrophys. J.*, 977, 220
- Arca Sedda, M., Kamlah, A. W. H., Spurzem, R., et al. 2023, *Mon. Not. Roy. Astron. Soc.*, 526, 429
- Arun, K. G., Buonanno, A., Faye, G., & Ochsner, E. 2009, *Phys. Rev. D*, 79, 104023, [Erratum: *Phys.Rev.D* 84, 049901 (2011)]
- Arvanitaki, A., Dimopoulos, S., Dubovsky, S., Kaloper, N., & March-Russell, J. 2010, *Phys. Rev. D*, 81, 123530

- Arvanitaki, A., & Dubovsky, S. 2011, *Phys. Rev. D*, 83, 044026
- Ashton, G., et al. 2019, *Astrophys. J. Suppl.*, 241, 27
- Aswathi, P. S., East, W. E., Siemonsen, N., Sun, L., & Jones, D. 2025, arXiv:2507.20979
- Atallah, D., Trani, A. A., Kremer, K., et al. 2023, *Mon. Not. Roy. Astron. Soc.*, 523, 4227
- Aubin, F., et al. 2021, *Class. Quant. Grav.*, 38, 095004
- Baibhav, V., Berti, E., Gerosa, D., Mould, M., & Wong, K. W. K. 2021, *Phys. Rev. D*, 104, 084002
- Baibhav, V., Gerosa, D., Berti, E., et al. 2020, *Phys. Rev. D*, 102, 043002
- Baibhav, V., & Kalogera, V. 2024, arXiv:2412.03461
- Baird, E., Fairhurst, S., Hannam, M., & Murphy, P. 2013, *Phys. Rev. D*, 87, 024035
- Banagiri, S., Callister, T. A., Adamcewicz, C., Doctor, Z., & Kalogera, V. 2025, *Astrophys. J.*, 990, 147
- Barkat, Z., Rakavy, G., & Sack, N. 1967, *Phys. Rev. Lett.*, 18, 379
- Barrera, O., & Bartos, I. 2022, *Astrophys. J. Lett.*, 929, L1
- Baryakhtar, M., Lasenby, R., & Teo, M. 2017, *Phys. Rev. D*, 96, 035019
- Baumann, D., Chia, H. S., & Porto, R. A. 2019, *Phys. Rev. D*, 99, 044001
- Bavera, S. S., Fragos, T., Qin, Y., et al. 2020, *Astron. Astrophys.*, 635, A97
- Bavera, S. S., et al. 2021, *Astron. Astrophys.*, 647, A153
- Belczynski, K., Holz, D. E., Bulik, T., & O’Shaughnessy, R. 2016a, *Nature*, 534, 512
- Belczynski, K., Kalogera, V., & Bulik, T. 2001, *Astrophys. J.*, 572, 407
- Belczynski, K., et al. 2016b, *Astron. Astrophys.*, 594, A97
- Berti, E., Cardoso, V., Gonzalez, J. A., et al. 2007, *Phys. Rev. D*, 76, 064034
- Berti, E., & Volonteri, M. 2008, *Astrophys. J.*, 684, 822
- Biscoveanu, S., Isi, M., Varma, V., & Vitale, S. 2021, *Phys. Rev. D*, 104, 103018
- Blanchet, L. 2014, *Living Rev. Rel.*, 17, 2
- Brito, R., Cardoso, V., & Pani, P. 2015a, *Lect. Notes Phys.*, 906, pp.1
- . 2015b, *Class. Quant. Grav.*, 32, 134001
- Broekgaarden, F. S., Stevenson, S., & Thrane, E. 2022, *Astrophys. J.*, 938, 45
- Buonanno, A., Kidder, L. E., & Lehner, L. 2008, *Phys. Rev. D*, 77, 026004
- Burrows, A., Wang, T., & Vartanyan, D. 2024, arXiv:2412.07831
- Calderón Bustillo, J., Sanchis-Gual, N., Torres-Forné, A., & Font, J. A. 2021, *Phys. Rev. Lett.*, 126, 201101
- Callister, T. 2021, *Reweighting Single Event Posteriors with Hyperparameter Marginalization*, LIGO DCC. <https://dcc.ligo.org/LIGO-T2100301/public>
- Callister, T. A., & Farr, W. M. 2024, *Phys. Rev. X*, 14, 021005
- Callister, T. A., Farr, W. M., & Renzo, M. 2021, *Astrophys. J.*, 920, 157
- Callister, T. A., Miller, S. J., Chatziioannou, K., & Farr, W. M. 2022, *Astrophys. J. Lett.*, 937, L13
- Campanelli, M., Lousto, C. O., & Zlochower, Y. 2006, *Phys. Rev. D*, 74, 041501
- Campanelli, M., Lousto, C. O., Zlochower, Y., & Merritt, D. 2007, *Phys. Rev. Lett.*, 98, 231102
- Cannon, K., Caudill, S., Chan, C., et al. 2021, *SoftwareX*, 14, 100680
- Capano, C. D., & Nitz, A. H. 2020, *Phys. Rev. D*, 102, 124070
- Capote, E., et al. 2025, *Phys. Rev. D*, 111, 062002
- Caputo, A., Franciolini, G., & Witte, S. J. 2025, arXiv:2507.21788
- Cardoso, V., Franzin, E., Maselli, A., Pani, P., & Raposo, G. 2017, *Phys. Rev. D*, 95, 084014, [Addendum: *Phys.Rev.D* 95, 089901 (2017)]
- Cardoso, V., & Pani, P. 2019, *Living Rev. Rel.*, 22, 4
- Carter, B. 1971, *Phys. Rev. Lett.*, 26, 331
- Chan, C., Müller, B., & Heger, A. 2020, *Mon. Not. Roy. Astron. Soc.*, 495, 3751
- Chatterjee, S., Fregeau, J. M., Umbreit, S., & Rasio, F. A. 2010, *ApJ*, 719, 915
- Chatterjee, S., Umbreit, S., Fregeau, J. M., & Rasio, F. A. 2013, *MNRAS*, 429, 2881
- Chattopadhyay, D., Stegmann, J., Antonini, F., Barber, J., & Romero-Shaw, I. M. 2023, *Mon. Not. Roy. Astron. Soc.*, 526, 4908
- Chatziioannou, K., Lovelace, G., Boyle, M., et al. 2018, *Phys. Rev. D*, 98, 044028
- Chen, H.-Y., Holz, D. E., Miller, J., et al. 2021, *Class. Quant. Grav.*, 38, 055010
- Chia, H. S., & Edwards, T. D. P. 2020, *JCAP*, 11, 033
- Colleoni, M., Vidal, F. A. R., García-Quirós, C., Akçay, S., & Bera, S. 2025, *Phys. Rev. D*, 111, 104019
- Cornish, N. J., & Littenberg, T. B. 2015, *Class. Quant. Grav.*, 32, 135012
- Cornish, N. J., Littenberg, T. B., Bécsy, B., et al. 2021, *Phys. Rev. D*, 103, 044006
- Coulter, D. A., et al. 2017, *Science*, 358, 1556
- Cutler, C., & Flanagan, E. E. 1994, *Phys. Rev. D*, 49, 2658
- Dal Canton, T., Nitz, A. H., Gadre, B., et al. 2021, *Astrophys. J.*, 923, 254

- Dall'Amico, M., Mapelli, M., Torniamenti, S., & Sedda, M. A. 2024, *Astron. Astrophys.*, 683, A186
- Damour, T., Deruelle, N., & Ruffini, R. 1976, *Lett. Nuovo Cim.*, 15, 257
- Darwin, C. 1959, *Proceedings of the Royal Society of London Series A*, 249, 180
- Davies, G. S., Dent, T., Tápai, M., et al. 2020, *Phys. Rev. D*, 102, 022004
- de Mink, S. E., & Mandel, I. 2016, *Mon. Not. Roy. Astron. Soc.*, 460, 3545
- Dhani, A., Völkel, S. H., Buonanno, A., et al. 2025, *Phys. Rev. X*, 15, 031036
- Divyajyoti, Krishnendu, N. V., Saleem, M., et al. 2024a, *Phys. Rev. D*, 109, 023016
- Divyajyoti, Kumar, S., Tibrewal, S., Romero-Shaw, I. M., & Mishra, C. K. 2024b, *Phys. Rev. D*, 109, 043037
- Doctor, Z., Farr, B., & Holz, D. E. 2021, *Astrophys. J. Lett.*, 914, L18
- Dorozsmai, A., Romero-Shaw, I. M., Vijaykumar, A., et al. 2025, *arXiv:2507.23212*
- East, W. E. 2018, *Phys. Rev. Lett.*, 121, 131104
- East, W. E., & Pretorius, F. 2017, *Phys. Rev. Lett.*, 119, 041101
- Essick, R., & Fishbach, M. 2021, On reweighing single-event posteriors with population priors, LIGO DCC. <https://dcc.ligo.org/LIGO-T1900895/public>
- Essick, R., Godwin, P., Hanna, C., Blackburn, L., & Katsavounidis, E. 2020, *Mach. Learn. Sci. Technol.*, 2, 015004
- Essick, R., et al. 2025, *arXiv:2508.10638*
- Ewing, B., et al. 2024, *Phys. Rev. D*, 109, 042008
- Fairhurst, S., Green, R., Hannam, M., & Hoy, C. 2020a, *Phys. Rev. D*, 102, 041302
- Fairhurst, S., Green, R., Hoy, C., Hannam, M., & Muir, A. 2020b, *Phys. Rev. D*, 102, 024055
- Farah, A. M., Edelman, B., Zevin, M., et al. 2023, *Astrophys. J.*, 955, 107
- Farr, B., Holz, D. E., & Farr, W. M. 2018, *Astrophys. J. Lett.*, 854, L9
- Farr, W. M., Stevenson, S., Coleman Miller, M., et al. 2017, *Nature*, 548, 426
- Favata, M., Hughes, S. A., & Holz, D. E. 2004, *Astrophys. J. Lett.*, 607, L5
- Fernandez, N., Ghalsasi, A., & Profumo, S. 2019, *arXiv:1911.07862*
- Finn, L. S., & Chernoff, D. F. 1993, *Phys. Rev. D*, 47, 2198
- Fishbach, M., Holz, D. E., & Farr, B. 2017, *Astrophys. J. Lett.*, 840, L24
- Fisher, R. P., Hemming, G., Bizouard, M.-A., et al. 2021, *SoftwareX*, 14, 100677
- Fitchett, M. J. 1983, *Mon. Not. Roy. Astron. Soc.*, 203, 1049
- Flanagan, E. E., & Hughes, S. A. 1998, *Phys. Rev. D*, 57, 4535
- Fragione, G., & Kocsis, B. 2020, *Mon. Not. Roy. Astron. Soc.*, 493, 3920
- Fragione, G., Kocsis, B., Rasio, F. A., & Silk, J. 2022, *Astrophys. J.*, 927, 231
- Fragione, G., & Silk, J. 2020, *Mon. Not. Roy. Astron. Soc.*, 498, 4591
- Friedberg, R., Lee, T. D., & Pang, Y. 1987, *Phys. Rev. D*, 35, 3658
- Fryer, C. L., Belczynski, K., Wiktorowicz, G., et al. 2012, *Astrophys. J.*, 749, 91
- Fuller, J., Cantiello, M., Lecoanet, D., & Quataert, E. 2015, *ApJ*, 810, 101
- Fuller, J., Lecoanet, D., Cantiello, M., & Brown, B. 2014, *ApJ*, 796, 17
- Fuller, J., & Ma, L. 2019, *Astrophys. J. Lett.*, 881, L1
- Galadage, S., Talbot, C., & Thrane, E. 2020, *Phys. Rev. D*, 102, 083026
- Galadage, S., et al. 2021, *Astrophys. J. Lett.*, 921, L15, [Erratum: *Astrophys. J. Lett.* 936, L18 (2022), Erratum: *Astrophys. J.* 936, L18 (2022)]
- Gamba, R., Breschi, M., Carullo, G., et al. 2023, *Nature Astron.*, 7, 11
- Gamboa, A., et al. 2025, *Phys. Rev. D*, 112, 044038
- Ganapathy, D., et al. 2023, *Phys. Rev. X*, 13, 041021
- Gayathri, V., Healy, J., Lange, J., et al. 2022, *Nature Astron.*, 6, 344
- Gerosa, D., & Berti, E. 2017, *Phys. Rev. D*, 95, 124046
- Gerosa, D., Berti, E., O'Shaughnessy, R., et al. 2018, *Phys. Rev. D*, 98, 084036
- Gerosa, D., & Fishbach, M. 2021, *Nature Astron.*, 5, 749
- Gerosa, D., Fumagalli, G., Mould, M., et al. 2023, *Phys. Rev. D*, 108, 024042
- Ghosh, A., Del Pozzo, W., & Ajith, P. 2016, *Phys. Rev. D*, 94, 104070
- Giersz, M., Leigh, N., Hypki, A., Lützgendorf, N., & Askar, A. 2015, *Mon. Not. Roy. Astron. Soc.*, 454, 3150
- Gilkis, A., & Soker, N. 2016, *ApJ*, 827, 40
- Goldstein, A., et al. 2017, *Astrophys. J. Lett.*, 848, L14
- Gondán, L., Kocsis, B., Raffai, P., & Frei, Z. 2018, *Astrophys. J.*, 860, 5
- Gonzalez, J. A., Hannam, M. D., Sperhake, U., Bruegmann, B., & Husa, S. 2007, *Phys. Rev. Lett.*, 98, 231101
- Gröbner, M., Ishibashi, W., Tiwari, S., Haney, M., & Jetzer, P. 2020, *Astron. Astrophys.*, 638, A119
- Gultekin, K., Coleman Miller, M., & Hamilton, D. P. 2006, *Astrophys. J.*, 640, 156

- Gupta, T., & Cornish, N. J. 2024, *Phys. Rev. D*, 109, 064040
- Gupte, N., et al. 2024, arXiv:2404.14286
- Hallinan, G., et al. 2017, *Science*, 358, 1579
- Hanna, C., et al. 2020, *Phys. Rev. D*, 101, 022003
- Hannam, M., Schmidt, P., Bohé, A., et al. 2014, *Phys. Rev. Lett.*, 113, 151101
- Hansen, R. O. 1974, *J. Math. Phys.*, 15, 46
- Harris, C. R., et al. 2020, *Nature*, 585, 357
- Harry, I., & Hinderer, T. 2018, *Class. Quant. Grav.*, 35, 145010
- Harry, I. W., & Fairhurst, S. 2011, *Phys. Rev. D*, 83, 084002
- Hendriks, D. D., van Son, L. A. C., Renzo, M., Izzard, R. G., & Farmer, R. 2023, *Mon. Not. Roy. Astron. Soc.*, 526, 4130
- Herdeiro, C. A. R., & Radu, E. 2014, *Phys. Rev. Lett.*, 112, 221101
- Hourihane, S., & Chatziioannou, K. 2025, *Phys. Rev. D*, 112, 084006
- Hoy, C., Fairhurst, S., & Mandel, I. 2025, *Phys. Rev. D*, 111, 023037
- Hoy, C., Mills, C., & Fairhurst, S. 2022, *Phys. Rev. D*, 106, 023019
- Hoy, C., & Raymond, V. 2021, *SoftwareX*, 15, 100765
- Hunter, J. D. 2007, *Comput. Sci. Eng.*, 9, 90
- Iglesias, H. L., et al. 2024, *Astrophys. J.*, 972, 65
- Islam, T., & Venumadhav, T. 2025, arXiv:2502.02739
- Islam, T., Vajpeyi, A., Shaik, F. H., et al. 2025, *Phys. Rev. D*, 112, 044001
- Janka, H.-T., Wongwathanarat, A., & Kramer, M. 2022, *Astrophys. J.*, 926, 9
- Jia, W., et al. 2024, *Science*, 385, 1318
- Johnson-McDaniel, N. K., Kulkarni, S., & Gupta, A. 2022, *Phys. Rev. D*, 106, 023001
- Joshi, P., et al. 2025a, arXiv:2506.06497
- . 2025b, arXiv:2505.23959
- Kalogera, V. 2000, *Astrophys. J.*, 541, 319
- Kaup, D. J. 1968, *Phys. Rev.*, 172, 1331
- Kerr, R. P. 1963, *Phys. Rev. Lett.*, 11, 237
- Kidder, L. E. 1995, *Phys. Rev. D*, 52, 821
- Kimball, C., et al. 2021, *Astrophys. J. Lett.*, 915, L35
- Kozai, Y. 1962, *Astron. J.*, 67, 591
- Kremer, K., Ye, C. S., Rui, N. Z., et al. 2020, *Astrophys. J. Suppl.*, 247, 48
- Krishnendu, N. V., Arun, K. G., & Mishra, C. K. 2017, *Phys. Rev. Lett.*, 119, 091101
- Krishnendu, N. V., Saleem, M., Samajdar, A., et al. 2019, *Phys. Rev. D*, 100, 104019
- Laarackers, W. G., & Poisson, E. 1999, *Astrophys. J.*, 512, 282
- Lange, J., et al. 2017, *Phys. Rev. D*, 96, 104041
- Lee, H. M. 1995, *Mon. Not. Roy. Astron. Soc.*, 272, 605
- Lee, H. M. 2001, *Classical and Quantum Gravity*, 18, 3977
- Lidov, M. L. 1962, *Planet. Space Sci.*, 9, 719
- Ligo Scientific Collaboration, VIRGO Collaboration, & Kagra Collaboration. 2024a, GRB Coordinates Network, 37776, 1
- . 2024b, GRB Coordinates Network, 38155, 1
- LIGO Scientific Collaboration and Virgo Collaboration. 2018, Data quality report user documentation, docs.ligo.org/detchar/data-quality-report/, ,
- LIGO Scientific, Virgo, and KAGRA Collaboration. 2018, LVK Algorithm Library - LALSuite, Free software (GPL), , , doi:10.7935/GT1W-FZ16
- . 2025, Zenodo, doi:10.5281/zenodo.17343574
- Littenberg, T. B., & Cornish, N. J. 2015, *Phys. Rev. D*, 91, 084034
- Littenberg, T. B., Kanner, J. B., Cornish, N. J., & Millhouse, M. 2016, *Phys. Rev. D*, 94, 044050
- Liu, B., & Lai, D. 2017, *Astrophys. J. Lett.*, 846, L11
- . 2018, *Astrophys. J.*, 863, 68
- Liu, B., Lai, D., & Wang, Y.-H. 2019, *Astrophys. J.*, 881, 41
- Lyu, Z., LaHaye, M., Yang, H., & Bonga, B. 2024, *Phys. Rev. D*, 109, 064081
- Ma, L., & Fuller, J. 2019, *Mon. Not. Roy. Astron. Soc.*, 488, 4338
- . 2023, *Astrophys. J.*, 952, 53, [Erratum: *Astrophys. J.* 965, (2024)]
- Mac Uilliam, J., Akcay, S., & Thompson, J. E. 2024, *Phys. Rev. D*, 109, 084077
- Macas, R., Pooley, J., Nuttall, L. K., et al. 2022, *Phys. Rev. D*, 105, 103021
- Macleod, D., Goetz, E., Davis, D., et al. 2025, [gwdetchar/gwdetchar](https://zenodo.org/record/15530809), Zenodo, doi:10.5281/zenodo.15530809
- Madau, P., & Fragos, T. 2017, *Astrophys. J.*, 840, 39
- Mahapatra, P. 2024, *Phys. Rev. D*, 109, 024050
- Mahapatra, P., Chattopadhyay, D., Gupta, A., et al. 2024, *Astrophys. J.*, 975, 117
- . 2025a, *Phys. Rev. D*, 111, 123030
- . 2025b, *Phys. Rev. D*, 111, 023013
- Mahapatra, P., Gupta, A., Favata, M., Arun, K. G., & Sathyaprakash, B. S. 2021, *Astrophys. J. Lett.*, 918, L31
- Mandel, I., & Müller, B. 2020, *Mon. Not. Roy. Astron. Soc.*, 499, 3214
- Mapelli, M., et al. 2021, *Mon. Not. Roy. Astron. Soc.*, 505, 339
- Marchant, P., Langer, N., Podsiadlowski, P., Tauris, T. M., & Moriya, T. J. 2016, *Astron. Astrophys.*, 588, A50
- Margutti, R., et al. 2017, *Astrophys. J. Lett.*, 848, L20

- May, T., East, W. E., & Siemonsen, N. 2025, *Phys. Rev. D*, 111, 044062
- McNeill, L. O., & Müller, B. 2020, *Mon. Not. Roy. Astron. Soc.*, 497, 4644
- Mehta, A. K., Buonanno, A., Cotesta, R., et al. 2023, *Phys. Rev. D*, 107, 044020
- Messick, C., et al. 2017, *Phys. Rev. D*, 95, 042001
- Mihaylov, D. P., Ossokine, S., Buonanno, A., et al. 2023, arXiv e-prints, arXiv:2303.18203
- Miller, M. C., & Lauburg, V. M. 2009, *Astrophys. J.*, 692, 917
- Miller, M. C., & Miller, J. M. 2014, *Phys. Rept.*, 548, 1
- Miller, S., Callister, T. A., & Farr, W. 2020, *Astrophys. J.*, 895, 128
- Mills, C., & Fairhurst, S. 2021, *Phys. Rev. D*, 103, 024042
- Mishra, C. K., Kela, A., Arun, K. G., & Faye, G. 2016, *Phys. Rev. D*, 93, 084054
- Morras, G., Pratten, G., & Schmidt, P. 2025, arXiv:2503.15393
- Morscher, M., Pattabiraman, B., Rodriguez, C., Rasio, F. A., & Umbreit, S. 2015, *ApJ*, 800, 9
- Mottola, E. 2023, arXiv:2302.09690
- Mould, M., & Gerosa, D. 2022, *Phys. Rev. D*, 105, 024076
- Nagar, A., Gamba, R., Rettengo, P., Fantini, V., & Bernuzzi, S. 2024, *Phys. Rev. D*, 110, 084001
- Neumayer, N., Seth, A., & Boeker, T. 2020, *Astron. Astrophys. Rev.*, 28, 4
- Ng, K. K. Y., Hannuksela, O. A., Vitale, S., & Li, T. G. F. 2021a, *Phys. Rev. D*, 103, 063010
- Ng, K. K. Y., Vitale, S., Hannuksela, O. A., & Li, T. G. F. 2021b, *Phys. Rev. Lett.*, 126, 151102
- Ng, K. K. Y., Vitale, S., Zimmerman, A., et al. 2018, *Phys. Rev. D*, 98, 083007
- Nitz, A. H. 2018, *Class. Quant. Grav.*, 35, 035016
- Nitz, A. H., Dent, T., Dal Canton, T., Fairhurst, S., & Brown, D. A. 2017, *Astrophys. J.*, 849, 118
- O’Leary, R. M., Rasio, F. A., Fregeau, J. M., Ivanova, N., & O’Shaughnessy, R. W. 2006, *Astrophys. J.*, 637, 937
- Pacilio, C., Vaglio, M., Maselli, A., & Pani, P. 2020, *Phys. Rev. D*, 102, 083002
- Pani, P., Cardoso, V., Gualtieri, L., Berti, E., & Ishibashi, A. 2012, *Phys. Rev. Lett.*, 109, 131102
- Pankow, C., Brady, P., Ochsner, E., & O’Shaughnessy, R. 2015, *Phys. Rev. D*, 92, 023002
- Pappas, G., & Apostolatos, T. A. 2012a, arXiv:1211.6299
- . 2012b, *Phys. Rev. Lett.*, 108, 231104
- Payne, E., Kremer, K., & Zevin, M. 2024, *Astrophys. J. Lett.*, 966, L16
- Paynter, J., & Thrane, E. 2023, *Astrophys. J. Lett.*, 945, L18
- Peters, P. C. 1964, *Phys. Rev.*, 136, B1224
- Planas, M. d. L., Ramos-Buades, A., García-Quirós, C., et al. 2025, arXiv:2504.15833
- Poisson, E., & Will, C. M. 1995, *Phys. Rev. D*, 52, 848
- Pompili, L., et al. 2023, *Phys. Rev. D*, 108, 124035
- Portegies Zwart, S., McMillan, S., & Gieles, M. 2010, *Ann. Rev. Astron. Astrophys.*, 48, 431
- Poutanen, J., et al. 2022, *Science*, 375, abl4679
- Pratten, G., Schmidt, P., Buscicchio, R., & Thomas, L. M. 2020, *Phys. Rev. Res.*, 2, 043096
- Pratten, G., et al. 2021, *Phys. Rev. D*, 103, 104056
- Press, W. H., & Teukolsky, S. A. 1972, *Nature*, 238, 211
- Pretorius, F. 2005, *Phys. Rev. Lett.*, 95, 121101
- Prix, R. 2007, *Class. Quant. Grav.*, 24, S481
- Puecher, A., Kalaghatgi, C., Roy, S., et al. 2022, *Phys. Rev. D*, 106, 082003
- Pürrer, M., Hannam, M., Ajith, P., & Husa, S. 2013, *Phys. Rev. D*, 88, 064007
- Qin, Y., Fragos, T., Meynet, G., et al. 2018, *Astron. Astrophys.*, 616, A28
- Racine, E. 2008, *Phys. Rev. D*, 78, 044021
- Ramos-Buades, A., Buonanno, A., Estellés, H., et al. 2023a, *Phys. Rev. D*, 108, 124037
- Ramos-Buades, A., Buonanno, A., & Gair, J. 2023b, *Phys. Rev. D*, 108, 124063
- Ray, A., et al. 2023, arXiv:2306.07190
- Rizzuto, F. P., Naab, T., Spurzem, R., et al. 2022, *Mon. Not. Roy. Astron. Soc.*, 512, 884
- Robinet, F., Arnaud, N., Leroy, N., et al. 2020, *SoftwareX*, 12, 100620
- Rodriguez, C. L., Amaro-Seoane, P., Chatterjee, S., et al. 2018a, *Phys. Rev. D*, 98, 123005
- Rodriguez, C. L., Amaro-Seoane, P., Chatterjee, S., & Rasio, F. A. 2018b, *Phys. Rev. Lett.*, 120, 151101
- Rodriguez, C. L., Zevin, M., Amaro-Seoane, P., et al. 2019, *Phys. Rev. D*, 100, 043027
- Rodriguez, C. L., Zevin, M., Pankow, C., Kalogera, V., & Rasio, F. A. 2016, *Astrophys. J. Lett.*, 832, L2
- Rodriguez, C. L., Weatherford, N. C., Coughlin, S. C., et al. 2022, *ApJS*, 258, 22
- Romero-Shaw, I., Stegmann, J., Tagawa, H., et al. 2025, *Phys. Rev. D*, 112, 063052
- Romero-Shaw, I. M., Gerosa, D., & Loutrel, N. 2023, *Mon. Not. Roy. Astron. Soc.*, 519, 5352
- Romero-Shaw, I. M., Lasky, P. D., & Thrane, E. 2022, *Astrophys. J.*, 940, 171
- Romero-Shaw, I. M., Lasky, P. D., Thrane, E., & Bustillo, J. C. 2020a, *Astrophys. J. Lett.*, 903, L5
- Romero-Shaw, I. M., et al. 2020b, *Mon. Not. Roy. Astron. Soc.*, 499, 3295

- Roulet, J., & Zaldarriaga, M. 2019, *Mon. Not. Roy. Astron. Soc.*, 484, 4216
- Ruffini, R., & Bonazzola, S. 1969, *Phys. Rev.*, 187, 1767
- Ryan, F. D. 1997, *Phys. Rev. D*, 55, 6081
- Sachdev, S., et al. 2019, arXiv e-prints, arXiv:1901.08580
- Sakon, S., et al. 2024, *Phys. Rev. D*, 109, 044066
- Salvesen, G., & Pokawanvit, S. 2020, *Mon. Not. Roy. Astron. Soc.*, 495, 2179
- Samsing, J. 2018, *Phys. Rev. D*, 97, 103014
- Samsing, J., Askar, A., & Giersz, M. 2018, *Astrophys. J.*, 855, 124
- Samsing, J., MacLeod, M., & Ramirez-Ruiz, E. 2014, *Astrophys. J.*, 784, 71
- Samsing, J., & Ramirez-Ruiz, E. 2017, *Astrophys. J. Lett.*, 840, L14
- Samsing, J., Bartos, I., D’Orazio, D. J., et al. 2022, *Nature*, 603, 237
- Santamaria, L., et al. 2010, *Phys. Rev. D*, 82, 064016
- Schmidt, P., Ohme, F., & Hannam, M. 2015, *Phys. Rev. D*, 91, 024043
- Schnittman, J. D., & Buonanno, A. 2007, *Astrophys. J. Lett.*, 662, L63
- Shaikh, M. A., Varma, V., Pfeiffer, H. P., Ramos-Buades, A., & van de Meent, M. 2023, *Phys. Rev. D*, 108, 104007
- Shaikh, M. A., Varma, V., Ramos-Buades, A., et al. 2025, *Class. Quant. Grav.*, 42, 195012
- Siemonsen, N., May, T., & East, W. E. 2023, *Phys. Rev. D*, 107, 104003
- Singer, L. P., & Price, L. R. 2016, *Phys. Rev. D*, 93, 024013
- Smith, J. R., Abbott, T., Hirose, E., et al. 2011, *Class. Quant. Grav.*, 28, 235005
- Soni, S., Glanzer, J., Effler, A., et al. 2024, *Class. Quant. Grav.*, 41, 135015
- Soni, S., et al. 2020, *Class. Quant. Grav.*, 38, 025016
- . 2025, *Class. Quant. Grav.*, 42, 085016
- Speagle, J. S. 2020, *Mon. Not. Roy. Astron. Soc.*, 493, 3132
- Spera, M., Giacobbo, N., & Mapelli, M. 2016, *Mem. Soc. Ast. It.*, 87, 575
- Spera, M., & Mapelli, M. 2017, *Mon. Not. Roy. Astron. Soc.*, 470, 4739
- Spruit, H. C. 1999, *Astron. Astrophys.*, 349, 189
- . 2002, *Astron. Astrophys.*, 381, 923
- Stegmann, J., & Klencki, J. 2025, *Astrophys. J. Lett.*, 991, L54
- Stott, M. J. 2020, arXiv:2009.07206
- Tagawa, H., Kocsis, B., Haiman, Z., et al. 2021, *Astrophys. J. Lett.*, 907, L20
- Talbot, C., Farah, A., Galaudage, S., Golomb, J., & Tong, H. 2025, *J. Open Source Softw.*, 10, 7753
- Talbot, C., Smith, R., Thrane, E., & Poole, G. B. 2019, *Phys. Rev. D*, 100, 043030
- Tauris, T. M. 2022, *Astrophys. J.*, 938, 66
- Thompson, J. E., Hamilton, E., London, L., et al. 2024, *Phys. Rev. D*, 109, 063012
- Thorne, K. S. 1980, *Rev. Mod. Phys.*, 52, 299
- Tiwari, V., & Fairhurst, S. 2021, *Astrophys. J. Lett.*, 913, L19
- Tong, H., Galaudage, S., & Thrane, E. 2022, *Phys. Rev. D*, 106, 103019
- Tsukada, L., et al. 2023, *Phys. Rev. D*, 108, 043004
- Uchikata, N., & Yoshida, S. 2016, *Class. Quant. Grav.*, 33, 025005
- Udall, R., Hourihane, S., Miller, S., et al. 2025, *Phys. Rev. D*, 111, 024046
- Usman, S. A., et al. 2016, *Class. Quant. Grav.*, 33, 215004
- Vaglio, M., Pacilio, C., Maselli, A., & Pani, P. 2022, *Phys. Rev. D*, 105, 124020
- van der Sluys, M. V., Röver, C., Stroeer, A., et al. 2008, *Astrophys. J. Lett.*, 688, L61
- Varma, V., Field, S. E., Scheel, M. A., et al. 2019, *Phys. Rev. Research.*, 1, 033015
- Viets, A., et al. 2018, *Class. Quant. Grav.*, 35, 095015
- Vigna-Gómez, A., et al. 2024, *Phys. Rev. Lett.*, 132, 191403
- Vijaykumar, A., Hanselman, A. G., & Zevin, M. 2024, *Astrophys. J.*, 969, 132
- Virgo Collaboration. 2021, PythonVirgoTools, git.ligo.org/virgo/virgoapp/PythonVirgoTools, vv5.1.1, ,
- Virtanen, P., et al. 2020, *Nat. Meth.*, 17, 261
- Vitale, S., Biscoveanu, S., & Talbot, C. 2022, *Astron. Astrophys.*, 668, L2
- Vitale, S., Lynch, R., Raymond, V., et al. 2017, *Phys. Rev. D*, 95, 064053
- Vitale, S., Lynch, R., Veitch, J., Raymond, V., & Sturani, R. 2014, *Phys. Rev. Lett.*, 112, 251101
- von Zeipel, H. 1910, *Astronomische Nachrichten*, 183, 345
- Wen, L. 2003, *Astrophys. J.*, 598, 419
- Wette, K. 2020, *SoftwareX*, 12, 100634
- Williams, D., Veitch, J., Chiofalo, M. L., et al. 2023, *J. Open Source Softw.*, 8, 4170
- Wongwathanarat, A., Janka, H. T., & Mueller, E. 2013, *Astron. Astrophys.*, 552, A126
- Woosley, S. E., Blinnikov, S., & Heger, A. 2007, *Nature*, 450, 390
- Woosley, S. E., & Heger, A. 2021, *Astrophys. J. Lett.*, 912, L31
- Wysocki, D., O’Shaughnessy, R., Lange, J., & Fang, Y.-L. L. 2019, *Phys. Rev. D*, 99, 084026
- Ye, C. S., Fishbach, M., Kremer, K., & Reina-Campos, M. 2025, arXiv:2507.07183

- Yu, H., Ma, S., Giesler, M., & Chen, Y. 2020, *Phys. Rev. D*, 102, 123009
- Zaldarriaga, M., Kushnir, D., & Kollmeier, J. A. 2018, *Mon. Not. Roy. Astron. Soc.*, 473, 4174
- Zdziarski, A. A., Veledina, A., Szanecki, M., et al. 2023, *Astrophys. J. Lett.*, 951, L45
- Zdziarski, A. A., Malyshev, D., Dubus, G., et al. 2018, *Mon. Not. Roy. Astron. Soc.*, 479, 4399
- Zevin, M., & Bavera, S. S. 2022, *Astrophys. J.*, 933, 86
- Zevin, M., Pankow, C., Rodriguez, C. L., et al. 2017, *Astrophys. J.*, 846, 82
- Zevin, M., Samsing, J., Rodriguez, C., Haster, C.-J., & Ramirez-Ruiz, E. 2019, *Astrophys. J.*, 871, 91
- Zweizig, J. 2006, The Data Monitor Tool Project, labcit.ligo.caltech.edu/~jzweizig/DMT-Project.html, ,